UNIVERSITY OF Southampton

University of Southampton Research Repository
ePrints Soton

Copyright © and Moral Rights for this thesis are retained by the author and/or other copyright owners. A copy can be downloaded for personal non-commercial research or study, without prior permission or charge. This thesis cannot be reproduced or quoted extensively from without first obtaining permission in writing from the copyright holder/s. The content must not be changed in any way or sold commercially in any format or medium without the formal permission of the copyright holders.

When referring to this work, full bibliographic details including the author, title, awarding institution and date of the thesis must be given e.g.

AUTHOR (year of submission) "Full thesis title", University of Southampton, name of the University School or Department, PhD Thesis, pagination

http://eprints.soton.ac.uk

UNIVERSITY OF SOUTHAMPTON

FACULTY OF SOCIAL and HUMAN SCIENCES

School of Mathematics

Optimising Plant and Soil Management

by

James Paul Heppell

Thesis for the degree of Doctor of Philosophy

October 2014

UNIVERSITY OF SOUTHAMPTON

ABSTRACT

FACULTY OF SOCIAL and HUMAN SCIENCES

SCHOOL OF MATHEMATICS

Doctor of Philosophy

Optimising Plant and Soil Management

by James Paul Heppell

This thesis is an accumulation of work regarding the role of phosphorus (P) and water in soils in relation to crop growth and food production. We use a multi-scale modelling approach to initially capture the interactions of soil and water on a single cylindrical root and further expand to a growing root structure. Moreover, we have a multi-physics problem involving fluid dynamics of water uptake in plants, and reactive solute transport in the soil for plant P uptake. We use detailed climate data and the super computer at the University of Southampton (Iridis 4) to parameterise our models. These facilities allow us to analyse the root structure as well as P and water in the soil in great detail. The collaboration of mathematics, biology and operational research makes it possible to complete this project.

The analytical models recently developed within our group have shown to agree remarkably well with full 3D simulation models. These analytical models help provide the structure for the models used within this thesis and will for the first time enable us to start using optimisation techniques to find the optimal conditions for increasing plant P uptake efficiency.

By using mathematical models to predict plant P and water uptake within the soil, we have addressed a number of questions surrounding the optimal plant root structure for P accumulation, and the survival of crops in a low P environment. In addition, we were able to predict the behaviour of water in the soil over the course of a full year. And finally, utilising all the above, we have outlined the optimal fertiliser and soil management strategy.

Contents

List of Figures

List of Tables

List of Publications

1. J. Heppell, S. Payvandi, K. C. Zygalakis, J. Smethurst, J. Fliege and T. Roose. 2014. Validation of a spatial-temporal soil water movement and plant water uptake model. *Geotechnique* **64**(7) 526-539.

2. J. Heppell, P. Talboys, S. Payvandi, K. C. Zygalakis, J. Fliege, P. Withers, D. Jones and T. Roose. 2014 How changing root system architecture can help tackle a reduction in soil phosphate (P) levels for better plant P acquisition. *Plant, Cell & Environment*, 1-33 (In Press) doi:10.1111/pce.12376.

3. J. Heppell, S. Payvandi, P. Talboys, K. Zygalakis, J. Fliege, D. Langton, R. Sylvester-Bradley, R. Walker, D.L. Jones and T. Roose. 2014. Modelling the optimal phosphate fertiliser and soil management strategy for crops. (will be submitted to Plant and Soil special edition 2014 - deadline November).

4. P. Talboys, J. Heppell, J. Daniel, T. Roose, J. Healey, D. Jones and P. Withers. 2014. Struvite: a slow-release P fertiliser for sustainable intensification? (Submitted to Agronomy for sustainable development 2014).

Declaration of Authorship

I, **James Paul Heppell**, declare that this thesis entitled **Optimising Plant and Soil Management** and the work presented in it are both my own, and have been generated by me as the result of my own research. I confirm that:

- this work was done wholly or mainly while in candidature for a research degree at this University;
- if any part of this thesis has previously been submitted for a degree or any other qualification at this University or any other institution, this has been clearly stated;
- where I have consulted the published work of others, this is always clearly attributed;
- where I have quoted from the work of others, the source is always given. With the exception of such quotations this thesis is entirely my own work;
- I have acknowledged all main sources of help;
- where the thesis is based on work done by myself jointly with others, I have made clear exactly what was done by others and what I have contributed myself;
- parts of this work have been published.

Signed: Date:

Acknowledgements

I would like to thank my supervisors Tiina Roose and Joerg Fliege for providing guidance throughout my PhD and answering my numerous questions. Konstantinos Zygalakis for giving critical feedback that has helped me grow as a scientist, Sevil Payvandi for putting up with my constant questions and having patience when working together throughout my PhD. My PhD would have been incomplete without Pete Talboys who ran numerous plant experiments to calculate much needed data; in addition the trips up to Bangor University were very enjoyable.

My PhD was funded by the Institute for Complex Systems Simulation (ICSS) Doctoral Training Centre (DTC) at Southampton and I am very grateful to Nicki Lewin who excelled at organising social events for our large group. This environment was a great opportunity to meet other post graduates of different disciplines that I would not have had the chance to meet otherwise. From years 2-4 of my PhD, I was based in the Maths department and would like to thank my office mates for putting up with my silly questions and providing much needed distractions from work, especially the 4 pm random question time.

While living in Southampton I have stayed with many groups of people and have had lots of great experiences. During my PhD years my flatmates have provided endless laughter and our Wednesday cinema trips were very enjoyable.

I would like to mention my parents for providing moral and financial support throughout my time at Southampton. Thank you for believing in me and always being there no matter what mess I got into. My twin brother, Charles, for whipping me into shape while he was also at Southampton and letting me learn from his experience as he went through every process of the PhD before me, graduating 2014. My sister in law Jin, my nephew Jack and my new nephew to come for sharing great experiences and letting me see that there is a lot more to life than work.

Speaking of not working, I would like to thank my group of badminton friends who have provided many hours of entertainment and kept me fit over the years. It was great fun playing with you, and without badminton I would not have met some very special friends.

Last but by no means least I would like to thank my significant other for being there for the last year and a half of my PhD. I am unable to thank you enough, for being truly amazing and putting up with me no matter my mood.

I have had a wonderful time at Southampton and have enjoyed all parts of my life here. Thanks!

Notation list for Chapter 1

$\mathbf{1}$	A vector of 1's	$\Re$	The set of real numbers
A_1	Weighting parameter	$\Re^+$	The set of positive real numbers
A_2	Weighting parameter	$\Re_d$	Set of real numbers of index d
a	Root radius	r	Polar radius
B	Function for calculating a lower bound	s^2	Estimated variance for a Kriging model
b	Soil buffer power	^{T}	Transpose
c_0	Far field concentration of P away from root	TOT_f	Cumulative fitness of all individuals
$Corr$	Correlation	t	Time
c	Concentration of P in pore water	V	Water flux into the root
D	Diffusion coefficient of P in pore water	X	Function for finding the next point for DIRECT search
D_H	Hyperrectangle	x	An element within $f(\bar{x})$
d	Distance between points in Kriging algorithm	x'	An element different to x within $f(\bar{x})$
det	Determinate	x_c	A contraction point in the Nelder-Mead Algorithm
exp	Exponential	x_e	An expansion point in the Nelder-Mead Algorithm
F_m	Maximum rate of P uptake	x_l	A lower bound
f	Actual fitness	x_m	Midpoint between x_l and x_u
$f(x)$	A functions for multi-objective optimisation	x_r	A reflection point in the Nelder-Mead Algorithm
$f(\mathbf{x})$	A generic function	x_u	An upper bound
$g(x)$	A functions for multi-objective optimisation	$y(x)$	An unknown function
$g(\mathbf{x})$	Inequality constraint	$\hat{y}(x)$	Surrogate model
$h(x)$	A functions for multi-objective optimisation	$Z(x)$	A local deviation from the global model
$h(\mathbf{x})$	Equality constraint	α	Reflection parameter in the Nelder-Mead Algorithm
K	Lipschitz constant	γ	Expansion parameter in the Nelder-Mead Algorithm
K_m	Michaelis constant	θ	Correlation vector parameter
N	Number of sampled points	κ	Parameter effecting the Gaussian distribution
n	Number of a given term	μ	A constant global model
n_{ic}	Number of inequality constraints	ρ	Contraction parameter in the Nelder-Mead Algorithm
n_{ec}	Number of equality constraints	Σ	A covariance matrix
P	Phosphorus	σ	Standard deviation
p	Probability	ϕ	Water saturation level
$\tilde{p}$	Bounded probability	$\phi(x)$	Probability density of sampling a new point in GBNM
p_{sel}	Probability of selection	Ω	A bounded space
q	Vector for Kriging	ω	Shrinkage parameter in the Nelder-Mead Algorithm
R	An n by n matrix		

Table 1: Notation list for Chapter 1.

Chapter 1

Introduction

This thesis is an accumulation of work accomplished by the author regarding the role of phosphorus (P) and water in soils in relation to crop growth and food production. By using mathematical models to predict plant P uptake within the soil, we address the following questions. What could the optimal plant root structure for P accumulation be? Can crops survive in soils with low P content? Can we predict the behaviour of water in the soil over the course of the year? What could the optimal fertiliser and soil management strategy be?

The material presented in this thesis has in part been used to address the Defra Link "Targeted P" project on "Improving the sustainability of phosphorus use in arable farming". The overall "Targeted P" project involves combining laboratory studies, field experiments and modelling to provide new insights to guide decisions on soil and fertiliser management strategies, to help farmers adapt for future P use. The academic papers presented in this thesis relate to the modelling work carried out and experimental data is used to validate the models and to provide a comparison against estimated plant P uptake.

This Chapter is split into four Sections. In Section 1.1 we cover the background of plant and soil management, in Section 1.2 we cover plant and soil models, in

Section 1.3 we cover operational research techniques used, and finally in Section 1.4 we cover the structure of the paper based Chapters within the thesis and declaration of work within them.

1.1 Background to Plant and Soil Management

All plants require 13 nutrients to survive, if any of these are lacking the plant can not complete its full life cycle. The combination of all of the nutrients is important, a message well described by Liebig's barrel [76]. Imagine a barrel full of water (signifying crop yield) and each plank of wood around the edge a key nutrient, where its height is equal to the amount available to the plant. The total amount of water in the barrel will be restricted by the most limited nutrient. Increasing the amount of other nutrients will not increase the water held in the barrel (yield). To make matters worse an excess of one nutrient can prohibit the uptake of another [154], essentially giving a finite amount of wood to use to construct the barrel. In addition to this scenario, different quantities of nutrients are required at different times throughout the crop life cycle and so the height of each plank of wood could be changing over time. It is therefore important to know the state of nutrients in the soil before applying fertilisers, and to stop over fertilisation of certain nutrients, such as phosphorus. For example, if a wheat field has an Olsen P index of 3 ($>$ 45 mg P/l) then no additional P from fertiliser is allowed for that harvest (RB209 fertiliser manual, UK).

Agricultural soils generally provide an adequate supply of all nutrients that plants need, but the ones that can be most limiting, are phosphorus (P) and nitrogen (N). The most limited nutrients in the soil are therefore topped up by the use of fertilisers. Two methods are commonly used to estimate the P fertiliser requirements for a given crop, soil tests every 5-10 years and sampling how much

P was taken out of the soil from the previous cropping season. The later is done by measuring the P content using the ascorbate/molybdate blue method of Murphy and Riley [126].

1.1.1 The Role of Phosphorus

The macro-nutrient phosphorus (P) is essential to crops since it is a major building block of adenosine triphosphate (ATP). ATP is found in all living cells and stores energy required for most processes. In addition, P plays an important role in photosynthesis, respiration, seed and fruit production and promotes root growth. P is taken up by plants in the form of orthophosphate (PO_4^{3-}) through the root system in the soil. Two signs that a crop is lacking P are the lack of growth and discolouring of leaves (yellow leaves with purple tips) [140]. Plants are affected by P in the soil, when in a low P environment plants allocate a greater biomass to the root system to grow longer root hairs in search for P [52, 72].

Generally 70% of the total phosphorus in soil is found in inorganic particulates [144, 201] and the three main elements that bind to phosphorus in soils are iron, aluminium and calcium [110].

P in the soil exists in at least two main states, bound and unbound. The unbound state includes P in solution, which has been dissolved into the soil solution via water pathways, and is taken up by the plant roots directly. A soil is fertile if the unbound P is repeatedly replenished by bound P, where bound P has reacted with calcium or aluminium to make it soluble. As the amount of P absorbed by the soil increases the amount of P in solution also increases. Bound P contains very insoluble inorganic phosphate compounds and organic compounds that are hard to mineralise by aid of micro-organisms. It is often the case that there is a very slow conversion of bound P to unbound P and this results in P being locked into the soil for many years.

One way for differentiating between soils, in terms of their P soil availability, is the soil buffer power. The buffer power is a term which describes the capacity of a soil to re-supply P to the soil solution, and relates to the time scale of release of bound P to unbound P. A high buffer power means the re-supply is low and P is kept in the bound state. Whereas, a low buffer power means the re-supply is high and the unbound P is being replenished quicker, generally giving a more fertile soil. Nutrients have different buffer power values in soil and P is generally much higher than others, Table (1.1) [161].

Nutrient	Buffer power
NO_3^-	1.0
K	39
S	2
P	239
Mg	1.2
Ca	156

Table 1.1: Soil buffer power values for different nutrients from [161].

There are many factors that effect P availability in the soil and hence the measurement of the P concentration of a soil. These factors include, soil pH, compaction, aeration, moisture, temperature, texture, organic matter, crop residues, plant root systems and mycorrhizae. Throughout history there have been many soil tests used to estimate the total amount of P in the soil and also the amount accessible by the plant root system. One of the earliest and simplest methods separates the total amount of P into three fractions, inorganic P extracted with 0.5 M sulphuric acid, inorganic P not extracted with 0.5 M sulphuric acid and organic P [202]. A variety of accepted methods for measuring soil P are used in different parts of the world due to varying soils conditions. In 1945 Bray and

Kurtz developed the Bray P1 and P2 method, the difference being the strength of the hydrochloric acid used (4 times stronger in P2) [19]. The Bray test was used to estimate the unavailable P in the soil contributed to by rock phosphate, which at the time farmers were "over-using". The Bray method is widely used in Midwestern and North Central United States of America [51]. In 1954, S.R. Olsen developed the Olsen (sodium bicarbonate) method which estimates the P concentration in alkaline soils, something the Bray test cannot do accurately [137]. The Olsen method however needs its own calibration method and therefore gives different results in labs across the world, because methods are not consistent. The Mehlich 1 method was developed in 1953 by Dr. Adolf Mehlichin for use on coastal plain soils of Eastern America [117]. Later in 1984, he developed the Mehlich 3 method which correlates well with the Bray P1 test in acid soils and with the Olsen method for alkaline soils [118]. Finally the Morgan's test, developed in 1932 by Morgan, can be used for a wide range of soils and is the main test for soils in Scotland [123]. An extension called modified Morgan's was introduced to include micro-nutrient analysis [189].

These current methods for estimating P in soil are not consistent across Europe, with a wide range of methods and techniques, causing similar soils to have uncorrelated results [90, 129]. This provides confirmation that due to the diversity of methods used, site specific treatments are needed and one method is not best for all soils. New methods however, are being developed that estimate the amount of available P within the soil. A more advanced technique compared to the very sensitive approach of Olsen P, uses iron oxide-impregnated paper to estimate P removal from soil [195]. Another method, Diffusive Gradients in Thin films (DGT) measures the diffusion of P taken from a soil sample to calculate the available P [185]. These new methods are trying to develop a robust method for all soils and if successful could result in a breakthrough and a better understanding of P

within the soil.

There has been a lot of discussion about how the readily available P reserves around the world will become depleted within the next 50-130 years [32, 35]. As a result, the agriculture systems will suffer severely as they heavily rely on constant supplies of this finite resource [191]. This need to reduce our reliance on rock phosphate may also become exacerbated by political control as the remaining reserves are highly spatially localised, being mainly owned by China, Morocco and the US, who together control 85% of the known global rock phosphate reserves [47].

P is typically applied in large quantities in most productive cropping systems ($>$ 20 kg P ha^{-1}). However, it is often used inefficiently with a large proportion of the added P subsequently becoming unavailable for plant P uptake or lost altogether. To achieve greater sustainability within agriculture requires that new strategies are developed to either reduce the P demand of the crop or to promote greater root recovery of the added P such that less fertiliser is required. This would reduce the negative aspects of P use in agriculture (e.g. eutrophication) as well as yielding higher economic returns for farmers. Due to repeated fertilisation over the last couple of decades many agricultural soils are now close to, or at, total P holding capacity [17]. While this makes P readily available to the plant, it also stimulates vertical loss down the soil profile and allows P to be readily released from particles when surface runoff enters freshwaters [68]. Therefore, one mitigation strategy is to "run down" soil P reserves by reducing P inputs relative to the amount of P taken up by the crop. Maintaining of yields, however, necessitates that P is used more efficiently by the crop. It is therefore important to assess how crops will cope under a reduced P environment, and if that is not plausible, determine what plant-based soil options are available for adapting to these conditions.

There are many potential strategies to help tackle the reduced P scenario, from changing plant traits by targeting plant breeding (e.g. desired seed P content and changes in root architecture), to altering the properties of soil [106, 196]. Plants are estimated to take up less than 15% of the P added into the soil, and therefore an alternative method to tackle this involves manipulating the chemistry and biology of the rhizosphere to make more of the added P available to plants [149]. As P is often highly immobile in soil, one method could be to adapt the root system architecture to obtain P more efficiently [73, 204]. From manipulating plant root traits to varying soil cultivation techniques, increasing P use efficiency is of great importance.

1.1.2 The Role of Water

In addition to studying how P behaves in the soil it is also important to consider the role of water. Water helps P become soluble in soil and increases its availability to plant roots. Water plays a vital role for crops providing them with their most useful resource. As seeds are planted they first grow deep roots down into the soil to look for water. Once this is established, the plant has a much better chance of being healthy and for a crop it means producing a greater yield [188]. The crop uses water for growth and to reduce its temperature via evapotranspiration. Evapotranspiration is made up of two processes, transpiration and evaporation. Transpiration is the term used to describe water lost from small openings on the surface of the leaves, called stomata. Evaporation is water lost from the plant surface or from wet soil. It is important not to put the plant under water stress as this can lead to a poor grain yield and therefore estimation of water in soil is important.

A common method used to measure the water saturation levels in soil is to use time domain reflectrometry (TDR) probes, which can produce readings of up to

every 10 minutes. Alternatively, a neutron probe can be dropped into the soil for an instant reading of the water saturation levels with depth. Neutron probes are only used a few times within the year (as they are a one-shot) to give a snap shot analysis of the water concentration levels within the soil; they are more accurate than TDR probes and are thus used in conjunction with TDR probes.

In 2001, world agriculture accounted for approximately 70% of freshwater consumption [145] and food production may soon be limited by the availability of water [92]. In the UK, significant reductions of crop yield by up to 30% can be seen from severe weather conditions, such as drought [11]. In order to optimize soil-water and plant management strategies it is necessary to understand current plant-soil systems and their reactions to varying rainfall and climate patterns. This becomes a more pressing question with the onset of global warming as climate patterns are likely to change. Simultaneously, the need for water is set to increase to critical levels due to the growing global population and corresponding increases in food production [203]. With both supply and demand varying, there is a need to optimise water management across all sectors: urban, industrial, environmental and agricultural.

1.1.3 Soil Cultivation and Fertiliser Strategies

There are many options available to farmers when deciding which crop management strategy to implement. Different ways of cultivating soil include: mixing the soil to different depths $0-25$ cm (ploughing), minimum tillage which distributes P in the soil into bands; $0-5$ cm, $5-10$ cm and $10-15$ cm with a P concentration ratio of $1.5:1:0.5$ respectively and an inverted plough which flips the current soil profile down to 15 cm. Each of these techniques are used and implementation generally depends on site specific conditions. Ploughing is the most common as it evenly distributes P within the soil profile and makes it available to the plant root

system. P fertiliser is applied by either, branding or broadcasting P within the seed bed, foliarly or as a seed coating. The branded application involves injecting fertiliser pellets $5 - 10$ cm below the soil and/or 5 cm away from the seed. The idea is to place the fertiliser close to the root system to try and maximise plant P uptake at the right time in the root system development. The broadcasted application evenly distributes fertiliser on top of the soil and is either mixed in or left to diffuse for future crops. Foliar applications are made part way through the crop life cycle as P is spread onto the leaves in a solution. However, difficulties can occur when trying to get P taken up directly by the leaves, as P solution instead drips off the leaves and onto the soil and slowly diffuses downwards. In addition, foliar P can negatively affect crops by lowering root colonization by arbuscular mycorrhizal fungi (AMF) thus potentially reducing uptake of other nutrients [170]. One solution to improve foliar application is to apply stickers or adhesive on the leaves to help P accumulation into the leaves [139]. Seed coating methods add fertiliser with seeds as they are planted producing a similar effect to the branded application. Fast- and slow-release P pellets are used, which provide P for early root growth and throughout the crop life cycle, respectively.

Methods that work well for specific sites are generally repeated to ensure similar crop yields, however, there is no 'best' method as strategies are different for sites around the world. A large European study assessing the effect of soil tillage on crop growth found that no tillage reduced yields by 8.5% while conservation tillage only reduced yields by 4.5% compared with conventional tillage [192]. These methods would save money on tillage costs to compensate for lower yields, and present viable solutions to areas that might have restrictions due to machinery requirements. In addition, negative effects of tillage (e.g. soil disturbance) could be reduced by applying a deep tillage in conjunction with crop rotation, including crops other than cereals [192]. Deep tillage in low rainfall ar-

eas can increase P supply to the root system, but may also lead to environmental degradation such as increased erosion, and rapid drying of soils can further lead to immobilisation of soil P [200]. When placing a mix of Nitrogen, Phosphorus and Potassium (NPK) fertiliser one study showed that to maximise total leaf area and yield for a maize crop, banded fertilisation was used which placed P 20 cm from the plant and 10 cm under the soil [141].

Climate conditions often have a big impact on which strategy farmers implement. For example, if the soil temperature has not risen enough over the spring then the summer crop cannot be planted and a late harvest can result in poor yields [58]. On the other hand if there is a forecast for heavy rain, applying fertiliser on top of the soil will mean that the applied P has a better chance of being taken up in the rooting zone (taking into account run-off effects).

1.2 Background to Plant and Soil Models

Models used to represent plant and soil systems can be split into those that consider nutrients and those that don't. We first look at models for plant water uptake (without nutrients) and then those that consider plant nutrient uptake, namely P.

Water Models

A number of agronomic models exist that estimate changes in water saturation levels within the soil in response to climate conditions and plant water uptake. However, many of these models only estimate the average water saturation levels within the plant root zone and do not include nutrients. Common examples used in agriculture (and to some extent, in engineering [29]) include Decision Support System for Agrotechnology Transfer (DASSAT) [89], the Agricultural Production

Systems Simulator (APSIM) [115] and Cropwat, a decision support tool developed by the Land and Water Development Division of FAO [31]. These macroscopic models are quick to implement as they use simple algebraic mass balance equations to estimate the total soil water content.

Cropwat carries out a water balance calculation for the rooting zone, determining an average soil saturation which varies in response to rainfall infiltration and plant evapotranspiration, calculated using the Penman-Monteith Equation [3]. Many of these models are adequate for simple crop management and irrigation purposes. However, applications in engineering and agricultural sciences need models to more accurately represent the soil-plant-atmosphere continuum, in particular the water movement and saturation within specific parts of the soil profile. For example, this is important for understanding crop behaviour in response to different patterns in climate [155]. In engineering, the stability of many embankments and cut slopes is dependent on the presence of soil suctions both within and below the rooting zone, and more advanced models are needed to investigate vegetation management options [21, 104].

A difficulty with trying to model the water saturation levels at different soil depths is the characterisation of the parameters that control the soil water saturation and flow processes. Both soil water retention and permeability can be difficult to measure accurately, and there is often little or no site specific data, yet modelling responses can be very sensitive to these parameters [164, 176]. Data on root structures and temporal soil and plant interactions with time can also be sparse. However, there are often good records for water saturation levels and climate conditions, which can be used to calibrate models.

Single Root Nutrients Models

Microscopic nutrient modelling began in the 1960's with models estimating nutrient uptake for a single cylindrical root surrounded by an infinite extent of soil, with a prescribed far field nutrient concentration [7, 133, 138]. Due to non-linearity in the root nutrient uptake boundary condition, only a numerical solution was found [7, 133], which meant that adapting a single root model to a more realistic root system was computationally expensive (Nye-Tinker-Barber model).

The Nye-Tinker-Barber absorption-diffusion model is described by Equations (1.2.1 - 1.2.4),

$$(\phi + b)\frac{\partial c}{\partial t} - \frac{aV}{r}\frac{\partial c}{\partial r} = \frac{\phi D}{r}\frac{\partial}{\partial r}(r\frac{\partial c}{\partial r}) \tag{1.2.1}$$

$$\phi D\frac{\partial c}{\partial r} + Vc = \frac{F_m c}{K_m + c} \text{ on } r = a, \tag{1.2.2}$$

$$c \to c_0 \quad \text{as} \quad r \to \infty, \tag{1.2.3}$$

$$c = c_0 \quad \text{at} \quad t = 0. \tag{1.2.4}$$

where ϕ is the water saturation level, b is the soil buffer power, c is the concentration of P in pore water, a is the root radius, V is the water flux into the root, r is the polar radius, t is time, D is the diffusion coefficient of P in pore water, F_m and K_m are properties of the root surface and c_0 is the far field concentration away from the root.

In 2001 a fully explicit analytical solution to the Nye-Tinker-Barber model was derived which enabled a more realistic model that utilises a more complex root branching structure [161, 162]. In all four papers [7, 133, 161, 162] the uptake of P by roots is represented by the Michaelis-Menten uptake law, and all of these models use a linear convection-diffusion model with a nonlinear root surface uptake condition. The rate of convective transport of P can be shown to be negligible relative to diffusion [91] and this has been fully analysed and justified

[161, 162]. For a complete solution of the convection-diffusion equations for P transport to plant roots see [162]. To estimate the total uptake of P an initial set of parameters is required, which represents the P concentration, water saturation and root parameters, such as length and radius [161]. Spatial components to represent P and water concentration are added in [159, 160] respectively. The P depletion zone along all roots is captured and this analytical solution for a single ordered root is scaled up to produce an accurate estimate for plant P uptake per soil surface area [161]; extrapolating surface area to produce field scale results. The assumption of a constant P concentration with depth is changed to a depth dependent P concentration in [159].

Although alternative models have been developed to investigate the influence of root architecture on plant P acquisition [54, 60, 107], these studies followed a detailed 3 dimensional approach [108] that presents difficulties with up-scaling to the field level [163]. A review of the current 3 dimensional models is well described in [44] providing strengths and weaknesses of each approach.

Crop Models

Statistical data based models (descriptive models) have been developed for crop growth, by scientists at Wageningen starting in the 1960's, by modelling the photosynthetic rate of crop canopies [36]. The static model in [36] was used to estimate potential food production for different areas within the world. Following this, in 1970 an Elementary CROp growth Simulator (ELCROS) was created which included the static photosynthesis model and added the effect of crop respiration being related to a fraction of the total biomass [37]. With the addition of micrometeorology, models could better predict transpiration and in 1978 the BAsic CROp growth Simulator (BACROS) was created [38]. BACROS is used as a reference model for further simulation models created at Wageningen, for example to

create a summary model called the Simple and Universal CROp growth Simulator (SUCROS) [194].

A simulation program (SISOL) compares different technical choices to assess the effect of tillage on the soil profile. The SISOL model simulates spatial variation of the soil structure in regards to precision agricultural and climate effects. In addition, the SISOL model has been validated with over 7 years of field studies on loamy soils [158].

Models used to describe the behaviour of a field, or fields owned by a farmer are useful for local decisions, however larger scale models are required to understand behaviour on a global scale. The ability to use these larger scale models, such as General Circulation Models (GCMs), has improved models for crop growth, as extra data enables more accurate predictions [119].

Conclusion

By simulating plant P uptake by a growing root system using mathematical models it is possible to capture many more scenarios, in less time and at significantly lower costs, than via experimentation. However, experimentation is essential to provide validation and parameters for models. In this thesis experimental data and model simulations are brought together to further advance the understanding of P uptake by plant root systems. Optimisation algorithms are used to further synthesise new knowledge from the models and to maximise the usage of the collected data.

The models presented by Roose in the literature [159, 160, 161] describing water and P uptake into plants and movement through soil, have been adapted and extended for use in this thesis. In order of progression we match Chapters to published work; Chapter 2 to [161], Chapter 3 to [160] and Chapters 4 and C to [159].

1.3 Background to Operational Research Techniques

In this Section we provide a background about operational research techniques and how they are applicable to solve certain practical problems. In addition, we outline and describe algorithms used within the thesis to provide context to the paper based Chapters.

1.3.1 Introduction

Operational research is a discipline that uses advanced analytical methods to help make better decisions. This might relate to finding a better solution for a problem (lower cost) or predicting what may happen to a commodity in the future (forecasting). The advanced analytical methods are generally in the form of algorithms which are used to find the optimal solution of a problem. The main properties of an algorithm include, the run time, convergence and function calls. These properties are different between algorithms, with each algorithm having its own strengths and weaknesses for certain types of problem. For a non-trivial problem, picking the 'best' algorithm increases the chance of finding an optimal solution given desired constraints.

An optimisation problem is generally of the form,

$$\begin{aligned} &\text{minimise} && f(x_1, x_2, ..., x_n) \\ &\text{subject to} && g_i(\mathbf{x}) \leq 0,\ i = 1, \ldots, n_{ic} \\ &&& h_i(\mathbf{x}) = 0,\ i = 1, \ldots, n_{ec}, \end{aligned} \tag{1.3.1}$$

for an objective function $f(\mathbf{x})$, with n variables, n_{ic} inequality constraints $g(\mathbf{x})$, and n_{ec} equality constraints $h(\mathbf{x})$. The type of variables used can either be integer, continuous or mixed depending on the problem, however in this thesis we will only

look at the most common type which is continuous. We only consider non-linear optimisation problems as the differential equation style models used within this thesis produce non-linear objective functions. In addition, the differential equation style models use only 'box constraints', where each variable is bounded. We will therefore now discuss unconstrained optimisation problems.

Non-linear unconstrained optimisation methods can be split into two categories, local and global optimisation methods. Local optimisation methods, or decent methods, can be categorised further into zero-, first- or second-order methods. Zero-order methods do not use any derivatives of the objective function throughout the optimisation process, for example Simplex search [127], Hooke and Jeeves method [2] and a Conjugate Direction method [148]. First-order methods take first-order derivatives of the objective function throughout the optimisation process, for example Gradient Descent [64], Quasi-Newtons method [39] and a Conjugate Gradient method [57]. As it follows, second-order methods use second-order derivatives throughout the optimisation process, for example Newtons method [8], a trust-region method [23] and Levenberg-Marquardts method [122]. The ability to use more information from the objective function generally improves, but slows down the optimisation process. Derivatives give an indication of how far to search in a possible optimal direction. Local optimisation methods however, converge to local optima and do not necessarily perform well on the global scale, heavily relying on good initial starting points. For non-linear objective functions, where there are many local optimal points, local search algorithms tend to perform worse than global search algorithms.

Global optimisation methods can be split into two types, deterministic and stochastic. Deterministic methods involve no element of randomness and therefore any change to the optimal solution comes from different initial starting points or parameters set at the beginning of the optimisation process. Deterministic

global optimisation algorithms include Lipschitz optimisation ideas [172], covering methods that iteratively tighten bounds on the global solution [65] and generalised descent methods where local optima are penalised to encourage global search [25]. Stochastic global algorithms include clustering methods [186], random search methods, for example simulated annealing [1] and genetic algorithms [143], and methods based on stochastic models, for example Bayesian methods [120], and Kriging [50] which in addition, approximates the objective function.

There are many algorithms available for use in global optimisation each having advantages and disadvantages for different types of problem. Models range from having cheap to expensive objective functions, where the number of function calls from an algorithm can become an issue. Expensive objective functions in combination with a large number of function calls makes certain algorithms unusable. A major concern with global optimisation is the number of variables used within a model, where the greater the number, the bigger the search space and less likely that optimal points will be found within a reasonable computational time. For problems with a large number of variables, approximations to models can be made which sacrifice accuracy for speed.

In Section 1.3.2 we describe how initial starting points are chosen and how they are used for a variety of different algorithms. In Section 1.3.3 we provide details of global algorithms including Lipschitz Optimisation, Genetic Algorithms, Multi-Start Nelder-Mead and Kriging. Finally, in Section 1.3.4 we explain how to handle problems that have more than one objective function.

1.3.2 Initial Sampling Methods

When trying to cover a search space (landscape) with a set of sample points, the higher the dimension the greater number of points are needed for the same resolution. The curse of dimensionality limits the potential power of an algorithm

and as such models are reduced down to a minimum number of variables. Increasing the number of variables exponentially increases the search space. Having n variables each with size a predictions, creates a search space of a^n.

Two basic steps to follow for a global optimisation problem are, where to start sampling (initial sampling methods) and once started, how to continue until optimal parameter values have been found (using an algorithm). The design of experiments (DOE) is the term used to describe the initial selection of parameters to be input into the model. This can be at one point or a set of points depending on the algorithm. However, which are the best starting points: the corners, the middle, a random point? The starting point for a given algorithm can be critical to its success, as getting stuck in local optima often happens. We describe three methods to show the process of how to find initial starting points, where some of these methods involve taking pseudo random numbers [55, 99].

There are many ways of sampling an n-dimensional space, including methods that use uniform points and/or randomly distributed points. Higher dimensions are harder to visualise so for a proof of concept we will only display sampling techniques in 2D and 3D. Randomly distributing points is an intuitive way to initially sample an n-dimensional space and implementation is not difficult, Figure 1.1. The main problem with a random distribution is that there are large spaces of un-sampled areas as well as areas with a high distribution of points. As the goal is to evenly cover the search space, these are not the ideal starting set of points. Uniform sampling is another method which evenly covers an n-dimensional space and will not produce a dense cluster of points. However, the rigid structure of the sampling points causes large planes of un-sampled areas. An objective function with a repeating pattern at certain intervals between the uniform points, would be missed by this set of sample points. In addition, the points do not project an even distribution in each direction (variable). A more advanced technique using

a space filling maximin Latin Hyper Cube (LHC) [84, 116, 124], tries to fill an n-dimensional space with points such that it maximises the minimum distance between them [50, 79]. The Latin hyper cube method is an extension of a Latin square, where for each n-dimension every column and row has a permutation of $1, 2, ..., n$. For a given n-dimensional space we look for the Latin square/hypercube where the minimum distance between two points is maximised (maximin). This provides a projection of each variable in each dimension and attempts to cover the search space evenly. Due to the large number of possible Latin squares, an evolutionary search algorithm is used to find this best solution, or a near best approximation.

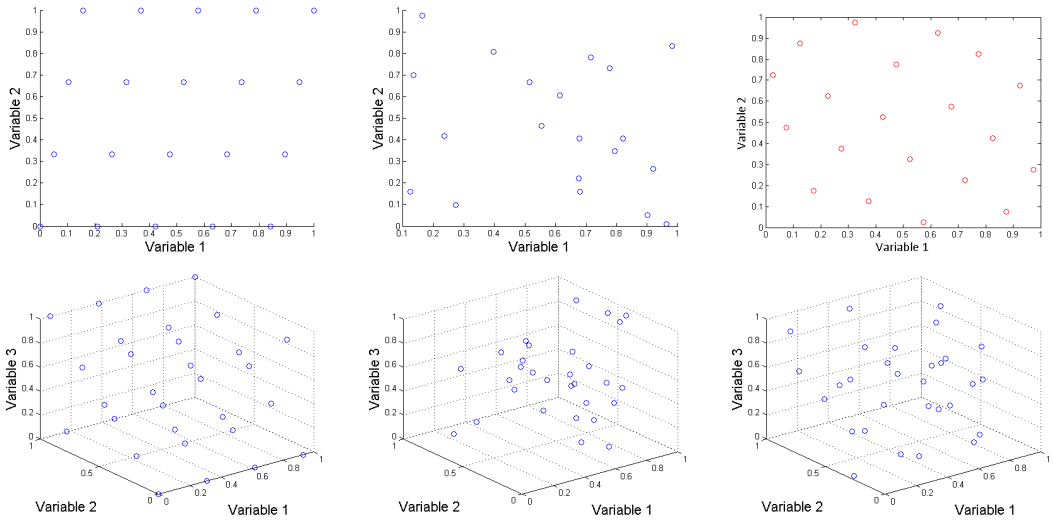

Figure 1.1: A diagram of initial sample plans, from left to right, for uniform, pseduo-random and Latin Hyper Cube techniques in 2 (top) and 3 (bottom) dimensions.

1.3.3 Global Algorithms

There are many global optimisation algorithms for solving non-linear models with one objective value. We look more closely at three types, a deterministic method (Lipschitz Optimisation), stochastic methods (Genetic Algorithms and

Multi-Start Nelder-Mead) and an approximation method (Kriging), and address their strengths and weakness for such problems.

Deterministic Methods - Lipschitz Optimisation

There are a number of deterministic methods for global optimization and we will address one of them, Lipschitz Optimisation, which is 'a sequential method seeking the global maximum of a function' [172]. To perform Lipschitz Optimisation we must first assume knowledge of a Lipschitz constant (K) which is a bound on the rate of change of the objective function. The idea behind Lipschitz Optimisation is to bound a function and then try to continuously tighten the bounds until the function is detailed enough that estimates for optimal points are satisfactory. Many advances have been made from this initial idea, so first we shall describe Lipschitz Optimisation (Shubert's algorithm) and follow with advances made to the original algorithm (namely, DIRECT search).

A function $f : D_H \subseteq \Re^d \rightarrow \Re$ is called Lipschitz-continuous if there exists a positive constant $K \in \Re^+$ such that,

$$|f(x) - f(x')| \leq K|x - x'|, \ \forall x, x' \in D_H. \tag{1.3.2}$$

For example, in 1D problems for a function $f(x)$ with lower and upper bounds x_l and x_u respectively, $x \in [x_l, x_u]$, we have

$$f(x) \geq f(x_l) - K(x - x_l), \tag{1.3.3}$$

$$f(x) \geq f(x_u) + K(x - x_u), \tag{1.3.4}$$

$$X(x_l, x_u, f, k) = \frac{x_l + x_u}{2} + \frac{f(x_l) - f(x_u)}{2K}, \tag{1.3.5}$$

$$B(x_l, x_u, f, k) = \frac{f(x_l) + f(x_u)}{2} - \frac{K(x_u - x_l)}{2}. \tag{1.3.6}$$

Equations (1.3.5) and (1.3.6) form the basis of Shubert's algorithm [172]. We start by computing the lower and upper limits (x_l and x_u respectively) of a function $f(x)$ and compute the value of X and B as in Equations (1.3.5) and (1.3.6) respectively, Figure 1.2.

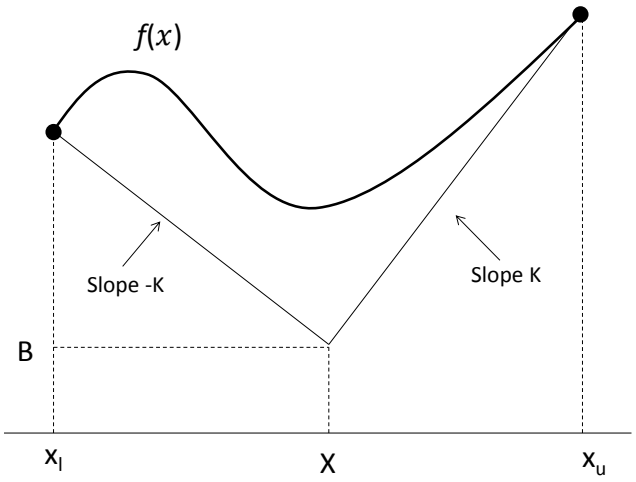

Figure 1.2: The initial set up for Shubert's algorithm in 1D, for a function $f(x)$ bounded by x_l and x_u.

The first point $x_1 = X(x_l, x_u, f, K)$ is computed with the objective function and divides the search space into two intervals, $[x_l, x_1]$ and $[x_1, x_u]$. Each interval is searched for the one with the lowest B value, which in the first iteration is the same. To settle ties a lower bound is chosen $x_2 = X(x_l, x_1, f, K)$ which divides the search space into three intervals, $[x_l, x_2]$, $[x_2, x_1]$ and $[x_1, x_u]$. This process is repeated until the minimum value of B is within a prespecified tolerance of the current optimal solution.

Shubert's algorithm is a deterministic global search which means there is no need for additional runs. There are few parameters and only K needs to be known, i.e., there is no need for fine tuning. The Lipschitz constant K gives a bound on

the error which means the algorithm does not need to rely on the number of iterations as a stopping condition. The disadvantages of Shuberts's algorithm is that finding K can be difficult for some problem types. In addition, the algorithm scales badly and the speed of convergence is slow as it has to evaluate all the corners. A larger value of K results in a more global search but leads to a slower convergence, and as K is a bound on the rate of change it is generally set quite high.

The DIRECT algorithm is an improvement on Shubert's algorithm as it reduces the number of function calls and more importantly removes the need to have a known Lipschitz constant [87]. To reduce the number of function calls the DIRECT algorithm evaluates points at the centre of each variable rather than at the end points. This requires a new set of equations for calculating which points to pick in each iteration and to check that the initial bound is satisfied for a given function.

For a 1D problem with a function $f(x)$ bounded by x_l and x_u, we find a centre point $x_m = (x_l + x_u)/2$. The function $f(x)$ must now satisfy,

$$f(x) \geq f(x_m) + K(x - x_m), \text{ for } x \leq x_m, \tag{1.3.7}$$

$$f(x) \geq f(x_m) - K(x - x_m), \text{ for } x \geq x_m, \tag{1.3.8}$$

which means that there is a weak lower bound of the function at $f(x_m) - K(x_u - x_l)/2$. To continue sampling midpoints and cutting the search space in half, the two new intervals ($[x_u, x_m]$ and $[x_m, x_u]$) are cut into thirds, sampling the third cut furtherest from x_m. Suppose a number of intervals have now been made $[x_{li}, x_{ui}], i = 1, \ldots, m$, and the midpoints have been calculated by the objective function. To choose which interval to sample next, a graph is drawn of $f(x_m)$ against $(x_u - x_l)/2$, for all points sampled. A pareto front is drawn through the

'best' sample points, and the slope between these points is calculated, resulting in different values for K.

This methods allows the sampling of all 'potentially optimal' intervals and continues by selecting one of the points from the pareto front. The centre points are calculated as described above and the algorithm continues its iteration. The 1D DIRECT algorithm is a modified Shubert's algorithm because it samples centre points and considers all potentially optimal intervals during an iteration. If the Lipschitz constant is known then a lower bound can be placed on the function and the search can stop within some tolerance of the current optimal solution.

To extend the DIRECT algorithm into multiple dimensions it is first assumed that every variable has a lower bound of 0 and an upper bound of 1, reducing the search space into an n-dimensional unit hypercube (essentially non-dimensionalisation). The DIRECT algorithm starts by sampling the points $x_m \pm \delta e_i,\ i = 1, \ldots, n$, where x_m the is centre of the hypercube, δ is a third of the side length of the hypercube, and e_i is the ith unit vector. These points $(x_m \pm \delta e_i)$ split the hypercube into a collection of hypercubes and hyperrectangles, where the 'best' points are given the largest splitting. This encourages the algorithm to search near points with good objective functions, increasing emphasis on local search. When dividing the rectangles only the long dimension is considered, ensuring that rectangles shrink on every iteration. The rest of the algorithm is similar to the 1D case where initially the centre is sampled. In each iteration we identify the potentially optimal hyper-rectangles, sample a midpoint and repeat, until a set number of iterations are completed or the given stopping criteria is met.

The global convergence of the DIRECT algorithm is guaranteed for a continuous function, due to the fact that, as the iteration number tends to infinity, the number of iterations within a subset of the unit hypercube become dense. There-

fore at any given point x, in the unit hypercube, and any $\delta > 0$, the DIRECT algorithm will eventually sample a point within a distance δ of x [87].

The main strength of the DIRECT algorithm is not requiring a known value for the Lipschitz constant, instead searching with all possible values. It was created to solve global optimisation problems with bound constraints [48]. The algorithm can operate in a high dimensional space, is derivative free, deterministic, and is most effective for low dimensions requiring relatively few function evaluations for six dimensions [87].

A review of other derivative-free deterministic global optimisation methods can be found in [157], in which other partitioning methods are described, such as Multilevel Coordinate Search (MCS) [78] and Branch-and-Bound (BB) search [147].

Stochastic Methods - Genetic Algorithms

Genetic Algorithms (GAs) have been around since the early 1960s and are adaptive heuristic search algorithms based on the ideas of evolution and Charles Darwin's principle of "survival of the fittest". The idea of a GA is to take a population of individuals and rank them by their fitness. Each member of the population has a binary string which represents a solution for a given model. Through some selective process, the 'best' individuals (parents) reproduce and create a new population (children) which will have similar traits (solutions). The child population is mutated to maintain diversity and unique individuals, such as in evolution. This mutated child population is then evaluated and ordered by fitness and the iteration continues. Stopping conditions for a GA consist of: a solution satisfying the minimum criteria, a fixed number of generations has been reached or time taken, the best solution has not improved after a certain number of iterations and/or by manual inspection to stop the code and taking the current best solution.

The initial population can be taken from a Latin Hypercube as explained in Section 1.3.2 and evaluation of the individuals just means computing the objective function of a model for the individual's parameter values. The main processes involved within a GA are selection (which parents should be chosen) and crossover (how to make the children from the parents). There is no known 'best' method for selection and crossover, each method provides different advantages.

The idea of selection is to pick the best individuals from the current population such that their good traits can be passed onto the next generation, producing fitter individuals. There are a number of traditional mechanisms for selection including, proportionate selection (Roulette wheel), ranking selection (truncation) and tournament selection [174], and these will be discussed below.

A popular method from proportionate selection is to use Roulette wheel selection [75], where individuals have a proportion of a roulette wheel associated with them based on their fitness. Individuals are randomly chosen to become parents based on their proportion. This is done by calculating the cumulative fitness of all individuals (TOT_f) and then computing the individuals' probability of selection (p_{sel}), which is their actual fitness (f) divided by the cumulative fitness, i.e. $p_{sel} = f/TOT_f$. The number of individuals (n) selected usually equals the current population size.

A common ranking selection method is truncation selection, where a proportion of the population ($0 < p \leq 1$) of the fittest individuals are selected and reproduced $1/p$ times, producing a new population of equal size. This method is quite basic and by only keeping the best individuals a very elitist population can arise.

Finally tournament selection is a method where two individuals are chosen at random and the fitter of the two is selected to be a parent with a given probability ($0.5 < p \leq 1$). This method can be extended for a given number of winners in

any size tournament.

The population size between each iteration is generally kept constant, this can avoid confusion and keep it easy to track the progress within each iteration. However, it has been shown that starting with a large population and decreasing to a small population compared to a constant size population (where the average population size is the same) can be beneficial. This is because greater information at the start of the algorithm provides a better initial signal for the GA evolution process [63].

The main difference between the selection methods is the diversity of the selected population. If selection is very elitist (only picking from the very best individuals) then the GA generally converges quicker, but sacrificing diversity means potentially converging on local optima. If selection is more general (weak members are allowed a chance to be selected) then the GA will converge slowly, but having too high a diversity means the GA could never converge as there needs to be a drive towards reaching an optimal solution. A balance is needed between diversity and convergence, and depending on the landscape of a given problem, some methods work better than others. Elitist picking is best if there are few local optima, whereas a more general selection is best for multiple local optima and/or noisy landscapes.

There are a number of crossover techniques that are used to create the child population, and they generally require two parents to create two children. Methods include single-point crossover, 2-point crossover, multi-point crossover, variable to variable crossover and uniform crossover [69].

Single point crossover takes two binary strings (two chosen parents) and randomly chooses one point as a crossover marker. Child one is made from the first part of parent one and the second part of parent two. Child two is made from the first part of parent two and the second part from parent one. Two- and multi-

point cross over work in the same way but with more crossover points, each time swapping between parent one and parent two.

Variable to variable crossover is used when the binary string of the parents can be separated into sub-strings. This can happen for a problem with more than one variable, as each variable is converted into a binary string. Single-point crossover is then used on each variable (sub-string) to create two children as before. This means that each design variable is more likely to change as they are being targeted separately.

Finally uniform crossover uses a different approach where a randomly created binary string of equal length to a parent is created (a mask). If the mask has a 1 then the child's binary digit for that gene is taken from parent one, if it is a 0 then the gene is taken from parent two. The opposite of the mask can be used to create a second child or a new random mask can be generated.

The number of crossover points determines how the GA searches, fewer crossover points encourages exploitation (local search), whereas uniform crossover encourages exploration (global search).

The child population is mutated before beginning the next iteration. Mutation helps to provide diversity within the population which stops early convergence at local optima. The mutation rate is usually equal to one over the binary string length, resulting in one gene being changed per individual on average. Mutation rates that are too high result in evolution having little effect and the GA becomes a random search algorithm; mutation rates that are too low can result in early convergence.

GAs use a lot of function calls due to each iteration generating a new population which has to be evaluated. GAs are partially useful in problems that are non-differential, non-continuous and multidimensional and are easy to implement. Difficulties occur when using GAs on constrained optimisation problems as check-

ing feasible solutions are not part of the algorithmic process. Tricks that 'repair' or 'mend' a gene sequence have to be implemented to keep feasible solutions which add to the computational time and in some cases are impossible. GAs have no guarantee of finding the optimal solution and bounds on the computational time are difficult, which limits their use in real time applications.

Stochastic Methods - Multi-Start Nelder-Mead

A classic method for multidimensional optimisation was developed in 1965 by Nelder and Mead, called the Nelder-Mead algorithm [127]. The Nelder-Mead algorithm is a local optimiser, however by adding a probabilistic restart it can be turned into a global search algorithm. The Nelder-Mead algorithm will be discussed, followed by the addition of the probabilistic restart, which results in the Globalized Bounded Nelder-Mead (GBNM) algorithm [105].

The Nelder-Mead algorithm starts by creating (n+1) vertices for an n-dimensional space. Each point is evaluated and the one with the worst objective value is replaced by a new point which is projected though the midpoint of the current set of vertices. This new point is either created via reflection (x_r in Figure 1.3), contraction (x_c in Figure 1.3) or expansion (x_e in Figure 1.3), or if all these points yield worse values than the current worst, then (n-1) new points are created via shrinkage. This process is then repeated with the updated set of (n+1) points until convergence. Each of the four operations, reflection, expansion, contraction and shrinkage comes with an associated parameter α, γ, ρ and ω respectively. The value of the parameters most used in applications are set from empirical observations, $\alpha = 1, \gamma = 2, \rho = -0.5, \omega = 0.5$. By altering these values the convergence of the Nelder-Mead algorithm changes.

To describe the Nelder-Mead algorithm we set up a minimisation problem for the function $f(y_1, y_2, ..., y_n)$ for n variables (dimensions). A set of parameters in

this space is given by $\mathbf{x}$ which has length n.

- Step 1. Evaluate and order the vertices $f(\mathbf{x}_1) \leq f(\mathbf{x}_2) \leq ... \leq f(\mathbf{x}_{n+1})$.
- Step 2. Calculate $\mathbf{x}_0$ the center of gravity of all points excluding $\mathbf{x}_{n+1}$.
- Step 3. Reflection: Compute the reflected point $\mathbf{x}_r = \mathbf{x}_0 + \alpha(\mathbf{x}_0 - \mathbf{x}_{n+1})$ If $f(\mathbf{x}_1) \leq f(\mathbf{x}_r) < f(\mathbf{x}_n)$ then obtain a new simplex by replacing the worst point $\mathbf{x}_{n+1}$ with the reflected point $\mathbf{x}_r$, and go back to step 1.
- Step 4. Expansion: If $f(\mathbf{x}_r) < f(\mathbf{x}_1)$ then compute the expansion point $\mathbf{x}_e = \mathbf{x}_0 + \gamma(\mathbf{x}_0 - \mathbf{x}_{n+1})$. If $f(\mathbf{x}_e) < f(\mathbf{x}_r)$ then obtain the new simplex by replacing $\mathbf{x}_{n+1}$ with $\mathbf{x}_e$ and go back to step 1, otherwise obtain a new simplex by replacing $\mathbf{x}_{n+1}$ with $\mathbf{x}_r$ and go back to step 1.
- Step 5. Contraction: We must have that $f(\mathbf{x}_r) \geq f(\mathbf{x}_n)$ therefore compute the contraction point $\mathbf{x}_c = \mathbf{x}_0 + \rho(\mathbf{x}_0 - \mathbf{x}_{n+1})$. If $f(\mathbf{x}_c) < f(\mathbf{x}_{n+1})$ then obtain a new simplex by replacing $\mathbf{x}_{n+1}$ with $\mathbf{x}_c$ and go back to step 1.
- Step 6. Shrinkage: We must have that $f(\mathbf{x}_c) \geq f(\mathbf{x}_{n+1})$ therefore compute a new simplex by replacing all points expect the best with $\mathbf{x}_i = \mathbf{x}_1 + \omega(\mathbf{x}_i - \mathbf{x}_1) \forall i \in \{2, ..., n+1\}$ and go back to step 1.

Convergence of the Nelder-Mead algorithm can be set from among: the current best point has not changed for a set number of iterations (flat), iteration number/time taken, and if the rate of improvement has slowed down below a certain threshold (small and/or degenerate). As the algorithm alone is deterministic, the final solution is sensitive to the initial simplex, methods such as multi-start (running the algorithm with different initial start points) can help provide global convergence.

The probabilistic restart is a way of restarting the algorithm if it has found a local optima, allowing it to search a different space with the hope of finding a

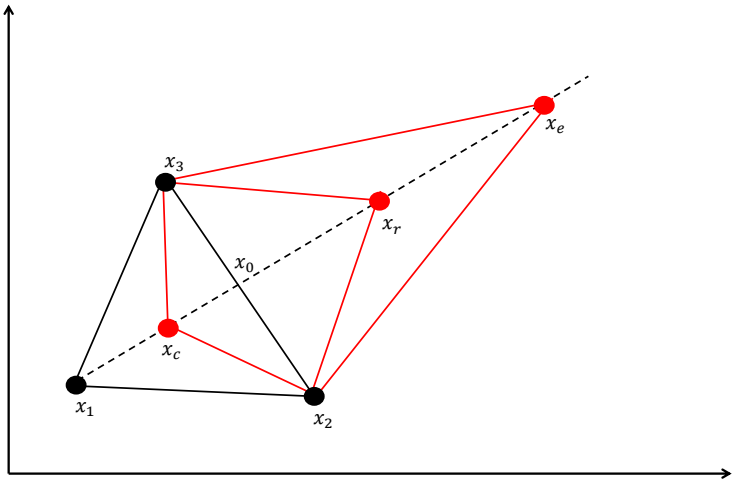

Figure 1.3: Nelder-Mead algorithm selection in 2D for the initial simplex $[\mathbf{x}_1, \mathbf{x}_2, \mathbf{x}_3]$ with a search direction through the mid-point $\mathbf{x}_0$ of the worst two points, for reflection $\mathbf{x}_r$, contraction $\mathbf{x}_c$ and expansion $\mathbf{x}_e$.

better solution. The number of restarts is unknown, as it depends on how the Nelder-Mead algorithm behaves.

The probability ($p(x)$) of having sampled a point x is given by a Gaussian Parzen-windows approach,

$$p(x) = \frac{1}{N} \sum_{i=1}^{N} p_i(x), \tag{1.3.9}$$

where N is the number of sampled points, and p_i is the normal multidimensional probability density function,

$$p_i(x) = \frac{1}{(2\pi)^{n/2}(det(\sum))^{1/2}} \cdot exp\left(-\frac{1}{2}(x - x_i)^T \sum^{-1} (x - x_i)\right), \tag{1.3.10}$$

where n is the number of variables and $\sum$ is the covariance matrix,

$$\sum = \begin{bmatrix} \sigma_1^2 & & 0 \\ & \ddots & \\ 0 & & \sigma_n^2 \end{bmatrix}, \tag{1.3.11}$$

where the variance (σ_j^2) is given by,

$$\sigma_j^2 = \kappa(x_j^{max} - x_j^{min})^2, \tag{1.3.12}$$

where κ is a positive parameter that governs the length of the Gaussian distributions and x_j^{max} and x_j^{min} are the bounds in the j^{th} direction.

A probability density function integrated over from negative infinity to positive infinity is equal to 1, however as a bounded space is considered (Ω) a bounded probability ($\tilde{p}(x)$) is calculated,

$$\tilde{p}(x) = \frac{p(x)}{M}, \qquad M = \int p(x) dx_\Omega, \tag{1.3.13}$$

such that $\int \tilde{p}(x) dx_\Omega = 1$.

The probability density of sampling a new point ($\phi(x)$) is equal to the probability density of not having sampled x before. An assumption is made such that only the best point x_H of $\tilde{p}(x)$ has zero probability of being sampled in the next iteration. Therefore the probability density of sampling a new point ($\phi(x)$) is given by,

$$\phi(x) = \frac{H - \tilde{p}(x)}{\int (H - \tilde{p}(x)) dx_\Omega}, \quad H = \max_{x \in \Omega} \tilde{p}(x). \tag{1.3.14}$$

The maximum of ϕ is equal to the minimum of p and therefore the parameters influencing p are: the points kept for the calculation of p (x), the number of points used to calculate the maximum of ϕ (N_r) and the parameter effecting

the Gaussian distribution (κ). These three parameters change how the GBNM performs and different values are used for different problems, much like the GA. The probabilistic restart is used when the Nelder-Mead converges for a particular reason, being small, flat or degenerate. A flow chart is presented in [105] (Figure 2 in Luersen) which runs through the algorithm. The GBNM algorithm is good for multi-modal, discontinuous optimisation problems where perhaps a global optimisation algorithm cannot be afforded. It is noted that the GBNM algorithm performs better than an evolutionary algorithm for both numerical cost and accuracy for given engineering problems [105].

Approximation Methods - Kriging

The Kriging algorithm carefully picks each sample point to reduce the number of function calls, and therefore the algorithm is mainly used for engineering systems, where the model's objective function is expensive to compute. In addition, the Kriging algorithm is efficient for small size problems under $20 - 30$ parameters.

The Kriging algorithm uses a set of radial basis functions to estimate a landscape, via a surrogate model, which is used to predict new possible points to sample. The idea is to minimise the number of expensive function evaluations while obtaining the global optimum. The surrogate model created by Kriging is an estimate of the actual objective function and goes through all the points evaluated by the objective function (a kind of interpolation). The Kriging algorithm assumes that the objective function is continuous and smooth. Some noise in the objective function is acceptable, but if this is high then it may need to be filtered or it will affect the performance of the Kriging algorithm, and cause early convergence. The surrogate model is used to search for potentially optimal points. Once a point or set of points are found they are evaluated in the actual objective function. Each point evaluated updates the surrogate model and provides a bet-

ter estimate for the next iteration. The Kriging algorithm uses a set of equations to find optimal points to search for, either locally or globally. There are many derivations of the Kriging procedure, first presented in [94]; however we will step through one below by [50] due to its clear explanation.

The Kriging model assumes that the unknown function $y(x)$ is

$$y(x) = \mu + Z(x), \tag{1.3.15}$$

where x is an n-dimensional vector (n design variables), μ is a constant global model and $Z(x)$ is a local deviation from the global model. The sample points x are interpolated with the Gaussian random function and the correlation between $Z(x_1)$ and $Z(x_2)$ is strongly related to the correlation between x_1 and x_2.

A special weighting distance between points ($d(x_1, x_2)$) is used rather than Euclidean, as the weights are not equal across all design variables,

$$d(x_1, x_2) = \sum_{k=1}^{m} \theta_k |x_{(1,k)} - x_{(2,k)}|^2, \tag{1.3.16}$$

where θ_k, for ($0 \leq \theta_k \leq \inf$), is the k_{th} element of the correlation vector parameter θ. Therefore the correlation between points x_1 and x_2 is,

$$Corr[Z(x_1), Z(x_2)] = exp[-d(x_1, x_2)], \tag{1.3.17}$$

and hence the Kriging prediction ($\hat{y}(x)$, the surrogate model) becomes,

$$\hat{y}(x) = \hat{\mu} + q' R^{-1}(y - \mathbf{1}\hat{\mu}), \tag{1.3.18}$$

where $\hat{\mu}$ is the estimated value of μ, R stands for the n by n matrix whose (i, j) term is $Corr[Z(x_1), Z(x_2)]$, q is a vector whose i_{th} element is $Corr[Z(x), Z(x_i)]$ and y is a vector $[y(x_1), ..., y(x_n)]$.

The unknown parameter θ is estimated by maximising the likelihood function below,

$$ln(\hat{\mu}, \hat{\sigma}^2, \theta) = -\frac{n}{2}ln(2\pi) - \frac{n}{2}ln(\hat{\sigma}^2) - \frac{1}{2}ln(|R|) - \frac{1}{2\hat{\sigma}^2}(y - \mathbf{1}\hat{\mu})'R^{-1}(y - \mathbf{1}\hat{\mu}). \quad (1.3.19)$$

Maximising this function creates an n-dimensional unconstrained non-linear optimisation problem, which can be solved for a given θ, knowing $\hat{\mu}$ and $\hat{\sigma}^2$ in the following forms,

$$\hat{\mu} = \frac{\mathbf{1}'R^{-1}y}{(\mathbf{1}'R^{-1}\mathbf{1})}, \quad (1.3.20)$$

$$\hat{\sigma}^2 = \frac{(y - 1\mu)'R^{-1}(y - 1\mu)}{n}. \quad (1.3.21)$$

The strength of Kriging lies in the fact that it is much quicker to evaluate potentially optimal points on the surrogate model compared with using the actual objective function. Kriging also uses the response of the surface of the surrogate model to determine where potentially optimal points are, thus using the maximum amount of information to carry out the optimisation procedure.

A key benefit of the Kriging algorithm is the ability to estimate the error in its predictions, where the estimated variance for an ordinary Kriging model [165] is

$$s^2(x) = \sigma^2 \left[1 - q'R^{-1}q + \frac{(1 - \mathbf{1}^T R^{-1}q)^2}{\mathbf{1}^T R^{-1}\mathbf{1}}\right], \quad (1.3.22)$$

which allows an estimate for the expected improvement on potentially optimal points found on the surrogate model. A Gaussian distribution is fitted in the space between sampled points to calculate the probability of expected improvement. New points can be picked that either have the best expected improvement (exploration) or just the best minimum (exploitation). A mixture of exploitation and exploration is generally used to converge to the global optimum.

To summarise, the Kriging algorithm takes an initial set of search points to

first construct the surrogate model; this is taken from an initial sampling plan, for example a maximin Latin Hyper cube. Additional points are sampled via two different search methods, exploitation and exploration. Convergence can be set from among: the current best point has not changed for a set number of iterations, iteration number/time taken, if the rate of improvement has slowed down below a certain threshold and/or if the expected improvement is below a certain threshold.

The Kriging algorithm is preferred over the GBNM and GA if the objective function is particularly expensive. The Kriging algorithm can also be used on cheap functions, but time is wasted on choosing search points rather than actually evaluating the objective function.

The models used within this thesis are expensive, solving complex non-linear differential equations, hence the Kriging algorithm is used to solve them. In addition, the Kriging algorithm is efficient for small size problems under $20 - 30$ parameters which also matches the models used within this thesis.

1.3.4 Multi-Objective Optimisation

In most optimisation problems there is more than one objective function that needs to be minimised or maximised, and it can be difficult to choose between them. A weighting can be given to each objective function to convert multiple objection functions into one objective function. For example, for two objective functions $f(x_1, x_2)$ and $g(x_1, x_2)$ for given variables x_1 and x_2, we might combine them and produce one objective function $h(x_1, x_2) = A_1 f(x_1, x_2) + A_2 g(x_1, x_2)$ for weighted parameters A_1 and A_2, where $A_1 = A_2$ gives equal weighting to both objectives. By solving for $h(x_1, x_2)$ for different values of A_1 and A_2 (generally set between 0 and 1) a set of solutions can be obtained, and to visually compare solutions we plot the objective functions ($f(x_1, x_2)$ and $g(x_1, x_2)$) against each other, Figure 1.4. A set of non-dominated solutions can be connected where any

increase in one object function causes a decrease in another objective function. The optimal solution is then chosen from this curve (pareto front) given other criteria. For example, there might be variability among the variables (x_1, x_2) and a small change (e.g. 1%) could alter the objective value in some way beyond the current constraints. Therefore opting for a 'safe' solution is best, keeping the objective functions within satisfactory constraints.

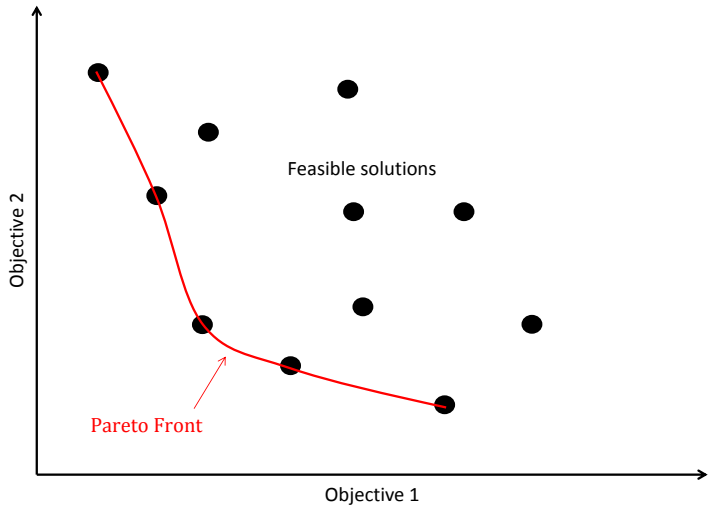

Figure 1.4: A set of solutions for two objective functions highlighting a non-dominated set, called the pareto front.

1.4 Structure of Paper Based Chapters and Declaration of Work

The structure of the thesis follows a paper style format in which each Chapter (2, 3 and 4) is an academic paper of the author, see publications page.

In Chapter 2 we describe how changing the root branching structure of a wheat plant can affect the amount of P taken up by the plant. Experimental work was carried out to validate the model (biological data collection carried out by Pete

Talboys at Bangor University) and we found that changing from a linear to an exponential distribution of first order branches (a high number of branches at the top of the soil) improves P uptake by 142% for low P soils. This is however not enough to compensate a drop from, a high P soil to a low P soil (35.5 to 12.5 mg P l^{-1} respectively, using Olsen P index). This paper was written by the author and edited by the co-authors, except for Section 2.3.1 which was written by Pete Talboys and edited by the co-authors. The modelling work was completed by the author and experimental data by Pete Talboys.

In Chapter 3 we describe the movement of water in the soil around a plant root system during a year. The model provides an estimate of the water saturation levels within the soil at different depths, and the uptake of water by the root system. The model was validated using field data, which includes hourly water content values at five different soil depths under a grass/herb cover over one year, to obtain a fully calibrated system for plant water uptake with respect to climate conditions. When compared quantitatively to a simple water balance model, our model achieves a better fit to the experimental data due to the variation of water content with depth. We find that to accurately model the water content levels in the soil profile, the sensitive Van Genuchten soil suction parameter and hydraulic conductivity values need to vary with depth. The Kriging algorithm is used here to find optimal parameter values which fit the model to the data set. This paper was written by the author and edited by the co-authors. The base code from [160] was written by Konstantinos Zygalakis and adapted and changed heavily by the author to enable simulation on Southampton's super computer, Iridis. Experimental data was taken from [175], carried out by Joel Smethurst.

In Chapter 4 we present a model for different fertiliser strategies to find which one maximises total P taken up by the plant. The model represents the development of P and water profiles within the soil as spatial systems. Current cultivation

techniques such as ploughing and a reduced till gradient are simulated along with fertiliser options to feed the top soil or below the seed. We find that a well-mixed soil (inverted and 25 cm ploughing) is critical for optimal P uptake and provides the best environment for the root system for a given crop cycle. This paper was written by the author and edited by the co-authors except for Section 4.3.4 which was written by the co-authors and edited by the author. The base code from [159] was written by Konstantinos Zygalakis and adapted and changed heavily, similar to the model in Chapter 3. The experimental work was carried out by Pete Talboys, field trial data was taken from Roger Sylvester-Bradley (ADAS) and Robin Walker (SRUC), and fertiliser and soil management strategies were guided by David Langton (Agrii).

In Chapter 5 we provide a summary of all the work included in the thesis, what was learnt and avenues for future progress, written solely by the author.

Notation list for Chapter 2

A	Maximum branching density distribution
a	Root radius
B	Strength of exponential root branching
b	Soil buffer power
c	P concentration in pore water
c_s	P held on the sold phase
c_{tot}	Total P in soil
D	Diffusion coefficient of nutrient in pore water
d	Denotes solution culture and soil systems
d_i	Length of final branching zone
F_D	Flux of nutrients
F_m	Maximum rate of P uptake
G	Number of roots per cm
K_i	The ith-order root length
K_m	Michaelis constant
L_i	Order i root growth rate
l	Current root length
l_a	Non-branching zone at the bottom of the root
l_b	Non-branching zone at the top of the root
l_n	Root branching interval
l_{ni}	Distance between 2 root hairs of order i
N_i	Total number of roots of order i
P	Phosphate
P	Probability
P_{sol}	Available P measured by Olsen $NaHCO_3$ extract method
r_i	Order i initial root growth rate
t	Time
t_2	Two-tailed t-test value
t_D	Time in days
α	Measure of effect of root hairs
γ	Euler's constant
ρ_b	Soil bulk density
ψ	Soil volumetric water content

Table 1.2: Notation list for Chapter 2.

Chapter 2

How changing root system architecture can help tackle a reduction in soil phosphate (P) levels for better plant P acquisition

J. Heppell[1,2,3,4], P. Talboys[6], S. Payvandi[5,4], K. C. Zygalakis[2,4], J. Fliege[3], P. J. A. Withers[6], D. L. Jones[6] T. Roose[5,4]

[1]Institute for Complex Systems Simulation, [2]Mathematical Sciences, Faculty of Social and Human Sciences, [3]Centre of Operational Research, Management Sciences and Information Systems, [4]IFLS Crop Systems Engineering, [5]Faculty of Engineering and the Environment, University of Southampton, Southampton and [6]School of Environment, Natural Resources and Geography, University of Bangor, Bangor 57 2UW, UK

2.1 Abstract

The readily available global rock phosphate (P) reserves may run out within the next $50 - 130$ years, causing soils to have a reduced P concentration which will affect plant P uptake. Using a combination of mathematical modelling and experimental data we investigated potential plant-based options for optimising crop P uptake in reduced soil P environments.

By varying the P concentration within a well-mixed agricultural soil, for high

and low P (35.5 to 12.5 mg l^{-1} respectively, using Olsens P index), we investigated branching distributions within a wheat root system that maximise P uptake.

Changing the root branching distribution from linear (evenly spaced branches) to strongly exponential (a greater number of branches at the top of the soil), improves P uptake by 142% for low P soils when root mass is kept constant between simulations. This causes the roots to emerge earlier and mimics topsoil foraging. Manipulating root branching patterns, to maximise P uptake, is not enough on its own to overcome the drop in soil P from high to low P. Further mechanisms have to be considered to fully understand the impact of P reduction on plant development.

2.2 Introduction

Fertiliser prices are continuing to increase, following a dramatic rise and fall in 2008. The increased volatility in the price of nutrients is linked to the price of oil, and doubt about the limitation of rock P availability in the medium term, maybe outweighed by limitations in energy and sulphur to process rock phosphate. Further, there have been repeated and increasing warnings stating that the readily available global rock phosphate (P) reserves will become exhausted within the next 50-130 years [32, 35]. Therefore careful use of this finite resource in agricultural systems is clearly warranted [191]. This need to reduce our reliance on rock P may also become exacerbated by political control as the remaining reserves are highly spatially localised, being mainly owned by China, Morocco and the US, who together control 85% of the known global phosphorus reserves [47].

P is typically applied in large quantities in most productive cropping systems (>20 kg P ha^{-1}), however, it is often used inefficiently with a large proportion of the added P subsequently becoming unavailable for plant P uptake or lost alto-

gether. To achieve greater sustainability within agriculture requires new strategies that will either reduce the P demand of the crop or promote greater root recovery of the added P such that less fertiliser is required [208]. This would reduce the negative aspects of P use in agriculture (e.g. eutrophication) as well as yielding greater economic returns for farmers. Repeated fertilisation over many decades can lead agricultural soils close to, or at, P saturated levels [17]. While this increases organic and readily available P in the soil it also stimulates vertical loss down the soil profile and allows P to be readily released from particles when surface run-off enters freshwaters [68, 179]. One mitigation strategy is therefore to 'run down' soil P reserves by reducing P inputs relative to the amount of P offtake in the crop. To maintain yields, however, necessitates that P is used more efficiently by the crop. It is therefore important to assess how crops will cope under a reduced P environment, and if that is not plausible, determine what plant-based options are available, for adapting to these conditions.

There are many potential strategies to help tackle the reduced P scenario, from changing the plant traits by targeted plant breeding (e.g. reduced seed P content, changes in root architecture), to altering the properties of the soil [106, 196]. Plants are estimated to take up less than 15% of the P added in the soil, and therefore an alternative method involves manipulating the chemistry and biology of the rhizosphere to make more of the added P available to plants [149]. As P is often highly immobile in soil, one method could be to adapt the root system architecture to obtain P more efficiently [73, 204].

Simulating P uptake by a growing root system using mathematical models enables us to capture a multitude of scenarios in less time and at significantly lower costs than via experimentation. However, the experimentation is essential to provide validation and parameters for the model. In this paper experimental data and model simulations are brought together to further advance the understanding

of P uptake by plant root systems. Optimisation algorithms are used to further synthesise new knowledge from the models and to get the most out of the collected data. Although previous models have been developed to investigate the influence of root architecture on plant P acquisition [54, 60, 107], these studies followed a pseudo 3 dimensional approach [108] that presents computational problems in up-scaling to the field level [163]. A review of the current 3D models is well described in [44] providing strengths and weaknesses of each approach. Here we present an alternative approach to modelling P uptake: using an adaptation of the more efficient root system model of [161] to simulate P uptake of a crop on a field scale. This model is comparable to other density based root models [46]. In addition, this model captures the nutrient depletion zone along all roots and scales up an analytical solution for a single-ordered root to produce an accurate estimate for plant P uptake per soil surface area; extrapolating surface area to produce field scale results [161].

Wheat (*Triticum aestivum L.*) is a key crop for global food production, with total worldwide yields for 2012 estimated to be 652.17 Mt [135]. In this study, the increasingly popular winter wheat cultivar variety Gallant was used to provide the root parameters for the model in [161]. This model has been adapted so that different root structural patterns can be simulated and the optimal root branching structure that maximises P uptake determined. To check if a certain root structure will give adequate compensation, the effect of lowering the soil P concentration level will be assessed.

2.3 Materials and Methods

2.3.1 Experimental Collection of Plant Parameters

Plant Root Growth

Given the variability of rooting within crop varieties [178], and the scarcity of studies quoting such basic root system characteristics, our own cultivar specific set of rooting parameters were produced, Table 2.1. In all experiments the soils were passed through a 5 mm sieve before use. All plants were grown in a greenhouse maintained at a minimum of 20^0C, supplied with artificial lighting providing at least 16 h days. Experiments were conducted in the UK winter, therefore the temperature and number of daylight hours rarely exceeded these values.

	Units	0 order root	1^{st} order root	2^{nd} order root
Growth rate	mm d^{-1}	15.83 ± 5.2^a	8.97 ± 2.6^b	4.00*
Inter-root branch distance	mm	n/a	3.64 ± 2.2^a	2.44 ± 1.3^b
Root diameter	mm	0.516 ± 0.090^a	0.229 ± 0.037^b	0.192 ± 0.049^c
Length of no branching zone	mm	43 ± 8^a	12.2 ± 3.4^b	n/a
Tip to root hair distance	mm	0.48 ± 0.15^a	0.0615 ± 0.037^b	0.376 ± 0.20^c
Root angle on lower ordered root	degrees	n/a	60.6 ± 9.0^a	63.8 ± 14.7^a
Number of root hairs on root	cm^{-1}	202 ± 52^a	250 ± 63^b	444 ± 120^c
Root hair length	mm	0.59 ± 0.25^a	0.49 ± 0.13^b	0.43 ± 0.11^c
Length of root	mm	1000**	79	2.8

Table 2.1: Experimental values for nine wheat root characteristics for zero-, first- and second-order roots used in the mathematical modelling of wheat. The only non-significant values are between the root angles for first- and second-order roots. Values represent means ± SD and those bearing the same alphabet are not significantly different within a row. *Result estimated from experimental data which is consistent with [142]. **Result taken from [183].

To measure the physical characteristics of the roots required by the model, seeds were planted to a depth of 1 cm in perspex rhizotrons (30 cm x 30 cm x 1 cm) filled with a Eutric Cambisol sandy clay loam textured soil (Abergwyngregyn, UK) which had a high available P content due to repeated long-term fertilisation (Olsen

P = 33 mg L^{-1} for further details of the soil see [88]). This soil was maintained at 80% water holding capacity by watering three times a week. We used two-dimensional rhizotrons as these have been shown to be representative of basic root architecture for cereal plants growing unconstrained [66]. The rhizotrons were tilted at a 30^0 angle to allow visualisation of the root system and measurement of root attributes: root growth of roots growing along the edge of the rhizotrons were measured by monitoring their progress with a ruler, and visible branching angles were measured using a protractor. It should be noted, however, the short length of the second order roots meant that measurement of their growth rate was not possible using this approach. At 21 d after emergence the plants were harvested. The roots were washed thoroughly by hand in distilled water, floated out on water in transparent plastic trays, and scanned using a flatbed scanner (Epson Perfection 4990 Photo, Epson America, Inc., California, USA). The diameter of each root order was then determined, using WinRhizo® software (Regent Instruments Inc., Québec, Canada). The inter branch distances, non-branching zone lengths and maximum root lengths were then measured manually for each root system using a ruler. To estimate root hair density and average lengths, 1 cm samples from the centre of each of these washed roots were mounted on slides in 50% glycerol and observed using a light microscope (Axioplan 2; Carl Zeiss Ltd, Cambridge, UK). The number of hairs protruding from each cm section of root as seen when mounted on microscope the microscope slide was doubled to account for half the root not being visible, and then used to define the root hair density for each root order. The length of the root hairs in these sections was measured using the microscopes eyepiece graticule, and then the average for each root order was then used to define the root hair lengths in the model.

Rooting Responses to P

A key component of the plant physiological response to P is the variation of root production [42]. To ensure this would be factored into the model, an experiment was designed to measure the difference in rooting characteristics in low and high P soils. Seeds were incubated in aerated de-ionised water overnight at room temperature and then grown on moist tissue paper until the roots reached ≈ 5 cm. This represents the start time in the model. These seedlings were then planted in 50 ml centrifuge tubes each containing 55 g of either Morfa Cambisol (low P, Olsen P = 12.6 mg L^{-1}) or Eutric Cambisol (high P, Olsen P = 33.0 mg L^{-1}) soils (both Abergwyngregyn, UK), maintained at 80% water holding capacity, and kept in a greenhouse (as previously described) for 10 d. Despite this being a small mass of soil, the plant available P supply remains significantly greater than the plants total P demand over such a limited timeframe, Table 2.2. As the model assumes the relationship of soil solution P to sorped P is at equilibrium, it was decided that using a soil high in native P that was already at equilibrium would provide better high-P model fits than applying soluble P fertiliser to a low-P soil, which would then perturb the sorption equilibrium. After 10 d the plants were harvested and the root systems were washed in water to remove the soil, excised from the remainder of the plant, dried to remove surface water with tissue paper and weighed to assess the differences in root mass between low- and high-P soil environments, Table 2.3. The same cultivation method was also used to produce plants with which to measure the impact upon inter-branch distance of order 1 branches in low and high P soils, Table 2.3: the inter-branch distance measured by scanning each root system using the flatbed scanner (Epson Perfection 4990 Photo) and then using the resulting images to measure the distance between each order 1 root branch on the seminal roots of each plant.

Days after sowing (initial root length was between 10 and 15cm over three roots)	0	1	2	4	6	8	10
Low P average uptake (μmol P plant^{-1})	0^a	0.058^a	0.14^a	0.37^a	0.79^a	1.3^a	2.1^a
Standard deviation (μmol P plant^{-1})	n/a	0.19	0.35	0.34	0.37	0.54	0.49
High P average uptake (μmol P plant^{-1})	0^a	0^a	0.12^a	0.70^a	1.5^a	2.1^a	3.2^b
Standard deviation (μmol P plant^{-1})	n/a	0.051	0.28	0.24	0.26	0.12	0.29

Table 2.2: Experimentally derived average P uptake (μmol plant^{-1}) measured over the 10 d growth period after sowing, for high- and low-P soil environments. After 10 d, the P uptake values become significantly different, for a two-tailed test with $P < 0.05$. Means bearing the same alphabet are not significantly different within a column.

	Low P	High P
Average inter-root branching distance (mm)	4.2 ± 2.4^a	3.7 ± 1.7^a
Average root mass (mg per plant)	586 ± 141.7^a	313 ± 117.1^b

Table 2.3: The average inter-root branching distances of first order roots and masses of fresh weight roots for high- and low-P soil environments. The average root mass was significantly different between high and low P, whereas the average inter-root branching distance was not. Values represent means ± SD and those bearing the same alphabet are not significantly different within a row.

Plant P Demand

To estimate plant P demand, wheat seeds were germinated on moist tissue paper until the roots had reached approximately 5 cm after which the seedlings were transferred to pots containing the high-P Eutric Cambisol soil (150 g). Over the next 10 d, plants were sequentially harvested, washed to remove the soil, and dried at 85^0C overnight. The plants were then dry-ashed (550^0C, 16 h), the residue dissolved in 0.5 M HCl and then their P content determined according to the ascorbate/molybdate blue method of Murphy and Riley [126].

Soil tests

The relationship between P in solution (c, mol/l) and P held on the solid phase of soil particles (c_s, mol/kg) is described by the soil buffer power (b),

$$b = dc_{tot}/dc, \tag{2.3.1}$$

for

$$c_{tot} = (c \cdot \psi) + (c_s \cdot \rho_b), \tag{2.3.2}$$

where ψ is the soils volumetric water content ($dm^3\ dm^{-3}$), and ρ_b is the soil bulk density ($kg\ dm^{-3}$).

To determine b (a constant (only when ψ is constant) used within the mathematical model), c_s and c a sorption isotherm was measured [7]. Using varying initial solution concentrations of ^{33}P-labelled KH_2PO_4 (0-1 mM; 1 kBq mL^{-1}, American Radiolabeled Chemicals Inc., USA), 5 mL of P solution was added to 1 g air-dry soil, shaken (200 rpm, 24 h), centrifuged (16000 g, 15 min), the supernatant solution mixed with the liquid scintilant Optiphase 'Hisafe' 3 (Perkin-Elmer, Boston, MA, USA), and ^{33}P concentration (c) measured using a Wallac 1404 a liquid scintillation counter (Perkin-Elmer, Boston, MA, USA). The amount of P sorbed to the solid phase (c_s) was calculated by difference. A Langmuir isotherm was then fitted to the experimental data using SigmaPlot v11 (Systat Software Inc., San Jose, CA) to enable calculation of c, c_s and b for each soil. This was done by using the middle of each Olsen P index band from DEFRA (2010) (Table 2.4) as the total P (c_{tot}) value for high and low P soils. The corresponding c, c_s and b values for that c_{tot} on the Langmuir isotherm were used as the initial conditions in the model, with b remaining fixed throughout the duration of the experiments.

DEFRA agronomic index value	P(mg L^{-1})	P(mmol L^{-1})	P_{sol}=c(μmol L^{-1})
Index 0 (very low P)	$0-9$	$0-0.2903$	$0-12.3$
Index 1 (low P)	$10-15$	$0.3226-0.4839$	$13.7-20.5$
Index 2 (moderate P)	$16-25$	$0.5161-0.8065$	$21.9-34.2$
Index 3 (high P)	$26-45$	$0.8387-1.4516$	$35.6-61.6$

Table 2.4: Relationship between the Department for Environment Food and Rural Affairs (2010) agronomic index values for available soil P measured using the Olsen $NaHCO_3$ extract method and actual levels in the soil and soil solution (P_{sol}). P_{sol} is equivalent to the concentration of nutrients in pore water c and is dependent upon the soil buffer power b and the water saturation (ψ).

Statistics Applied to Experimental Data

To test whether means from experimental data are significantly different to each other a two-tailed t-test was performed, where $P < 0.05$ would yield a positive significance. For two means, x_1 and x_2, with corresponding standard deviations, s_1 and s_2, and sample numbers, n_1 and n_2, Equation (2.3.3) calculates the value of t_2,

$$t_2 = \frac{\bar{x}_1 - \bar{x}_2}{\sqrt{\left(\frac{(n_1-1)s_1^2+(n_2-1)s_2^2}{n_1+n_2-2}\right)\left(\frac{1}{n_1}+\frac{1}{n_2}\right)}}. \tag{2.3.3}$$

The following assumptions are made; there are two independent samples, the data is normally distributed and the samples have the same variance. Once t_2 is known the degrees of freedom (calculated from $(n_1-1)+(n_2-1)$) is needed to produce a P value which is then compared to the confidence interval, 0.05 for 5%. If $P < 0.05$ then the means are significantly difference.

2.3.2 Phosphate Uptake Model

Previous models for nutrient uptake of a single cylindrical root surrounded by an infinite extent of soil have been studied [7, 133], where the nutrient concen-

tration is equal to the farfield nutrient concentration away from the root. Due to nonlinearity in the root nutrient uptake boundary condition, the models were only solved numerically, which meant that adapting a single root model to a more realistic root system was computationally expensive [7, 133]. However, model advancements made it possible to provide a fully explicit 'approximate' analytical solution to the Nye-Tinker-Barber model which enabled a more realistic model that utilises a more complex root branching structure [161, 162]. In all four previous studies [7, 133, 161, 162] the uptake of P by roots is represented by Michaelis-Menten uptake kinetics and a convection-diffusion model containing a linear diffusion equation with a nonlinear root surface uptake condition. The rate of convective transport of nutrients is assumed to be negligible relative to diffusion [91, 161, 162]. For a complete solution of the convection-diffusion equations for P transport to plant roots see [162]. The total uptake of nutrients given an initial set of parameters are calculated in [161], which represent the nutrient concentration, water saturation and root parameters, such as length and radius. The analytical solution for the flux of nutrients $F_D(t;a)$ into a root of radius a in [161] is given by,

$$F_D = \frac{2F_m c}{K_m + c + L + (4cK_m + (K_m - c + L)^2)^{1/2}}, \tag{2.3.4}$$

with,

$$L = \frac{F_m a}{2\psi D} ln\left(1 + 4e^{-\gamma}\frac{\psi D}{(\psi + b)a^2}t_D\right), \tag{2.3.5}$$

where F_m represents the maximum rate of P uptake (μmol cm^{-2} s^{-1}), c is the far field concentration of P in pore water (μmol cm^{-3}), K_m is the Michaelis constant (μmol cm^{-3}), $\gamma \approx 0.5772$ is Eulers constant, ψ is the water saturation (dm^3 solution dm^{-3} soil), D is the diffusion coefficient of nutrient in pore water (cm^2 s^{-1}), b is the soil buffer power (dimensionless) and t_D represents time (days). The values of these parameters, taken from [161], are presented in Table 2.5, and it

is assumed that the farfield concentration of P is constant within the soil. The model calculates the uptake of P for one zero order root (as in Equation (3.13) in [161]), and this is extrapolated to five to account for the number of primary root axes in a developing wheat root system.

Parameter	Description	Value	Unit
ψ	Soil volumetric water content	0.3	L solution L soil^{-1}
D	P diffusion coefficient in pore water	0.3×10^{-5}	cm^2 s^{-1}
b	P buffer power in soil	239	-
F_m	Maximum rate of root P uptake	3.26×10^{-6}	μmol cm^{-2} s^{-1}
γ	Euler's constant	0.5772	-
K_m	Michaelis constant for root P uptake	5.8×10^{-3}	μmol cm^{-3}

Table 2.5: Soil and nutrient uptake parameters, with values and units, taken from [161].

To capture the effect of root hairs on nutrient uptake, we will apply the method of [101] where three different models for nutrient uptake were considered. A dimensionless parameter α is calculated and depending on the morphological and physiological properties of the root hairs 3 scenarios occur. For $\alpha \sim 1$, a concentration gradient dynamically develops within the root hair zone, for $\alpha > 1$, the uptake by root hairs is negligibly small and for $\alpha < 1$, P in the root hair zone is taken up instantaneously. The dimensionless parameter α is given by,

$$\alpha = log_e \left(\frac{dl_{ni}}{DK_m} F_m \right) \Big/ log_e \left(\frac{l_{ni}}{K_i} \right), \tag{2.3.6}$$

where d is dimensionless factor that distinguishes between solution culture and soil systems (in the solution culture $d = 1$; in soil $d = 1/(\psi + b)$), l_{ni} is the distance between two root hairs on the i_{th}-order root (cm) and K_i is the i_{th}-order root length (cm).

The value of α for zero-, first- and second-order roots is $0.466, 0.703$ and 1.477, respectively. For zero- and first-order roots $\alpha < 1$, which means root hairs effectively extend the root radius by the root hair length. For second-order roots $\alpha > 1$, which means the roots hairs have a small uptake compared to the roots and are neglected. Experimental data showed root hairs appearing everywhere on all ordered roots and as a result, increased root radius occurred over the entire root length.

Equation (2.3.4) is used to construct a model for the nutrient uptake of a plant root system. The root system consists of a distribution of roots of radius a and length l. Figure 2.1 shows the layout of the root structure where the top section of the root is labelled l_b and the bottom section l_a, which are the non-branching zones. The main root is called 0 order, side branches of this are called 1^{st} order and so forth. The root system branches by creating smaller side roots between the non-branching zones l_b and l_a, and this starts commencing when the original root reaches the length $l_b + l_a$. Given a root of length l, there are $[(l - l_a - l_b)/l_n]_+$ branches, where l_n is the interval for each branching root.

Different order growing roots will have different radii a_i, and will grow at different rates $L_i(t)$. The elongation of roots of order i decreases with age and is described by,

$$\frac{dl}{dt} = L_i = r_i \left(1 - \frac{l}{K_i}\right), \tag{2.3.7}$$

where l is the length of the root (cm), r_i is the initial rate of growth (cm d^{-1}) and K_i is the i_{th}-order root length (cm).

The model in [161] uses a constant branching rate to define root architecture, thereby creating an even branching distribution. To change the root architecture we replace the constant value by a root branching distribution parameter, which interpolates between an even branching distribution and one which exponentially decreases in root length density down the soil profile. An exponential branching

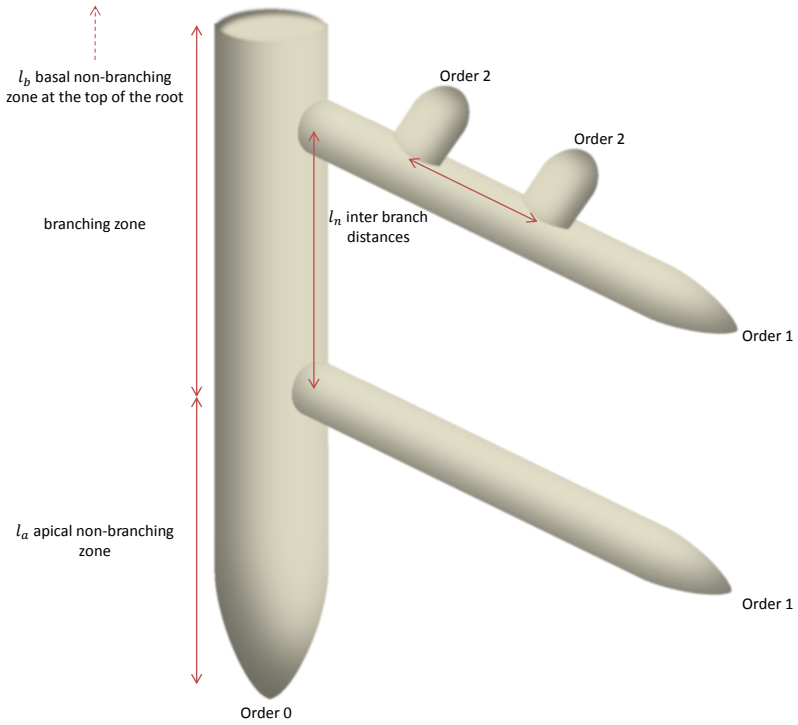

Figure 2.1: Branching structure of a root system, with non-branching zones l_a and l_b, and inter-root branch distance l_n. The main root, order 0, branches order 1 roots which in turn branch order 2 roots.

distribution is used where the same final volume of roots is grown; however, it creates a root system where top soil foraging is maximised [197]. This also matches observations of root proliferation in top soils ($0 - 30$ cm) when fertilisers are strategically placed [114]. The exponential branching distribution (G, the number of roots per cm) is described by,

$$G = Ae^{-Bl}, \tag{2.3.8}$$

where two variables define the branching structure, A (cm^{-1}) denotes the maximum density distribution (i.e. the maximum number per cm) and B (cm^{-1}) denotes how density decays towards the tip of the main root l. For example, at a linear branching distribution of 0.7 cm we set $A = 1/0.7$ cm^{-1} and $B = 0$ cm^{-1}.

The branching points are calculated by first varying l between 0 and d_i, where

d_i is the length of the final branching zone along the main root. Secondly, the total area created by the curve in Equation (2.3.8) from $l = 0$ to $l = d_i$ is calculated. Thirdly, a point l such that the area covered by the curve from $l = 0$ to $l = l_1$ is calculated to be equal to the total area divided by the number of branching roots. The next point l_2 is chosen such that the area created between the two points l_1 and l_2 is the same as between 0 and l_1. Finally, continuing this approach will generate an equal number of branching roots, but the distribution will be exponential rather than linear.

The two-parameter family in Equation (2.3.8) can be reduced to a single parameter if the total final length of the root system is kept the same. This simplifies the fitting process, discussed in Section 2.4.3, as fewer parameters reduce the search space and thus the computational time of the model. The method is described in the set of equations below, which begins with the total number of roots N_i, which are in the length range $(0, d_i)$ for root order i.

$$\int_0^{d_i} Ae^{-Bl} dl = N_i. \tag{2.3.9}$$

Simplifying and solving Equation (2.3.9) for A produces,

$$A = -\frac{N_i B}{e^{-Bd_i} - 1}, \tag{2.3.10}$$

which generates the root branching distribution G that conserves the final size of the root system, just in terms of the new variable B.

$$G = \frac{N_i B}{1 - e^{Bd_i}} e^{-Bl}. \tag{2.3.11}$$

The values of d_i are prescribed to be equal to 100 and 7.9 cm for the main root and order 1 root, respectively, and N_i equal to the number of roots for

each given order calculated from the experimental data presented in Table 2.1. The chosen variable B will be bounded, such that at its minimum, 0 cm^{-1}, the root branching is linear and at its maximum, 10 cm^{-1}, the root branching is exponential and almost all the side roots branch at the top of the branching zone. Figure 2.2 shows the root structure (with only 50 side roots for simplification) for the cases where B is $0, 5$ and 10 cm^{-1} and the different initial branching scenarios can be clearly seen between Figure 2.2a ($B = 0$ cm^{-1}) and Figure 2.2c ($B = 10$ cm^{-1}). The minimum branching distance measured from the experimental data (0.067 cm) was also set as the minimum branching distance in the model, i.e. at the upper bound when $B = 10$ cm^{-1}. As we assume there is a constant P concentration within the soil, every root is therefore given their own depletion zone which does not overlap with others (no inter-root competition) for the entire growth of the root system.

For modelling purposes the growth angles of the roots in our experiments are not used, all other values in Table 2.1 are used in the model. This is due to the fact that the initial P concentration in the soil is constant, and roots will achieve the same uptake from any position; it is therefore sufficient to just calculate the time at which a root started growing. This simplification in the root system is justified by the comparison made in [100], where the P uptake from the roots in the model by [161] was shown to be comparable to the one of a 3D plant root system.

The second-order roots are experimentally shown to grow where the density of root mass is greatest rather than in a linear or exponential distribution. The greatest density of second-order roots on a first-order branch was experimentally calculated to be 1.153 second order roots per mm. Therefore the second-order roots were modelled such that there were a greater number of branches at higher density areas with the greatest density capped at 1.153 roots per mm. This

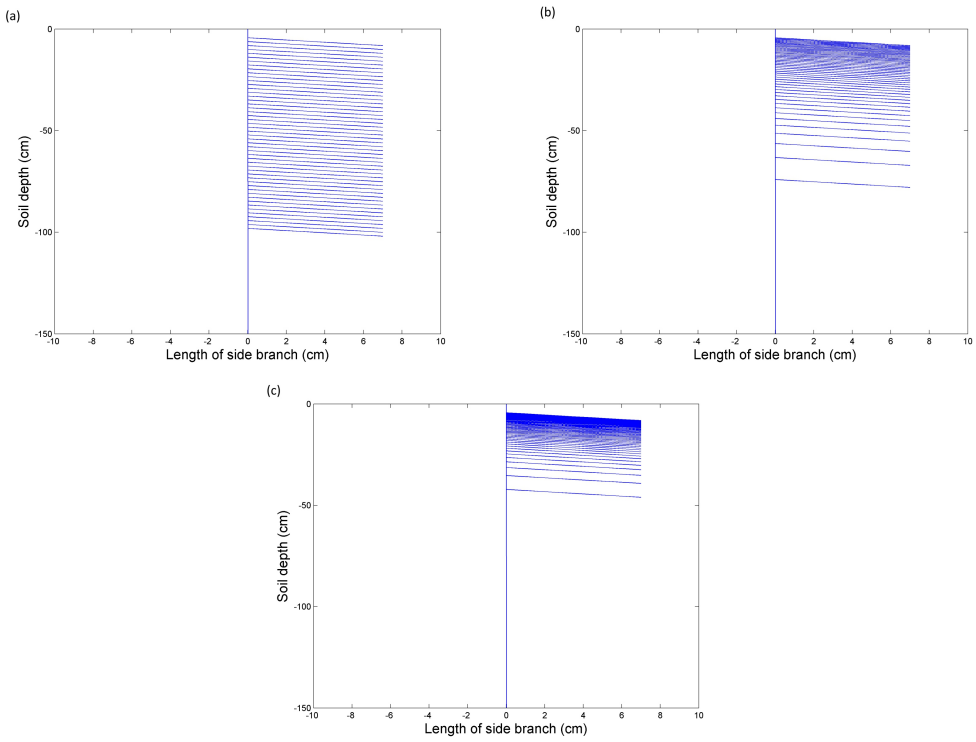

Figure 2.2: The simulated root structure (with only 50 order 1 roots for simplification) for three different branching distributions; (a) shows a linear branching distribution ($B = 0$ cm^{-1}), (b) shows a slight exponential distribution ($B = 5$ cm^{-1}), and (c) shows a strong exponential distribution ($B = 10$ cm^{-1}).

distribution can be seen in Figure 2.3 where the position of the second-order roots is affected by the exponential distribution of the first-order roots. In the linear branching distribution case all of the root branches are constant whereas for the exponential branching distribution case, the majority of second-order roots appear nearer the top of the plant as there is a greater density of roots there.

2.4 Results

2.4.1 Model Parameterisation

The experimentally derived values for wheat root characteristics for zero-, first- and second-order roots are summarised in Table 2.1. Significant differences were apparent for all characteristics for the different root types, except for 'root angle

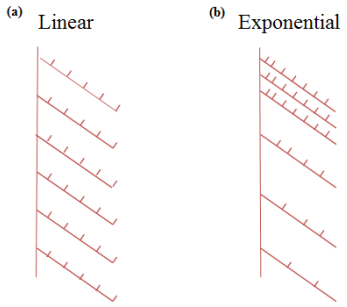

Figure 2.3: The root distribution of order 2 roots; (a) shows the distribution of order 2 roots for a linear branching distribution of order 1 roots, and (b) shows the distribution of order 2 roots for an exponential distribution of order 1 roots. The greater the exponential distribution the denser the order 2 roots become.

on lower ordered root'. We used these values to parameterise the model to estimate the P uptake for different root branching distributions in soil possessing two contrasting P contents, 35.5 mg L^{-1} (high P) and 12.5 mg L^{-1} (low P)(Table 2.4).

Experimental analysis showed that the biomass of roots grown in a low P soil was reduced on average by 45% in 10-day-old plants compared to those grown in a high P soil, and yielded a significant difference ($P < 0.05$; Table 2.3). However, the inter-branch distance for the emergence of first order roots was not significantly greater when the roots were grown in a high P environment ($P > 0.05$; Table 2.3). To capture this P-induced change in root architecture within the model, the simulation scenarios for the low-P soil had the maximum root length for all order roots capped to match the experimental data. To determine the impact of this capping, simulations were undertaken with both reduced and constant root mass. The effects of a reduced root mass could present problems with current plant nutrition strategies, and perhaps placement of nutrients could produce greater yields [152].

2.4.2 Model Simulations

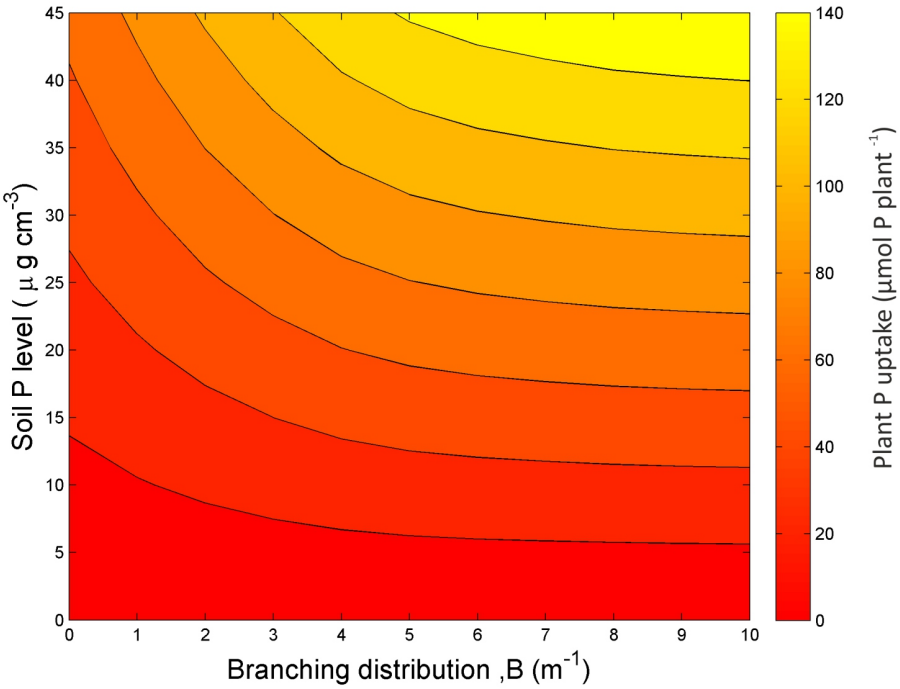

Figure 2.4: Model estimates for whole plant P uptake (μmol P plant^{-1}) for different branching distributions (B) and initial soil P concentrations. At $B = 0$ we have a uniform branching distribution and for increasing values of B we have more concentrated branching at the top of the soil profile.

Figure 2.4 shows the model predictions of plant P uptake across a range of P concentrations within the soil for the different root branching distributions. For a given line of constant branching distribution, there is a linear relationship between P concentration and P uptake ($R^2 = 1$ due to the model being deterministic). However, for the line of constant P concentration, there is non-linear relationship between branching distribution and P uptake.

Three scenarios in particular were studied; a linear branching distribution in a low- and high-P soil and an exponential branching distribution in a low-P soil. For each of these scenarios our model estimated the amount of P uptake by the whole root system, Figure 2.5. In the high-P soil, the model predicted that the plant would acquire 183% more P than a plant grown in the low-P soil. When the

root branching distribution was changed from a linear to an exponential pattern the model predicted that this improved plant P uptake by 142% in the low-P soil. This represents a reduction of 14.5% in comparison with plants grown in a high-P soil with a linear branching pattern.

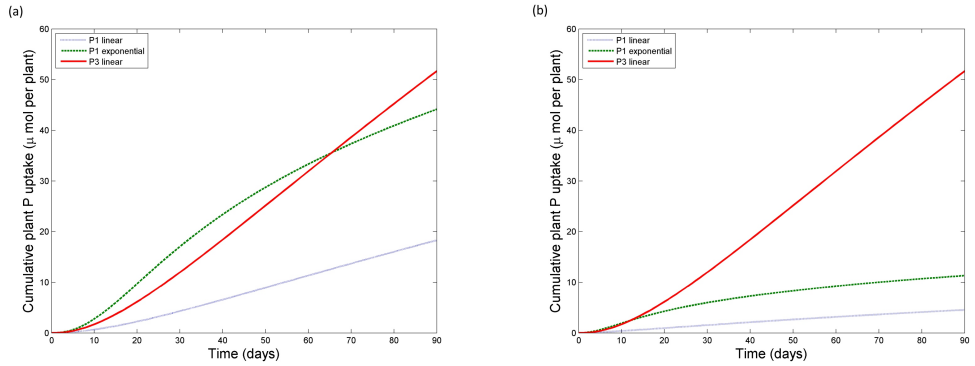

Figure 2.5: Predicted cumulative plant P acquisition for three root branching scenarios, a linear branching distribution in a high- and low-P soil and an exponential branching distribution in a low-P soil; Panel (a) shows P uptake when the final volume of roots is conserved, while panel (b) shows P uptake where there is a 45% reduced root biomass after 10 d for the low P scenarios.

The results for cumulative P uptake for the 3 root branching scenarios over a 90 d crop growth period are shown in Figure 2.5a. The end time of 90 d was chosen as it gave suitable long-term behaviour for wheat growth. For the majority of the time period, up to around 65 d, the exponential branching distribution in a low-P soil (green-dashed) possessed the greatest P uptake even when compared with the linear branching distribution in a high-P soil (red-solid). This is due to the fact that the side roots emerge earlier and therefore there is a greater surface area to enable earlier P uptake. After 65 d, the linear branching distribution in a high-P soil catches up with and overtakes the exponential branching distribution in a low-P soil and can take advantage of the rich P environment. The shape of the P uptake curve is defined by the branching distribution. In both linear root branching examples (red-solid and blue-dotted) there is smooth hinge shape curve, however in the exponential root branching example (green-dashed) a saturation

growth curve is observed, which is expected as the root system grows to its full length.

With the negative effect of reduced root mass in the low-P soil (Figure 2.5b), the difference between the low- and high-P soil was magnified. Plant P uptake for the exponential branching distribution in a low-P soil (green-dashed) fell by 74% compared to when the root system growth was not capped (Figure 2.5a) and matches a linear exponential branching distribution with an effective Olsen P index of 3.7 (39 mg L^{-1}). Changing from a linear to an exponential branching distribution improves P uptake by 151% in the low-P soil, but this is a large decrease of 78% when compared with a high-P soil using a linear branching pattern; which is expected given the large reduction in root mass.

2.4.3 Model Validation and Optimisation

The estimated P uptake from our model was compared with the experimental data collected for a root system grown in a high- and low-P environment (Table 2.2, Figure 2.6). The parameter for the root branching structure, B, was fit to minimise the sum of squares difference between our model and the experimental data. The estimated total plant P uptake fits well with experimental data within the initial 10 d of growth; for the comparisons, high P with $B = 1.5$ cm^{-1} and high P data, and low P with $B = 7$ cm^{-1} and low P data. The scenario for a low-P soil with $B = 7$ cm^{-1} is not enough to capture the effects of the experimental high P uptake, because it is difficult to overcome the 45% reduced root mass and beyond the 10 d mark this difference is amplified.

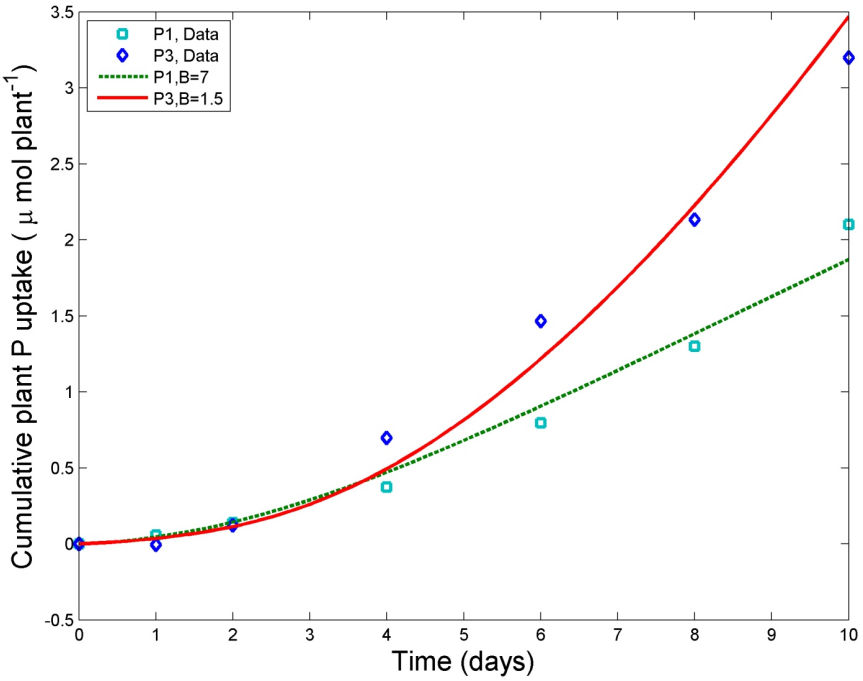

Figure 2.6: Experimental and model values for the cumulative uptake of P by wheat seedlings over a 10 d period when grown in high- and low-P soil for a range of root branching distributions. The model values comprise of, a high-P soil with a weak exponential distribution ($B = 1.5$ cm^{-1}), and a low-P with a strong exponential distribution ($B = 7$ cm^{-1}).

2.5 Discussion

The important question that needs addressing is how alteration of root system architecture could (by breeding or genetic manipulation) produce greater P uptake. To that end, the model in [161] has been adapted by introducing a parameter that changes the root branching distribution. Our model has two parameters that we will directly manipulate, the nutrient concentration in the soil c and the root branching distribution parameter B. By looking at the effect of changing the P level against the root branching distribution, by altering c (Table 2.4) and B, the P uptake is estimated.

Our study estimated the P uptake using our experimental soil and plant parameters found in Table 2.1. Our model is adapted from [161] such that the

branching density distribution is allowed to change from linear to exponential, to see the effects that root structure with different P concentrations in the soil, has on P uptake. Three scenarios were considered, a high and low P concentration level with a linear branching distribution and a low P concentration with an exponential branching distribution. In these scenarios the effect of reduced root mass in low P soils is considered, as seen in our experimental results.

The experimental P uptake (Table 2.2, Figure 2.6) fits best with a weak exponential root branching distribution for P3 data, which can be seen for certain crops. A shift towards increased early lateral rooting has previously been shown experimentally to increase P uptake efficiency [213], and this scenario is successfully captured in the model. The strong exponential branching modelled here is however more aggressive than our data suggests and is currently seen within wheat root developmental plasticity. Perhaps breeding varieties to adopt this rooting strategy would be limited by carbon availability from photosynthesis. Although our model simulates a uniform soil P profile, that top soil foraging has been shown to be an essential component of plant P acquisition [212], provides further emphasis upon the need to produce lateral roots early in the plants growth; helping to improve root-foraging strategies [156]. By modelling a non-uniform soil P profile [159] a better fit to the data could be achieved, given necessary depth dependent data of available soil P. This is the subject of our follow on work which will be published separately.

Our model shows that changing the root structure of the plant, to produce more lateral roots earlier, has a positive effect on the uptake and can help plants survive in lower phosphate environments. This is corroborated by previous experimental approaches [213]. On average a 147% increase in P uptake is achieved from having a highly exponential root branching distribution over a linear one. However this positive increase is not enough to completely overcome the difference

between a high- and low-P soil environment. Therefore, although increasing early lateral root production will enhance P uptake, other plant- and fertiliser-based strategies would be required to produce the required yields at low soil P levels. For example, an increase to all root lengths of all orders in combination with the exponential root branching distribution is sufficient, as only an 8% improvement is needed to match an exponential branching distribution in a low-P soil, with a linear branching distribution in a high-P soil (without accounting for the reduced root mass in a low-P soil).

The exponential branching distribution however does provide greater early P uptake in low-P soils when compared to linear branching root systems grown in high-P, Figure 2.4a. Early growth, and yield size, have been shown to be most significantly correlated with early P uptake levels [16, 20, 59, 62], and greater early P uptake, and the corresponding early vigour seedlings display is also viewed by industry as insurance against problems which may occur in the growing period such as adverse weather conditions. Vigorous early growth also provides quicker soil surface cover, and therefore is useful in the reduction of soil erosion which can be a significant driver of environmental problems, and loss of P from agricultural systems [146]. The diminished uptake that exponential branching in low P displays over linear branching in high P could still potentially impact final yields, where P-uptake from the environment is still required to augment grain filling [15, 59, 121], and also to facilitate carbohydrate translocation into the ripening grain [182]. However, such a small difference in final P uptake could potentially be met by a small targeted application of P late in the growing season, whilst still allowing for significantly lower application rates of P fertiliser than in current systems. The enhanced effectiveness of the exponential branching distribution provides an insight into the potential benefits possible from crop breeding, Figure 2.4a. The extent of the wheat root system already varies significantly between

varieties [178], and plant breeding efforts have been made to use plant breeding to produce cultivars with an enhanced ability to acquire P [53]. Significant improvements in crop growth and output have been demonstrated to be possible from targeted breeding to improve varieties [173], therefore a re-profiling of root branching distribution is potentially possible, and could drive an increase in crop P-acquisition. Additional and more rigorous experiments would need to be undertaken to properly validate possible improved root structures and their effects in high- and low-P soil. Given the variations in root system size present in commercially available wheat varieties [178], a targeted breeding programme has the potential to provide a range of root architectural variations which may prove to be more suited to low-P soils. Furthermore, other parameters from Table 2.1, such as root hair dynamics, could be re-calculated to find possible differences between high- and low-P soils.

Due to the root structure being diminished in a low-P environment we implemented the reduced root mass scenario. The difference between the high- and low-P soils generated a substantial 45% root mass decrease after 10 days which heavily affected the P uptake values in the low-P environment. In a low-P environment, targeting P close to early root growth (seed dressing or placement of fertiliser in bands 5 cm down from seed) is emphasised as even more essential due to the fact that the plants ability to search out P in a low P soil is severely limited by the smaller area of soil the root system can cover.

In this Chapter we provided modelling basics towards the development of whole plant nutrient uptake models, by assessing what root structures are needed for given concentrations of P in the soil to maximise plant P uptake.

Notation list for Chapter 3

a	Zero order root radius	$\mathbf{u}$	Volume flux of water
a_1	First order root radius	W	Volume flux of water into the soil at the surface
a_k	Fourier Transformation Signalling algorithm parameter	WS	Wind Speed
b_k	Fourier Transformation Signalling algorithm parameter	x	Depth
c	Correction constant for estimating water flux	x_i	The i_{th} model data value
D_0	Diffusivity of water in non-saturated soil	$\hat{x}_i$	The i_{th} experimental data value
F_w	Uptake of water by plant roots	y	Objective value for sum of squares equation
g	Gravitational acceleration	z	Depth
H	Humidity	α	Parameter for the linear estimation of W
k	Soil permeability	α_1	Parameter for the non-linear estimation of W
$\hat{\mathbf{k}}$	Unit vector in the downwards direction	α_2	Parameter for the non-linear estimation of W
k_r	Root radial water conductivity parameter	α_3	Parameter for the non-linear estimation of W
K_s	Saturated hydraulic conductivity	β	Parameter for the linear estimation of W
k_s	Water permeability in fully saturated soil	β_1	Parameter for the non-linear estimation of W
k_z	Root axial hydraulic conductivity	β_2	Parameter for the non-linear estimation of W
L	Maximum length of the order 0 root	β_3	Parameter for the non-linear estimation of W
L_1	Maximum length of the order 1 root	γ	Parameter for the linear estimation of W
l_d	Root length density	γ_1	Parameter for the non-linear estimation of W
l_w	The depth at which zero flux occurs	γ_2	Parameter for the non-linear estimation of W
m	Van Genuchten soil suction parameter	γ_3	Parameter for the non-linear estimation of W
N	Number of points	δ	Parameter for the estimation of W
P	Initial water pressure	θ	Volumetric water content
p	Water pressure in the soil	θ_r	Residual water content
p_a	Atmospheric pressure	θ_s	Soil porosity
p_c	Characteristic suction pressure	λ_1	Parameter for the estimate of P
p_r	Root internal xylem pressure	λ_2	Parameter for the estimate of P
p_r^0	Baseline root pressure	λ_3	Parameter for the estimate of P
R	Rainfall	μ	Dynamic viscosity of water
S	Relative water saturation	ρ	Density of water
T	Temperature	ϕ	Angle between zero and main order root
t	Time	ψ_1	Density of first order roots on the zeroth order roots

Table 2.6: Notation list for Chapter 3.

Chapter 3

Validation of a Spatial-Temporal Soil Water Movement and Plant Water Uptake Model

J. Heppell[1,3,4,5], S. Payvandi[2,4], K. C. Zygalakis[3,4,5], J. Smethurst[2], J. Fliege[3,5] and T. Roose[2,4]

[1]Institute for Complex Systems Simulation, University of Southampton, Southampton, UK. [2]Faculty of Engineering and the Environment, University of Southampton, Southampton, UK. [3]CORMSIS, University of Southampton, Southampton, UK. [4]IFLS Crop Systems Engineering, University of Southampton, Southampton, UK. [5]School of Mathematics, University of Southampton, Southampton, UK.

3.1 Abstract

Management and irrigation of plants increasingly relies on accurate mathematical models for the movement of water within unsaturated soils. Current models often use values for water content and soil parameters that are averaged over the soil profile. However, many applications require models to more accurately represent the soil-plant-atmosphere continuum, in particular, water movement and saturation within specific parts of the soil profile. In this paper a mathematical model for water uptake by a plant root system from unsaturated soil is presented. The model provides an estimate of the water content level within the soil at different

depths, and the uptake of water by the root system. The model was validated using field data, which includes hourly water content values at five different soil depths under a grass/herb cover over 1 year, to obtain a fully calibrated system for plant water uptake with respect to climate conditions. When compared quantitatively to a simple water balance model, the proposed model achieves a better fit to the experimental data due to its ability to vary water content with depth. To accurately model the water content in the soil profile, the soil water retention curve and saturated hydraulic conductivity needed to vary with depth.

3.2 Introduction

In the UK, shrink and swell displacements caused by seasonal changes in clay soil water content can cause serviceability problems for vegetated earthworks [5, 134] and exacerbate the progressive failure of clay slopes [198]. Clay shrinkage in dry summers also regularly causes damage to older buildings constructed on shallow foundations [43].

With the onset of global warming, weather systems and in particular rainfall patterns are likely to change. This climatic change will have an impact on plants that interact with engineered structures such as earthworks and shallow foundations [29]. In order to optimise soil water and plant management strategies it is necessary to understand current plant-soil systems and their reactions to varying rainfall and climate patterns.

A number of agronomic models exist that calculate changes in water content within the soil in response to climate and plant water uptake. However, many of these models only estimate the average water saturation level within the plant root zone. Common examples used in agriculture (and to some extent, in engineering, e.g. [29]) include Dassat [89], Apsim [115] and Cropwat [30, 31].

Cropwat carries out a water balance calculation for the rooting zone, determining an average soil saturation which varies in response to rainfall infiltration and plant evapotranspiration, calculated using the Penman-Monteith Equation [3]. Many of these models are adequate for simple crop management and irrigation purposes. However, applications in engineering and agricultural sciences need models to more accurately represent the soil-plant-atmosphere continuum, in particular the water movement and content within specific parts of the soil profile. In engineering, the stability of many embankments and cut slopes is dependent on the presence of soil suctions both within and below the rooting zone, and more advanced models are needed to investigate vegetation management options [21, 104].

A difficulty with trying to model the water content levels at different soil depths is the characterisation of the parameters that control the soil water content and flow processes. Both soil water retention and permeability can be difficult to measure accurately, and there is often little or no site specific data, yet modelling responses can be very sensitive to these parameters [132, 151, 164, 176]. Data on root structures and temporal soil and plant interactions with time can also be sparse. However, there are often good records for water content and climate conditions, which can be used to calibrate models.

In this paper we develop a computational approach to calculate the water content at different depths in the soil based on an extension of the model for water flow and plant water uptake given by [160]. Environmental inputs are added which estimate the water flux into the soil and root internal pressure. This model is validated against climate and water content data measured by [176] at a site in Newbury. A numerical procedure is then used to optimise the model input parameters and distributions of some of the more uncertain soil parameters (such as soil permeability, soil-water retention and root density) to obtain a best fit to

the measured water content data. The model is spatially explicit, allowing the distribution of water within the soil profile to be determined.

3.3 Materials and Methods

3.3.1 Field Data

The field data used to calibrate the numerical model have been taken from instrumentation installed into a cut slope adjacent to the A34 Newbury bypass in England (Ordnance Survey grid reference SU455652). The site, and the full range of instrumentation installed, is described in detail in [175, 176]. The 16^o, 8 m high slope is cut entirely within London Clay, which is weathered over a depth of about 2.5-3.0 m below the original ground level, Figure 3.1.

The vegetation cover is primarily rough grass with herbs, with some small shrubs mainly of Hazel, which towards the start of the study (the data used are from 2005) were generally less than 0.5 m high. Recent observations made from shallow vertical faces cut into the slope indicate that the roots extend to about 0.8 m depth. Although detailed root density measurements were not taken in 2005, the plants had been growing on the slope for over 6 years, and therefore were well established.

Time domain reflectrometry (TDR) probes were installed at depths of 0.3, 0.45, 0.6, 0.9 and 1.5 m at different locations (A and C; Figure 3.1) on the slope, to record volumetric soil water content (units of m^3 of water per m^3 of soil) every hour. A climate station was installed at the site to measure rainfall, air temperature, humidity, wind speed and solar radiation. Surface runoff and interflow (flow of water through the topsoil) were measured using an interceptor drain cut to 0.35 m depth across the face of the slope. Soil pore water pressures (or suctions) were also recorded every hour, as described in [176].

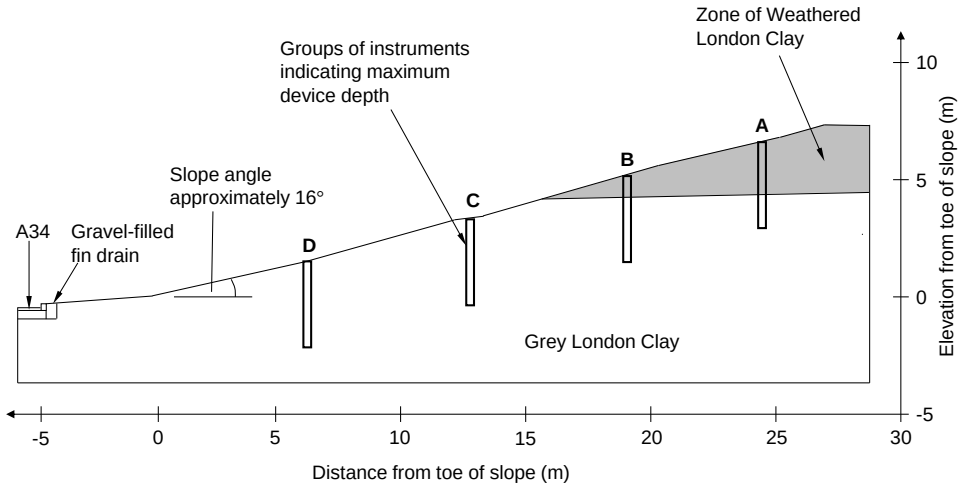

Figure 3.1: A cross section through the Newbury site showing the locations of installed instrumentation. Taken from [176].

3.3.2 Model

Water Movement and Plant Water Uptake Model

A model describing the movement of water within an unsaturated soil surrounding a root was developed by [160]. The model provides an estimate of the soil water content at different depths, and the uptake of water by the root system. The important aspects of the model are presented here; full details are given in [160].

A 1 year data set (2005) collected from [176] was used to validate the model from [160], which included determining optimal values of some root and soil water parameters. These were then used within the model with further climate data to see if the optimised model was able to produce predictions of changes in water content comparable with those measured in later years. A number of changes were made to the model in [160] to allow it to link with climate parameters such as rainfall, air temperature, wind speed and humidity and hence to the measured data; these changes are discussed below.

The model is based on the equation for the conservation of water in the soil (Richards Equation), which is given by:

$$\theta_s \frac{\partial S}{\partial t} + \nabla \cdot \mathbf{u} = -F_W, \tag{3.3.1}$$

where S is the relative water saturation in the soil ($S = (\theta - \theta_r)/(\theta_s - \theta_r)$, where θ is the volumetric water content, θ_s is soil porosity and θ_r is the residual water content; S also denotes the normalized volumetric water content, with the Eurocode 7 descriptor Θ), $\mathbf{u}$ is the volume flux of water (m s^{-1}) and F_W is the uptake of water by the plant roots (volume per unit time per unit volume of soil). The residual water content θ_r was taken as zero since at very high suctions in clay soils it does become close to zero [34], Figure 3.2. The volume flux of water is represented by Darcy's law,

$$\mathbf{u} = -\frac{k}{\mu}[\nabla p - \rho g \hat{\mathbf{k}}], \tag{3.3.2}$$

where k is the soil permeability (m^2), p is the water pressure in the soil (Pa), μ is the dynamic viscosity of water (kg s^{-1} m^{-1}), ρ is the density of water (kg m^{-3}), g is the gravitational acceleration (m s^{-2}) and $\hat{\mathbf{k}}$ is the unit vector in the downward direction.

It is also possible to write the water pressure in the partially saturated soil pores in terms of the relative saturation via the soil water retention curve [193],

$$p_a - p = p_c f(S), \qquad f(S) = (S^{-1/m} - 1)^{1-m}, \tag{3.3.3}$$

where p_a (Pa) is the atmospheric pressure, p_c (Pa) is a characteristic suction pressure determined from experimental data for different types of soil and m denotes the Van Genuchten soil suction parameter, where $0 < m < 1$. Measuring

gauge pressures relative to atmospheric pressure gives $p_a = 0$.

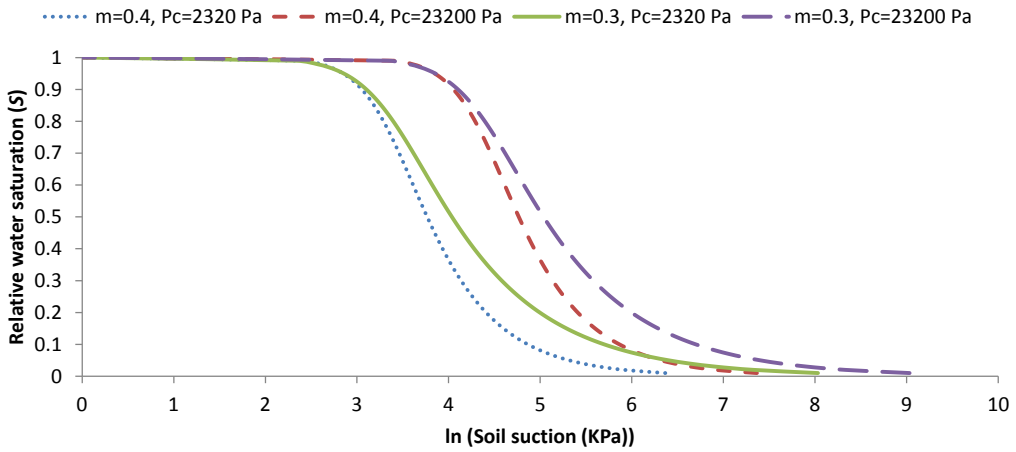

Figure 3.2: Soil water retention curves for two different values of m(0.3 and 0.4) and p_c (23200 Pa and 2320 Pa). The curves for $p_c = 23000$ Pa are representative of those used to model the Newbury site.

Soil permeability is influenced by soil saturation, and therefore the soil permeability is written in terms of relative water content using [193],

$$k = k_s K(S) = k_s S^{1/2} \left[1 - (1 - S^{1/m})^m\right]^2, \tag{3.3.4}$$

where k_s is the water permeability in fully saturated soil (m^2), and $K(S)$ represents the reduction in water mobility in the soil due to the reduction in relative saturation. The air entry value (the soil suction at which the volumetric water content reduces from full saturation) is represented in the Van Genuchten expression (Equation (3.3.3)) by a combination of m and p_c. It is most sensitive to p_c and decreases as p_c decreases, Figure 3.2.

The water uptake by a single cylindrical root is calculated from the difference between soil pore water pressure and root xylem pressure (the water pressure in the root), and is given by

$$F_W = 2\pi a l_d k_r (p - p_r) = 2\pi a l_d k_r (-p_c f(S) - p_r), \tag{3.3.5}$$

where $2\pi a l_d$ is the root surface area density, l_d is the root length density (m of roots per m^3 of soil), a is the average zero order root radius (m), k_r is the root radial water conductivity parameter (m s^{-1} Pa^{-1}) and p_r is the root internal xylem pressure (Pa).

Using Equations (3.3.3) and (3.3.4), we can write Equation (3.3.1) in terms of the relative saturation S only,

$$\theta_s \frac{\partial S}{\partial t} = \nabla \cdot \left[D_0 D(S) \nabla S - K_S K(S) \hat{\mathbf{k}} \right] - F_W, \tag{3.3.6}$$

where the water "diffusivity" in the soil is $D_0 D(S) = (k/\mu)|\frac{\delta p}{\delta S}|$,

$$D_0 = \frac{p_c k_s}{\mu} \left(\frac{1-m}{m} \right), \tag{3.3.7}$$

$$D(S) = S^{1/2-1/m} \left[(1 - S^{1/m})^{-m} + (1 - S^{1/m})^m - 2 \right], \tag{3.3.8}$$

and K_s is the saturated hydraulic conductivity (m s^{-1}) given by,

$$K_s = \frac{\rho g k_s}{\mu}. \tag{3.3.9}$$

The boundary conditions for the model are

$$D_0 D(S) \frac{\partial S}{\partial x} - K_s K(S) = \begin{cases} -W & at \quad x = 0 \\ 0 & at \quad x = l_w \end{cases}, \tag{3.3.10}$$

where W is the volume flux of water into the soil at the surface, representing both infiltration due to precipitation and evaporation (volume of water per unit soil surface area per unit time), and l_w is the depth at which zero water flux occurs.

The balance between the axial and radial fluxes of water inside a single cylin-

drical root is given by

$$2\pi a k_r(-p_c f(S) - p_r) = -k_z \frac{\partial^2 p_r}{\partial x^2}, \tag{3.3.11}$$

with the following boundary conditions,

$$\frac{\partial p_r}{\partial x} - \rho g = 0 \qquad \text{at} \qquad x = L, \tag{3.3.12}$$

$$p_r = P \qquad \text{at} \qquad x = 0, \tag{3.3.13}$$

where k_z is the root axial hydraulic conductivity calculated using Poiseuilles law (m^4 Pa^{-1} s^{-1}), P is the initial water pressure at the top of the root (Pa) and L denotes the maximum length of the root (m). The single root uptake equation is scaled up using the multi-scale analysis presented in [160] to represent macroscopic behaviour (e.g. many roots within a vegetated soil profile) in determining F_W with the depth of the soil.

The model is written in terms of relative water saturation (S) as it is more stable to numerically solve for Richards Equation via a finite volume method. To summarise, the one-dimensional (1D) model describing water movement in the soil and plant water uptake is,

$$\frac{\partial S}{\partial t} = \frac{\partial}{\partial z}\left[D_0 D(S)\frac{\partial S}{\partial z} - K_s K(S)\right] - F_W, \tag{3.3.14}$$

where

$$F_W = \frac{2\pi a_1 k_r + (2\pi a_1 k_r k_z)^{1/2}\psi_1(z)}{\pi(a + L_1 cos\phi)^2}[-p_c f(S) - p_r]. \tag{3.3.15}$$

where ψ_1 is the density of first order roots on the zeroth order roots, a_1 is the first order root radius, L_1 is the maximum length of the first order branches and ϕ is the angle between the main root and the first order branches.

The boundary conditions for the model are

$$D_0 D(S)\frac{\partial S}{\partial x} - K_s K(S) = \begin{cases} -W & at \quad x = 0 \\ 0 & at \quad x = l_w \end{cases}. \tag{3.3.16}$$

The root internal pressure p_r is calculated from

$$2\pi a k_r(-p_c f(S) - p_r) = -k_z \frac{\partial^2 p_r}{\partial x^2}, \tag{3.3.17}$$

with

$$\frac{\partial p_r}{\partial x} - \rho g = 0 \qquad \text{at} \qquad x = L, \tag{3.3.18}$$

$$p_r = P \qquad \text{at} \qquad x = 0. \tag{3.3.19}$$

In the following sections we validate this model against the soil saturation data provided by [176].

Adjustments to the Model and Dataset

Figure 3.3 shows the water content measured with the TDR probes at different depths at location A for the year 2005. A reduction in the water content is observed at 0.3 m, 0.45 m and 0.6 m depths between June and October, reflecting the summer drying period. The traces for the shallowest three probes show a series of short upward spikes in response to heavy winter rainfall events. The spikes in water content are likely caused by pulses of water passing downward through the upper (more silty) part of the profile after heavy rainfall events, returning after the event to field capacity (the equilibrium water content of soil held against gravity).

The very rapid spikes in the measured traces of water content were difficult to model as they were misleading the model fitting procedure. The model cannot represent these short time dynamic conditions, as it is designed to track seasonal

variations on the timescale relevant to plant water uptake rates than response to fast hourly/daily extreme weather events. It was decided therefore to focus on modelling the saturation level at field capacity during the winter, and its reduction during the summer and early autumn. A Fourier Transformation Signalling algorithm [177] was used to eliminate the spikes found in raw data and produce smoother curves that reflect the long-term change in the soil saturation level. The algorithm uses the following equation:

$$p(x) = \sum_{k=0}^{N} a_k cos(kx) + b_k sin(kx), \tag{3.3.20}$$

where a_k and b_k are variables to be solved for a fixed N and at a set of chosen points, x, and their value $p(x)$. The spike smoothing process involves taking uniformly spaced points along the x-axis and smoothing the curve between them using Equation (3.3.20). The result of this process is shown in Figure 3.3 which shows the smoothed data for the corresponding raw data. Initially curves consist of about 2000 data points, which when smoothed reduce to about 50 data points. In order to generate a full data set again, the 50 data points are extrapolated back to 2000. The sum of squares scores between the original and new (with spikes removed) data sets is low at an average of 2.7 for location A and 0.2 for location C. The smoothing method eliminates the peaks while maintaining the main characteristics of the curves. The physical meaning of removing the spikes relates to removing surface water accumulation and run-off effects, essentially scaling how much rainfall water actually makes it into the soil. From now on mention to the probe/experimental data is referring to the smoothed data, of Figure 3.3.

The water flux at the ground surface is modelled by considering the net flux of water into the soil W, which is based on environmental factors such as rainfall (R), humidity (H), wind speed (WS), temperature (T) and a constant (c), using

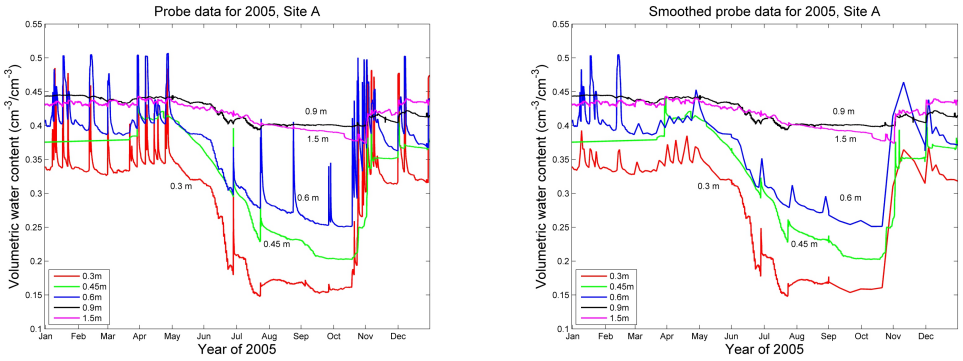

Figure 3.3: TDR probe data at location A for 2005 showing the volumetric water content at different soil depths: (left) the raw data; and (right) the data smoothed by the Fourier Transformation signalling algorithm.

either linear (Equation (3.3.21)) or non-linear (Equation (3.3.22)) expressions,

$$W = \delta R + \alpha H + \beta T + \gamma WS + c, \tag{3.3.21}$$

$$W = \delta R + \alpha_1 H + \alpha_2 H^2 + \alpha_3 H^3 + \beta_1 T + \beta_2 T^2 + \beta_3 T^3 + \gamma_1 WS + \gamma_2 WS^2 + \gamma_3 WS^3 + c, \tag{3.3.22}$$

where the parameter vectors $\delta, \alpha, \beta, \gamma$ and c are to be determined from the optimal fit to the soil water content data of [176]. The flux of water W has units ms^{-1} of water and from this units can be assigned to the remaining parameters as shown in Table 3.1. Equations (3.3.21) and (3.3.22) can essentially be considered as Taylor expanded versions of other non-linear relationships often used for calculation of evaporation/transpiration such as the Penman-Monteith Equation.

The driving pressure (P) inside the root is dominated by atmospheric humidity and temperature as the stomata in the leaves open and close depending on the environmental conditions [190]. When the air temperature is high and/or humidity is low the plant closes its stomata to slow down the loss of water and this leads to an increase in the pressure of water inside the roots. Due to the direct change to the water pressure within the plant roots, we use the following formula

for P for the boundary Equation (3.3.19) to model the total pressure,

$$P = (p_r^0 + \lambda_3) + \lambda_1 T + \lambda_2 H, \tag{3.3.23}$$

where p_r^0 is the baseline root pressure and λ_1 (Pa/degC), λ_2 (Pa/% humidity) and λ_3 (Pa) are determined by seeking the optimal fit to the soil water content data. The parameter values are given in Table 3.1 while the inputs and outputs for this model are given in Table 3.2.

3.3.3 Numerics

To solve Equations (3.3.14-3.3.19) numerically the x-axis was discretised into 800 equidistant points over the depth of the assumed soil profile (0-2 m depth). A high-resolution Monotone Upstream-centred Scheme for Conservation Laws (MUSCL) proposed by [95] was used which set 1600 cells as that required to obtain the true solution for the soil profile; it was found that 800 cells gave a less than 1% error for the model output (plant water uptake) with a significant reduction in run time (between a factor of 5 and 6) and this was selected as the final grid size.

3.3.4 Validation Techniques

In Roose and Fowler (2004) the flux of water into the soil at the soil surface (W) and the pressure down the root ($p_r(z)$) were set to have a constant value in time. To more accurately represent the effect of the climate on these factors they were set as external time dependant inputs.

Equations (3.3.21) and (3.3.22) for the flux of water into the soil (W, in essence rainfall minus the runoff and evaporation) are simpler than other models for potential evapotranspiration (PET) such as the Penman-Monteith Equation [3]. Simple linear and non-linear relationships between evaporation/evapotranspiration, tem-

perature, humidity and wind speed (similar to Equations (3.3.21) and (3.3.22)) have been proposed in the literature, and demonstrated to work well for site specific locations [18, 49].

The water flux into the soil is calculated from the climate data collected by [176]. Since the characteristics of the climate data vary across the different seasons, the climate data were split into blocks of about 3 months representing each of winter, spring, summer and autumn, and the model used to simulate each 3-month period separately. The initial model starting condition for each seasonal period was based on the finishing point of the preceding season.

The field data are taken from a highway cutting in which the ground slopes at about 16^o. A one- and two-dimensional unsaturated finite element simulation of a clay slope was carried out by [21], with the one-dimensional column model having the same vertical geometry as the mid-slope of the two-dimensional model. Both were analysed with the same surface boundary flux representing climate and vegetation, and the results of the one-dimensional column model agreed closely with the two-dimensional model. This was because horizontal water flow due to gravity was found to be small compared with vertical water flow due to the flux boundary at the ground surface. It was therefore considered reasonable to model the effects of the vegetation here in one-dimension only. In this case, use of a one-dimensional model allows an optimisation of some of the soil parameters (described in Section 3.3.5) that would be difficult to do with a two-dimensional model. The impermeable base of the model was assumed to be at 2 m depth. This was based on there being only a small change in measured water content and pore pressure at this depth [176] with most of the change due to the vegetation occurring in the top 0.8 m of the profile. The impact of a more diffuse boundary condition at the bottom could be investigated within future work.

The water permeability in fully saturated soil k_s and the soil suction parameter

m are linked in Equation (3.3.7), and control how the water moves through an unsaturated soil. These values were assumed to be constant in the original model in [160]. However, measurements and modelling indicate that these values can vary both with depth and time [4, 102]. For example, surface soils are often quite structured with a higher organic matter content and larger cracks/fissures caused by root penetration and repeated drying and wetting cycles. A greater number of larger voids in the soil will give a lower air entry value and more rapid water drainage from the soil at lower suction, thus changing the shape of the soil water retention curve (SWRC). In this case, there are no site specific data for variation of m with depth, and few if any measurements of this type appear to have been carried out for a stiff clay soil. The parameter m was allowed to vary to obtain an optimal fit to the water content data, with m modelled using a bounded arbitrary function. The value of m was allowed to change between the points at which the experimental water content levels were recorded (at $0, 0.3, 0.45, 0.6, 0.9$ and 1.5 m), giving 6 different values of m for the full soil profile. The values of m were optimised for each of seasonal time periods considered.

At location A there is a variation of soil characteristics with depth, going from a layer of more silty weathered London Clay at the top to a layer of lower permeability grey London Clay below, Figure 3.1. This transition occurs around $x_2 = 0.9$ m, which for the purpose of the numerical simulations is taken to be an exact depth, Figure 3.4. Two scenarios were considered for location A: in scenario 1, k_s has a constant value for both types of soil, whereas in scenario 2, k_s linearly decreases with depth in the weathered London Clay region and is constant in the grey London Clay. Since location C consists only of grey London Clay, k_s was set to linearly decrease with depth, as seen in scenario 3. Some measured data for permeability at the site were available, from deeper depths in the clay (mainly below 1.0 m; [176]). The site data were used to define the value of k_s at depth, and

arbitrary increases were applied to the relevant scenarios above this. The model is found to be more sensitive to changes in m compared to k_s, hence the values of k_s were held constant over the full year of modelled data where scenario 2 was set for location A, and scenario 3 was set for location C. This means that the model does not incorporate the influence of potential surface desiccation cracking. Evidence is investigated in Section 3.4 to support the hypothesis that water permeability decreases with greater depths.

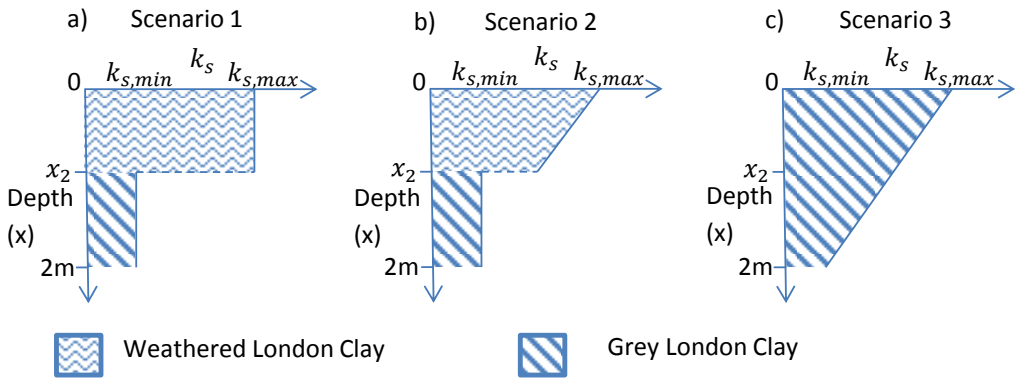

Figure 3.4: Three scenarios used to model the change in saturated water permeability (k_s) with depth: (a) scenario 1; (b) scenario 2; (c) scenario 3. The value of k_s is bounded between $k_{s,min}$ and $k_{s,max}$ which are 5.78×10^{-9} and 5.78×10^{-8} m^2 respectively (Table 3.1).

The exact root distribution of the vegetation at the site in Newbury is not known and the water uptake parameter k_r and root length density l_d were set as constant with time within each seasonal period but allowed to vary between these. It was assumed the roots at the Newbury site had already grown to full length, and the length of the main root (zero order) was fixed at 0.8 m.

3.3.5 Optimisation Procedure

The optimisation model output is the optimal set of values for the following parameters: 2 for the water uptake (Equation (3.3.17)), 2 for the root length param-

eters (Equation (3.3.5)), 5 or 11 respectively for the linear or non-linear systems for the flux of water at the soil surface (Equations (3.3.21) and (3.3.22)), 3 for the water pressure inside the root (Equation (3.3.23)) and 6 for the Van Genuchten soil suction parameter m. This set of parameters was combined with the model to produce an accurate representation of the water movement within the soil, from the given climate data and the root and soil parameters seen in Table 3.1 (please see page 94 at end of Chapter).

An upper bound for the input flux of water W was imposed, because at high values of rainfall (conditional to parameters such as water uptake into the plant roots and water diffusivity) the model becomes invalid as the soil profile becomes fully saturated, and Equation (3.3.16) no longer holds. The upper bound was distributed between the parameters in Equations (3.3.21) and (3.3.22), as they sum to the value of W. These bounds restricted the parameters to be within realistic values and Table 3.1 shows the enforced upper bounds. The experimental data show that the surface was never fully saturated and therefore Equation (3.3.16) holds for unsaturated soil.

Once the values for the flux of water W are determined together with the rest of the model parameters, Equation (3.3.14) can be solved numerically to obtain the resulting water profile. The calculated water profile was then compared to the experimental data (i.e. the values for the water content at different depths) by using the sum of squares differences between observed and simulated data. Equation (3.3.24) denotes the formula for the sum of squares (SOS) difference for the objective value y,

$$y = \sum_{i=1}^{N} (x_i - \hat{x}_i)^2, \tag{3.3.24}$$

where x_i are the model points and $\hat{x}_i$ are the data points, for a set of N points. The optimisation procedure used the global optimisation method Kriging [50], which stops as the objective value either reaches 0, shows no sign of change after

a set number of iterations, or until a maximum number of iterations has occurred. A large number of the simulation runs stopped due to no sign of change as they converged on the global/local optima.

As described above, the simulation has up to 24 parameters in the non-linear case and just one output, the sum of squares fit. An optimisation procedure was used as opposed to an exhaustive search (evaluating every combination), to find the optimal set of parameters which minimises the sum of squares fit. The optimisation procedure was twofold; firstly a set of initial starting points are chosen and then evaluated; secondly a process takes these points and converges on an optimal solution.

The initial search plan was based on the Latin Hyper Cube Technique [79], where the points picked are as far away from each other as possible. This method uses a Genetic Algorithm to optimise for the greatest distance between the initial points. The conventional number of points to pick is ten times the number of dimensions (parameters).

Once these initial search points are found their objective value was calculated using the full model given in Section 3.3.2. The next set of points to be sampled was calculated from the Kriging algorithm [50], which produced a surrogate model to imitate the full model. The Kriging procedure was iterative and used all of the information from the points calculated at the previous time step to estimate the best local and global points using two techniques; exploitation and exploration. Exploitation works like a local search or hill climber, as opposed to exploration which fills the gaps between existing sample points, placed at the maximum estimated error. These points were found on the surrogate model as it was much less expensive to traverse and find potentially optimal points within the surrogate than for the full model. This process was continued until the desired stopping condition was reached, which depended on the convergence of the opti-

mal set of parameters, the number of sample points and the value of the expected improvement.

3.4 Results

The model was validated using the climate data from [176] following the approach described in Section 3.3.4. The difference between the sum of squares fit for the two locations A and C, with linear and non-linear expressions for the climate input data, and the different seasons (wet and dry periods), is compared below. The profile of the Van Genuchten parameter m is also considered.

3.4.1 Fitting the 2005 data

In Figure 3.5 we show the fitting for the whole year (reconstructed from the seasonal segments) for all of the probes in both locations A and C for the year 2005 for a linear formulation of the climate conditions, and demonstrate that the model simulation accurately represents the soil water content. The model fluctuates a little around the experimental data, and better fits were obtained at deeper depths due to the smaller overall change in the water content.

In Figure 3.5 there are large differences between the model and experimental data in the autumn season, indicating a poor fit, especially for 0.6 m depth at location A. This is in contrast to the other seasons where good fits are obtained. The reason for the poor fit in autumn is due to the change in climate and soil conditions from mid-October to mid-November, where there is a large and sudden increase in the soil water content at 0.3 m depth from 0.17 to 0.36. In this period the model changes more slowly than the measured trace, and takes several days to catch up with it, matching it again in December when the winter season starts. This could be due to the values for saturated permeability used in the

model, which may not reflect the near-surface clay cracking that occurs during the summer period. The model does not capture the hysteresis of the SWRC, which would also potentially allow a rapid increase in water content on wetting.

Better fits were obtained for the sum of squares (SOS) values for location C compared to location A by roughly a factor of 2.5, when normalised. The fittings are much tighter for location C than location A, especially at 1.5 m depth. However, in autumn at 0.3 m depth the fitting again takes some time to catch up with the sudden increase in measured water content. In winter and spring, the model fits the data very well, especially at location C where the SOS values are below or close to 1. The smoothed experimental data for location A provided a better landscape for the model fit compared to the raw data.

There was found to be little difference in the model fit to the field data resulting from the linear and non-linear climate expressions, Equations (3.3.21) and (3.3.22) respectively. However, there was a difference between the different locations and seasons as seen in Table 3.3, which shows the final sum of squares scores for each of the scenarios.

3.4.2 Soil Suction Parameter (m)

The Van Genuchten soil suction parameter m denotes a fitting parameter which is normally determined by fitting a curve to data points obtained experimentally from samples of soil. Small samples of soil are usually tested under zero total stress, and the laboratory results may not capture either the bulk structure of the soil (and its variability throughout locations A and C), nor the likely change in water retention properties with increasing total stress. It would not be unreasonable to expect the value of m to change, both between locations A and C, and with depth below the ground. The effects of volume changes and stress states have been considered on the SWRC by [130], who show that under higher

stress there are lower rates of desorption, likely caused by the existence of average smaller pore size distributions in the soil. The value of p_c which largely controls the air entry value of the SWRC was fixed at a value of 23 kPa, intended to be representative of a structured clay soil [21]. Changes in the air entry value due to the particle size and structure of the soil, and changes in soil stress, are thus not modelled; this is a limitation of the current simulations and may be incorporated in further investigations.

In analysis of the SWRC, an increase in the value of m gives a smaller value of soil suction for the same value of volumetric water content; thus coarser soils or those with structure should have water retention behaviour defined by higher values of m. At higher stresses the pore sizes will decrease, consistent with a smaller value of m at depth.

Previous models (Hydros, which uses the ROSETTA pedotransfer functions by [167] and a plant water uptake model by [160]) use one value of m for the full soil profile, but here the optimisation was able to determine the values for m that produce the best fit to the measured water content data. The results of the optimisation procedure showed that the profile of m with depth generally conformed into one distribution, where the averages are seen in Figure 3.6.

The profiles in Figure 3.6 indicate that the value of m varies with depth. The four profiles for locations C and A (linear and non-linear formulation of the climate conditions) are very similar. Below 0.9 m the value of m is fairly uniform with depth, perhaps as a result of increasing soil uniformity deeper within the profile. For the layer of soil between 0 and 0.9 m there is an increase in the value of m immediately below the soil surface followed by a decrease. A high value of m indicates a coarser soil, which is consistent with a generally more structured soil around the root system. As explained earlier, water permeability changes with depth [102] and it is therefore plausible that m will also change with depth (they

are coupled by Equation (3.3.7)). The values for m can be estimated using a fractal approach, for different soil types, and improve the root mean square error values given from the ROSETTA model [56]. However, the range of values estimated for m still differed widely; for example in a silty clay loam the maximum and minimum values were 0.48 and 0.09 respectively. No experimental studies seem to have been carried out to quantify the change in m with depth within a stiff clay; nonetheless the profiles obtained from the model look sensible, and in future could be checked against experimental measurements.

3.4.3 Predictions and Comparisons

To test how effective the validation of the model was, the optimal fitting parameters from the 2005 validation were used to run the model for the following year, 2006. Figure 3.7 shows the results of the model plotted with the experimental data for 2006; these look quite similar to that of 2005 (Figure 3.5), where the model achieved a good fit. The SOS scores for the 2006 model run (Table 3.3) are slightly worse than for the 2005 fitting procedure as may be expected; the 2006 scores were approximately twice as large, summing over the year. Averaging the input parameters from 2 or more years of fittings would help improve the forecasting ability, as the unknown soil and water parameters would likely be matched to a higher degree of accuracy with more available data.

The average soil water content from the model was compared with that calculated using Cropwat with the Penman-Monteith Equation, as used by [176] to model the same site. In Figure 3.8 we show the comparison of the Cropwat model, the updated model from [160], and the average soil water content for locations A and C calculated from the TDR probe data (a weighted average of the probe readings at different depths). Throughout the year the average water content at location C is 11% lower than location A, despite the climate conditions being

equal. This is due to the different soil properties between the measurement locations, and the different initial saturation of the soil. The updated model from [160] accounts for this whereas the simple water balance in Cropwat does not. The updated model from [160] produces a much better fit to the TDR probe data, due to the more detailed mathematical formulation used to describe the plant, soil and water movement, when compared with models such as Cropwat which produce an average value for the depth of the soil column.

A separate sensitivity analysis on all of the parameters in the model was carried out; where the new SOS score was calculated after individually changing each parameter by $\pm 5\%$. It was found that the most sensitive parameters were those associated with the pressure in the xylem vessels, i.e. plant parameters appear to be very important. This indicates that it is important that the good estimates of these parameters are determined (if they can be experientially measured, which is the case) and future work will involve more careful measurements and modelling of the pressure in the xylem vessel.

Finally, to demonstrate that the parameter optimisation procedure is valuable when dealing with large parameter uncertainty, the model was used to fit the 2005 data, but this time using fixed and uniform with depth 'best guess' values for k_s and m. This model run (Figure 3.9) gave poor results with an SOS of 203. The fittings at 0.45 and 0.6 m were acceptable due to the value of m being close to the earlier values used at these depths. However, the model did not match the other probe depths well, as there was a difference in the value of m from the fully optimised model fit. This also supports the idea that k_s and m are depth dependent, and that outputs from models of this type can be sensitive to having the correct soil-water parameters.

Location	A				C			
Season	Winter	Spring	Summer	Autumn	Winter	Spring	Summer	Autumn
2005 Linear W, SOS	5.79	6.45	17.30	19.94	0.28	0.65	4.07	4.52
2005 Non-linear W, SOS	3.77	4.70	15.07	16.62	2.08	0.39	2.57	3.31
2006 Non-linear W, SOS	22.23	8.91	26.79	18.78	1.72	1.28	3.94	9.77

Table 3.3: The SOS results for linear and non-linear W, in the different locations and seasons: fitted results for 2005 and forecast model run results for 2006.

3.5 Discussion

The modified Roose and Fowler (2004) model has made use of climate data and soil information to estimate the water content within the soil. It provides a variation in water content with depth in the soil profile rather than an average such as obtained from simple water balance models. The proposed model also estimates the uptake of water into plant roots. A procedure for fitting the model to measured data has been used to estimate and optimise soil-water and plant parameters which may be particularly uncertain and to which the outputs from this type of model can be particularly sensitive.

The fitting procedure was used on water content data measured at a clay cutting slope site near Newbury, Berkshire. The changes made to the profiles for saturated water permeability k_s (Figure 3.4) had relatively little effect on the model outputs compared to the change in the Van Genuchten soil suction parameter m. The permeability does vary with saturation (Equation (3.3.4)), however, permeability was not allowed to sufficiently increase to represent clay cracking, and this resulted in generally poor model fits to the real data during the autumn/winter soil re-wetting. The model could be adjusted to allow optimisation of saturated permeability, as well as the water retention parameter m. The profiles of m from the model output (Figure 3.6) show an average larger pore size for the root zone; this is where the soil is likely to be more disturbed or structured in

practice.

A sensitivity analysis was carried out and showed that the most sensitive parameters in the model were those involved with the pressure in the xylem vessel. It is therefore important to measure these plant parameters accurately; to help with this, the optimisation procedure is useful for estimating values that are uncertain.

The model may be used for sites such as vegetated clay earthworks to estimate the extent of drying and effective stress changes in the soil in response to climate or changes in vegetation. Where measured water content or pore water pressure data are available, these may be used with the fitting procedure to assess difficult parameters such as k_s and m.

The model has the potential to be used for different soil types, climate conditions and for growing root systems; as long as the set of parameters in Table 3.1 are obtained or estimated. Therefore the model should aid soil and plant management strategies through better understanding the soil and water configuration, and by forecasting soil conditions for potential scenarios.

Variables	Range	Units
δ	0 to 5×10^{-3}	-
α_1	0 to 5×10^{-6}	ms^{-1} of water
α_2	0 to 2.5×10^{-11}	ms^{-1} of water
α_3	0 to 1.25×10^{-16}	ms^{-1} of water
β_1	0 to 5×10^{-5}	ms^{-1} of water/degC
β_2	0 to 2.5×10^{-9}	ms^{-1} of water/degC^2
β_3	0 to 1.25×10^{-13}	ms^{-1} of water/degC^3
γ_1	0 to 2.5×10^{-3}	ms^{-1} of water/ms^{-1} of air
γ_2	0 to 6.25×10^{-6}	ms^{-1} of water/m^2s^{-2} of air
γ_3	0 to 1.5625×10^{-8}	ms^{-1} of water/m^3s^{-3} of air
λ_1	-5×10^{-3} to 5×10^{-3}	Pa
λ_2	-1.5×10^{-3} to 1.5×10^{-3}	Pa/% humidity
λ_3	-0.25 to 0.25	Pa/degC
c	0 to 2.5×10^{-3}	ms^{-1} of water
m	0.1 to 0.5	-
k_r	0 to 2.5×10^{-4}	ms^{-1}Pa
k_z	0 to 4.6×10^{-11}	$m^4s^{-1}Pa^{-1}$
Fixed values	**Value**	**Units**
ϕ	0.4	-
ρ	2.6×10^3	kg m^{-3}
p_c	0.232×10^5	Pa
D_0	1.1574×10^{-6}	m^2s^{-1}
k_S	5.78×10^{-9} to 5.78×10^{-8}	m^2
a	5×10^{-4}	m
l_d	1.785×10^3	m of roots per m^3 of soil
L	0.8	m

Table 3.1: A list of variables and fixed values used within the model in Chapter 3.

Inputs	Outputs
Water flux at the top of the soil	Water uptake by root system
Root parameters	Water saturation levels overtime for any given depth up to 2 m
Soil parameters	

Table 3.2: Inputs and outputs for the model in Chapter 3.

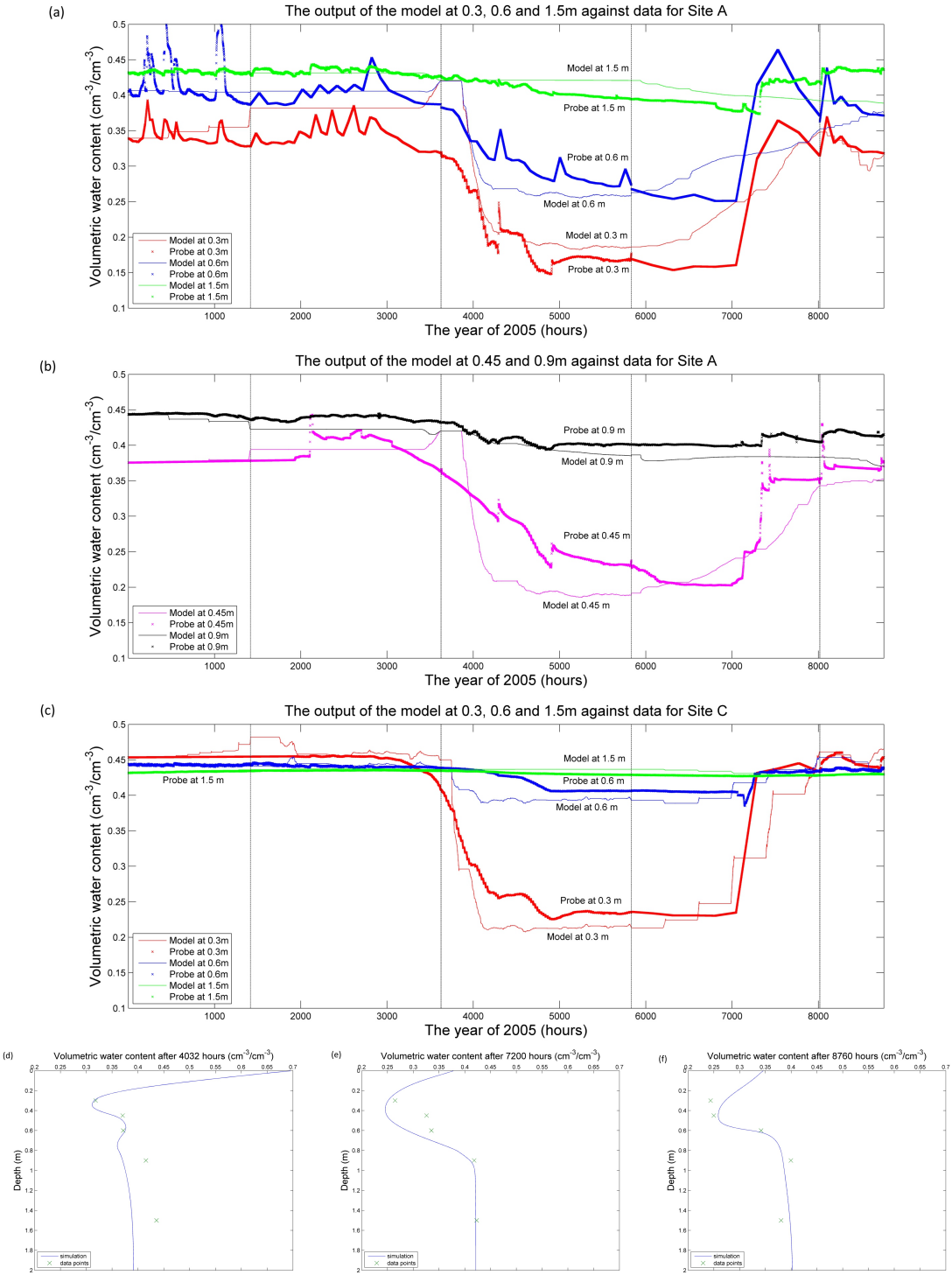

Figure 3.5: Model fittings for 2005 for locations A and C for five and three probe depths, respectively, with a linear formulation of the climate conditions. Output of model at (a) 0.3, 0.6 and 1.5 m against data for site A; (b) 0.45 and 0.9 m for site A; (c) 0.3, 0.6 and 1.5 m for site C. Graphs (d), (e), (f) show volumetric water content taken at 4032, 7200 and 8760 h respectively.

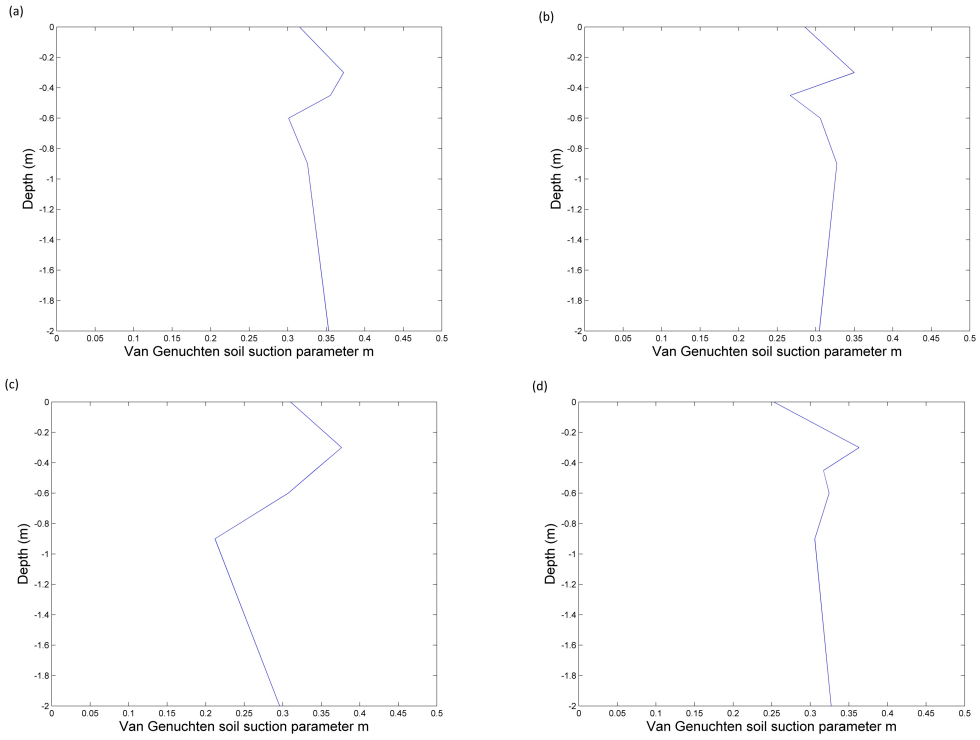

Figure 3.6: The profile for m for locations A (a, c) and C (b, d) with linear/non-linear input water flux formulations, respectively.

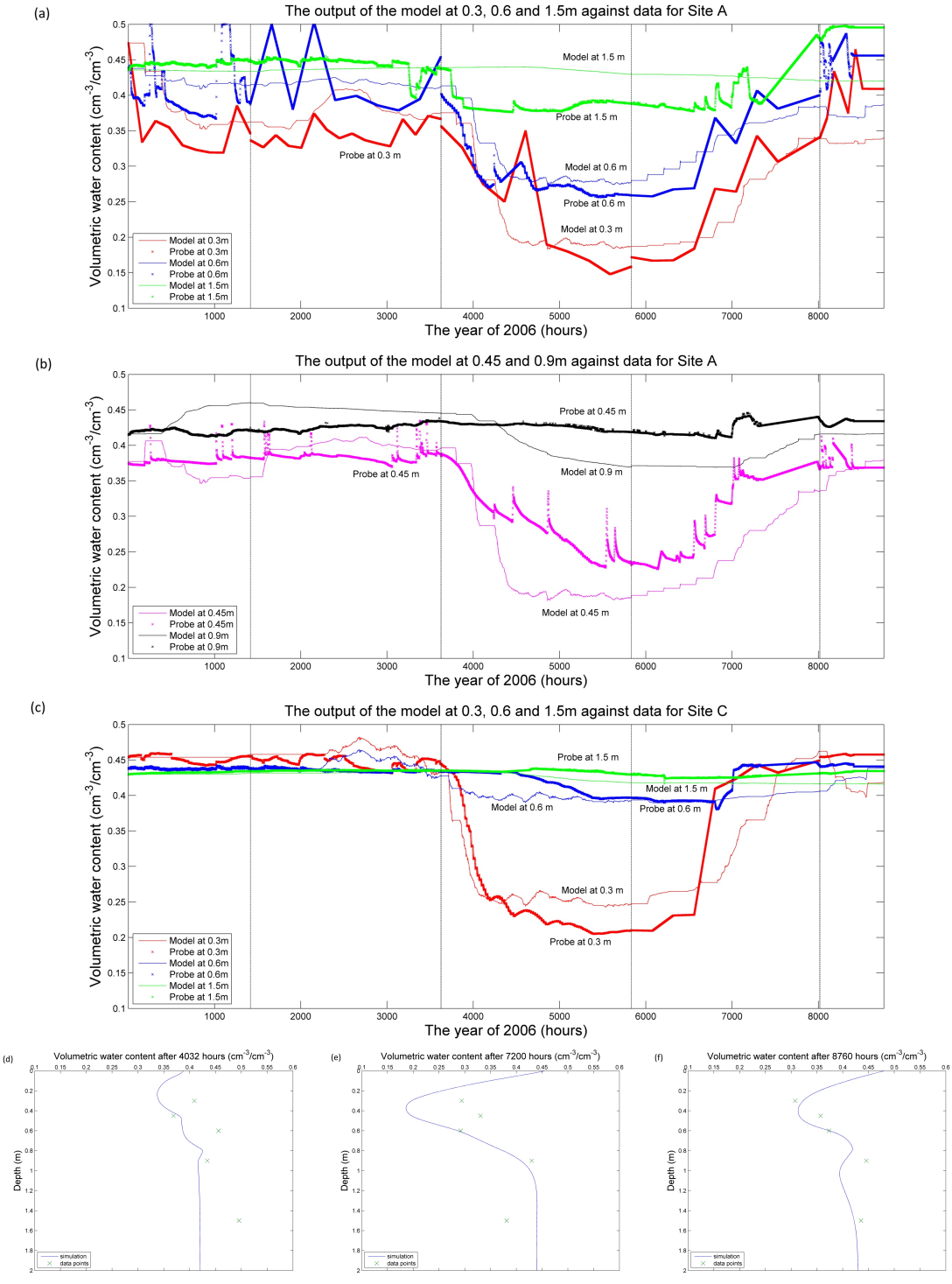

Figure 3.7: Model run to forecast water content changes in 2006 for locations A and C for five and three probe depths, respectively, with a linear formulation of the climate conditions. Output of model at (a) 0.3, 0.6 and 1.5 m against data for site A; (b) 0.45 and 0.9 m for site A; (c) 0.3, 0.6 and 1.5 m for site C. Graphs (d), (e), (f) show volumetric water content taken at 4032, 7200 and 8760 h respectively.

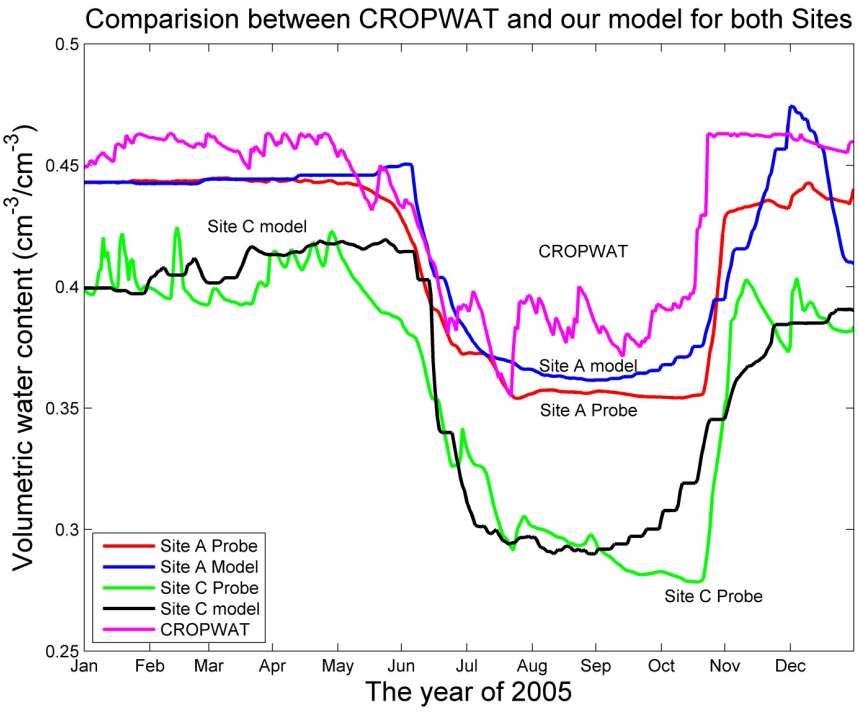

Figure 3.8: The comparison between the Penman-Monteith/Cropwat model, the validated Roose and Fowler model and the measured TDR data for both sites.

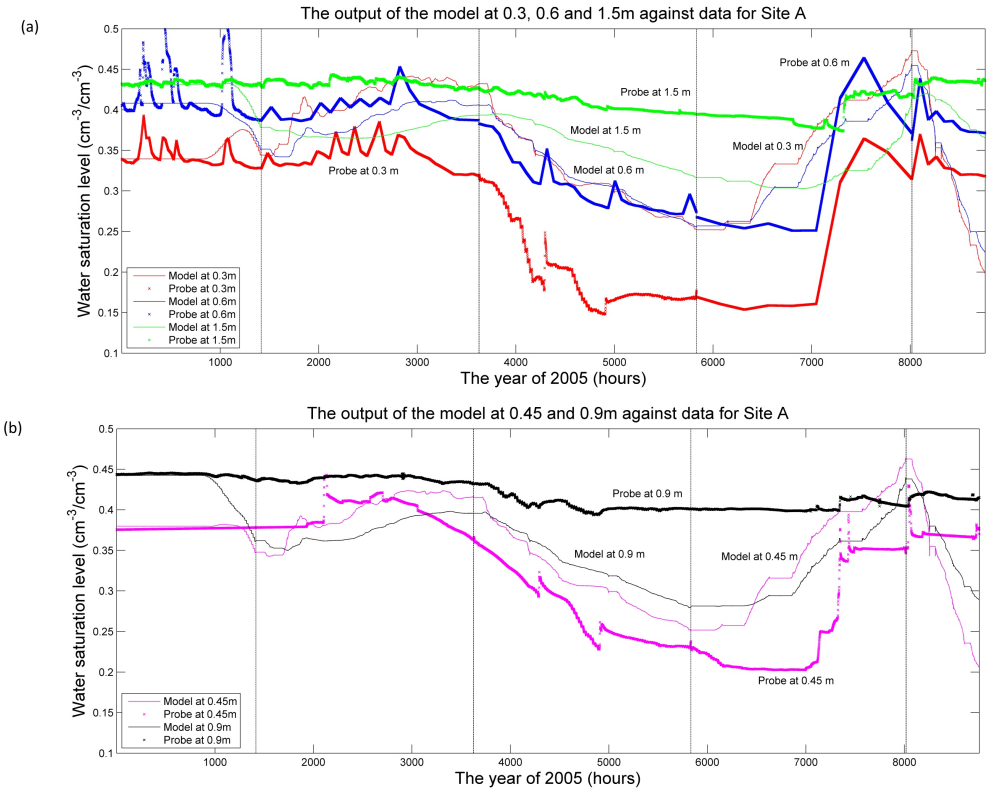

Figure 3.9: The model fittings for 2005 for location A for constant values of m and k_s: (a) output of model at 0.3, 0.6 and 1.5 m against site data; (b) output of model at 0.45 and 0.9 m against site data.

Notation list for Chapter 4

b	Soil buffer power
c	P concentration in pore water
D_0	Water diffusivity
D_f	P diffusivity in free water
$D(S)$	Reduction in water diffusivity in response to S decrease
d	Impedance factor
E	constant for the linear estimation of W_{dim}
F	Rate of P uptake
F_w	Uptake of water by plant roots
H	Humidity
K_i	Maximum length of order i root
K_s	Saturated hydraulic conductivity
$k(S)$	Reduction in hydraulic conductivity in response to S decrease
$\hat{\mathbf{k}}$	Unit vector in the downwards direction
l_i	Current length
l_w	The depth at which zero flux occurs
m	Van Genuchten soil suction parameter
P	Phosphate
P	Pressure at top of xylem in root
p_r^0	Baseline root pressure
Q_{dim}	Rate of fertilisation
R	Rainfall
R_T	Rate of root growth
r_i	Initial rate of growth for order i root
S	Relative water saturation
T	Temperature
t	Time
$\mathbf{u}$	Volume flux of water
W_{dim}	Volume flux of water into the soil at the surface
WS	Wind speed
z	Depth
α	Parameter for the linear estimation of W_{dim}
β	Parameter for the linear estimation of W_{dim}
γ	Parameter for the linear estimation of W_{dim}
δ	Parameter for the linear estimation of W_{dim}
λ_1	Parameter for the estimate of P
λ_2	Parameter for the estimate of P
λ_3	Parameter for the estimate of P
ϕ	Soil porosity
ϕ_1	Volumetric water content

Table 3.4: Notation list for Chapter 4.

Chapter 4

Modelling the Optimal Phosphate Fertiliser and Soil Management Strategy for Crops

J. Heppell[1,3,4,5], S. Payvandi[2,5], P.Talboys[6], K. Zygalakis[3,5], J. Fliege[3,4], D. Langton[7], R.Sylvester-Bradley[8], R.Walker[9], D.L.Jones[6] and T. Roose[2,5]

[1]Institute for Complex Systems Simulation, University of Southampton, Southampton, UK. [2]Faculty of Engineering and the Environment, University of Southampton, Southampton, UK. [3]School of Mathematics, University of Southampton, Southampton, UK. [4]CORMSIS, University of Southampton, Southampton UK. [5]IFLS Crop Systems Engineering, University of Southampton, Southampton, UK. [6]School of Environment, Natural Resources and Geography, University of Bangor, Bangor 57 2UW, UK. [7]Agri-intelligence, UK. [8]ADAS Boxworth, Cambridge CB23 4NN, UK. [9]Scotlands Rural College, Aberdeen, AB21 9YA.

4.1 Abstract

The readily available global rock phosphate (P) reserves may run out within the next $50 - 130$ years, causing soils to have a reduced P content thus affecting plant P uptake. Careful use of this finite resource in agriculture systems is clearly warranted. We develop a model that allows us to assess a range of P fertiliser and soil management strategies, in order to find which one maximises plant P uptake for a given set of climate conditions. In this paper we present the results

for Barley; however the model is adaptable for other types of crops, subject to root structure data being available. The model describes the development of the P and water profiles within the soil space. Current cultivation techniques such as ploughing and a reduced till gradient are simulated along with fertiliser options to feed the top soil or below the seed. We find that a well-mixed soil (inverted and 25 cm ploughing) is critical for optimal plant P uptake and provides the best environment for the root system. However, the model is sensitive to the initial state of P and its distribution within the soil profile; experimental parameters which are sparsely measured. The combination of modelling and experimental data provides useful predictions for site specific locations.

4.2 Introduction

Within the agricultural industry, the management of soils and crops varies widely around the world [90], and slight adjustments to reduce costs and/or increase crop yields can make substantial differences on the global scale. The demand for food is increasing; from 1992 to 2012 the production of cereals worldwide increased from 1.97 bn to 2.55 bn tonnes (http://faostat.fao.org/). In 2012 the UK alone produced 19.5 m tonnes of cereals, 5.52 m of which was barley. One of the most important nutrients for plant growth is phosphate (P), which is often the most limiting due to its low mobility in soils [24]. The current world rate of P consumption for fertilisers is not sustainable, and there are warnings that readily available global rock P reserves may be depleted within the next $50 - 130$ years [32, 35, 191].

As an attempt to increase the sustainable use of P, European governments [40, 96] are reducing the amount of P in agricultural sites from a high Olsen P index 3 ($26 - 45$ mg P/l) to either index 2 ($16 - 25$ mg P/l) or index 1 ($10 - 15$

mg P/l), thereby reducing P fertilisation. However, lower P content soils can lead to reduced yields [208]. Therefore it is vital to identify optimal soil management strategies for more efficient use of P [45]. However, optimal strategies can depend upon the current climate and the distribution of P within the soil. The distribution of P is a feature which is generally unknown for field situations, but is becoming more regularly sampled [200, 179].

Farmers implement a range of soil strategies based on information from a variety of sources. The fertiliser manual (RB209) published by the Department for Environmental, Food & Rural Affairs (DEFRA) provides a guide to farmers as to the amount of fertiliser to use for given soil types [40]. Field-specific advice is also given by agronomists based on this "tribal memory" about P use. Previous history of any specific site also remains an important factor as repeating cropping strategies for similar environments provides experience on which strategies perform best [153]. The general guidelines in the RB209 manual for applying fertiliser are based on soil P concentrations, often taken from spot measurements. The amounts of P application recommended are classified into different categories. However, this classification means that soils, which have similar soil P concentrations, but lie across the boundaries of the classification can have entirely different fertiliser recommendations. This leads to a varying selection of treatments on similar plots of land and makes it difficult to reduce the amount of P in soils, as a recent study in Ireland showed [96]. Site-specific guidelines may provide a better basis to implement optimal fertiliser and soil cultivation strategies when it comes to cultivating crops. The aim is to more efficiently use applied P, not over-apply in cases where it is not needed or under apply it and not meet crop yield targets. Therefore, instead of having a table of discrete amounts of fertiliser to add, a simple linear or saturating continuously graded expression could govern how much P to add. Also, a better classification of soils is needed; much like the

varied descriptions of soils in Scotland [181].

Increasing information collected about soil type and characteristics can provide a better understanding of which fertiliser treatment to apply, resulting in a more successful crop for a given season. However, collecting detailed data about soils is expensive. In addition, it is difficult to ascertain how much data is actually needed to give the best prediction for a successful strategy [93]. Models can provide the analysis needed to evaluate a large range of strategies that cannot all be tested at the field scale, due to time, money and location specific restrictions [82, 171]. Once optimal strategies are found, they can be tested and evaluated among other strategies to prove their validity, in the hope to support evidence for a better understanding of applying P to soils.

Many models used to describe the root system consider a density of root mass for a given volume in soil. The root mass can be estimated from averaging a 3D growth approach [27, 108] or considering a 3D growth model, for example L systems [100]. These approaches however cannot be easily assessed experimentally (due to image analysis of segmenting root radii) and can lead to numerical inaccuracies of up to 30% when compared to computed plant P uptake, when up-scaling to the field level [163]. In this paper, we model the movement of P and water within the soil profile over time. We extend the models in [71, 159] to estimate the uptake of P by crop roots for a given surface area of soil. This extended model is comparable to other density-based models [46], and accounts for the P depletion zone along all roots. We compare the extended model's output, estimating plant P uptake (kg P/ha), against two sets of field trial data for barley. Following this, the extended model is used to predict the optimal fertiliser and soil cultivation strategy which maximises plant P uptake. As a result, the optimal strategy should also maximise 'P efficiency use' within a low P environment.

In Section 4.3 we discuss P and water uptake models, looking more closely

at [71, 159] and our adaptations made to them. We then describe how the data is collected and the values used for the extended model. Modelling results are described in Section 4.4 followed by Section 4.5 where we describe our findings and future avenues for work.

4.3 Materials and Methods

4.3.1 Phosphate and Water Uptake Model

It is expensive to experimentally determine, in detail, the distribution and movement of water and P within the soil and the consequent uptake into the plant root system. The use of modelling in combination with experimental data allows us to predict optimal management strategies in agricultural systems. Many models exist that estimate water and P movement within soil. For example a model was developed that predicts plant P uptake by estimating the distribution of P in 3D [44]. The 3D P information can be combined with other models, such as one that estimates the fractal geometry of simulated root systems in 1, 2 and 3D [108]. However, due to memory and computational limitations, these models are not appropriate for up-scaling to the field level [163]. Other models focus on the root architecture and the uptake of P by the root system [54, 60, 107, 161], one of which captures the P depletion zone along all roots and obtains an analytical solution [161]. The model in [161], estimates plant P uptake per soil surface area and can be used to predict plant P uptake on a field scale. The model is further advanced by estimating the movement of water and P spatially [159]. In this paper, for the first time, we extend the model in [159] by adding the effect of climate, via surface water flux and xylem pressures as in [70]. This extension allows comparing of the model's output, estimating plant P uptake, against field study experimental data, for different environmental conditions. In addition, we

incorporate temperature-dependent root growth so that the model can be used for winter crops, as there is little or no growth at low temperatures. We first describe details of the model by [159] and then the adaptations made to it.

4.3.2 Roose and Fowler Model

Roose and Fowler model water and P flow through soil to calculate uptake into a surrounding plant root system using Richards Equation coupled to a diffusion-convection equation describing P movement in the soil [159]. They assume that the soil is homogeneous and neglect horizontal movement for water and P, since at the field scale the differences in the horizontal variation for the root length density are negligible compared to the vertical variation [160]. The dimensional model is described by the following two equations for water and P conservation, respectively,

$$\phi \frac{S}{\partial t} = \nabla \cdot \left[D_0 D(S) \nabla S - K_S k(S) \hat{\mathbf{k}} \right] - F_w(S, Z, t), \tag{4.3.1}$$

$$\frac{\partial}{\partial t}[(b + \phi S)c] + \nabla \cdot [c\mathbf{u}] = \nabla \cdot [D_f \phi^d S^d \nabla c] - F(c, S, t)., \tag{4.3.2}$$

where the speed of water movement in the soil, $\mathbf{u}$, is given by Darcys law,

$$\mathbf{u} = -D_0 D(S) \nabla S + K_S k(S) \hat{\mathbf{k}}, \tag{4.3.3}$$

with S being the relative water saturation given by $S = \phi_1/\phi$, ϕ_1 being the volumetric water content, and ϕ being the porosity of the soil. D_0 (cm^2 day^{-1}) and K_S (cm day^{-1}) are the parameters for water 'diffusivity' and hydraulic conductivity, respectively. $D(S)$ and $k(S)$ characterize reduction in water 'diffusivity' and hydraulic conductivity in response to the relative water saturation decrease, where the functional forms for partially saturated soil are given by [193]. $\hat{\mathbf{k}}$ is the

vector pointing vertically downwards from the soil surface and F_w is the water uptake by the plant root system per unit volume of soil as given by [160].

For the P conservation equation, c is the P concentration in pore water, b is the soil buffer power, D_f is the P diffusivity in free water and d is an impedance factor given by the range $1.5 \leq d \leq 3$ [7, 133]. $F(c, S, t)$ describes the rate of P uptake by a surrounding root branching structure as in [161]. Both F_w and F are affected by the root structure which is predefined, water is only taken up by the main order roots while P is taken up by all roots.

For the soil surface boundary condition, a flux of water due to rainfall at the soil surface is applied, W_{dim} (cm s^{-1}) [159], which is the volume flux of water per unit soil surface area per unit time;

$$-D_0 D(S)\frac{\partial S}{\partial z} + K_S k(S) = W_{dim} \text{ at } z = 0. \tag{4.3.4}$$

The P soil surface boundary condition, given a rate of fertilisation Q_{dim} (μmol cm^{-2} s^{-1}), is,

$$-D_f \phi^d S^d \frac{\partial c}{\partial z} + W_{dim} c = Q_{dim} \text{ at } z = 0. \tag{4.3.5}$$

The boundary condition at the 'bottom' of the soil is assumed to be a zero flux boundary condition at a given level l_w, and is shown below for both water and P, respectively,

$$-D_0 D(S)\frac{\partial S}{\partial z} + K_S k(S) = 0 \text{ at } z = l_w. \tag{4.3.6}$$

$$-D_f \phi^d S^d \frac{\partial c}{\partial z} = 0 \text{ at } z = l_w. \tag{4.3.7}$$

Solving for relative water saturation (S) and P concentration (c) produces water and P profiles in depth and time.

The root growth rate equation used in the model by [161], allows the rate of

growth to slow down over time, i.e., the rate of growth is given by,

$$\frac{\partial l_i}{\partial t} = r_i \left(1 - \frac{l_i}{K_i}\right), \tag{4.3.8}$$

where l_i is the length of the order i root, r_i is the initial rate of growth of the order i root and K_i is the maximum length of an order i root.

4.3.3 Adaptations to Roose and Fowler Model

To combine the model in [159] with experimental data, climate parameters from a weather station are used, including rainfall, wind speed, temperature and humidity. These parameters allow for a more accurate calculation of the plant transpiration rate and the movement of water inside the soil and within the plant. These adaptations are made in [70] and successfully capture the movement of water within the soil profile and plant transpiration rates.

To model the water saturation levels in the soil, the flux of water into the soil (W_{dim}) is estimated from a combination of environmental factors. These include rainfall (R), humidity (H), wind speed (WS), temperature (T) and a constant (E), using a linear expression,

$$W_{dim} = \delta R + \alpha H + \beta T + \gamma WS + E, \tag{4.3.9}$$

where the parameters $\delta, \alpha, \beta, \gamma$ and E are to be determined from the optimal fit to the soil water saturation and climate data [70]. The flux of water (W_{dim}) can essentially be considered as Taylor expanded versions of any other non-linear relationships, for example the Penman-Monteith Equation [12]. Therefore, the formulation of Equation (4.3.9) allows for easy comparison with other models, should this be necessary.

The driving pressure, P (Pa), inside the root is determined by the environ-

mental conditions (humidity and temperature) causing the stomata in the leaves to open and close [190]. When the air temperature is low and/or humidity is high, the plant opens its stomata to speed up the loss of water and cause cooling, and this leads to a decrease in the pressure of water inside the roots. Thus the water pressure within the plant roots (P) is given by,

$$P = (p_r^0 + \lambda_3) + \lambda_1 T + \lambda_2 H, \tag{4.3.10}$$

where p_r^0 (Pa) is the baseline root pressure and λ_1 (Pa/^{o}C), λ_2 (Pa/% humidity) and λ_3 (Pa) are determined by seeking the optimal fit to soil saturation data and are used to help calculate F_w [70]. These parameters have been determined by [70] for a given geographical monitoring site.

A new feature is added to the model to match the root growth over the cropping season (where little growth is seen over the winter period) by making the rate of growth, temperature dependent. This transforms Equation (4.3.8) into,

$$\frac{\partial l_i}{\partial t} = r(T(t)) \left(1 - \frac{l_i}{K_i}\right), \tag{4.3.11}$$

where $r(T(t))$ is taken from experimental data on temperature dependant root growth rates, Table 4.1.

In summary, the data needed for the adapted model to run includes: initial distributions of water and P concentrations in the soil, climate data for rainfall, humidity, wind speed and temperature values, fertiliser application and amount, soil cultivation strategy and temperature dependant root growth rates which are obtained from experimental data. Henceforth, when referring to the 'model' we mean the adapted model extended from the one in [159], unless otherwise stated.

Temperature (^{o}C)	5	10	20	30
Average root growth rate (cm day^{-1})	0	0.2340	0.8234	1.299
Standard deviation / number of samples	0	0.0175	0.0150	0.0129

Table 4.1: Wheat root growth rates at four different temperature, 5, 10, 20 and 30^{o}C measured by WINRHIZO after 24 hours.

Type of data	Parameter	Value	Units	Source
Model parameter	D_0	10^3	cm^2 day^{-1}	[159]
Model parameter	K_S	5	cm day^{-1}	[159]
Model parameter	D_f	10^{-5}	cm^2 day^{-1}	[159]
Model parameter	d	3	-	[159]
Model parameter	l_w	200	cm	[159]
Model parameter	p_r^0	1	Pa	[159]
Model parameter	K_0	150	cm	[183]
Model parameter	K_1	7.9	cm	[71]
Model parameter	b	23.28	-	[71]
Model parameter	m	0.1 to 0.5	-	[70]
Model parameter	δ	2.69×10^{-2}	-	[70]
Model parameter	α	1.2×10^{-6}	m s^{-1} of water	[70]
Model parameter	β	2.22×10^{-6}	m s^{-1} of water/degC	[70]
Model parameter	γ	5.35×10^{-4}	m s^{-1} of water/ m s^{-1} of air	[70]
Model parameter	E	5×10^{-4}	m s^{-1} of water	[70]
Model parameter	λ_1	2.7×10^{-3}	Pa/ degC	[70]
Model parameter	λ_2	8.46×10^{-4}	Pa/% humidity	[70]
Model parameter	λ_3	7.9×10^{-2}	Pa	[70]
Model input	ϕ	0.3	-	[159]
Type of data	Description			Source
Model parameter	Temperature dependant root growth as in Table 4.1			Bangor pot experiment
Model input	Fertiliser strategies, Figure 4.2			Agrii*
Model input	Cultivation methods, Figure 4.2			Agrii*
Model input	Climate values for rainfall, wind speed, temperature and humidity			[70]
Model input	P concentrations at different depths, Figure 4.1			Bangor field experiment
Model output comparison	P uptake (kg P/ha) at GS39 and GS92 for Barley, Figure 4.3			ADAS field experiment
Model output comparison	P uptake (kg P/ha) at GS31, GS45 and GS91 for Barley, Figure 4.4			SRUC field experiment

Table 4.2: Types of data used in the modelling and where it is sourced. *General strategies used on fields across the UK were provided by Agrii.

4.3.4 Data Collection

From the Literature

To run the adapted mathematical model a set of parameters were taken from [70, 71, 159, 183], consisting of values for plant root dynamics and soil characteristics, Table 4.2.

Pot Trials

Triticum aestivum seeds were soaked overnight in aerated, de-ionised water to induce germination. They were then placed on filter papers, moistened with deionised water, put in parafilm sealed Petri dishes covered in aluminium foil and incubated at 20^oC. After 48 hours the root lengths of each emerged seminal root were measured non-destructively using a ruler. The filter papers were re-moistened and the Petri dishes were grouped into different controlled temperatures, heating at 5, 10, 20 and 30^oC. After another 24 hours the lengths of the seminal roots were again measured, and the differences in root length for each root were recorded as the average root growth rate per day.

Plant root growth rates increased from 5^oC at which a zero growth rate was observed, Table 4.1. A linear curve was fitted to the data such that the information could be translated into the mathematical model, for temperature T we set the growth rate R_T to be,

$$R_T = \begin{cases} 0 & \text{for} \quad T \leq 5^0 C \\ 0.053(T-5) & \text{for} \quad T > 5^0 C \end{cases}. \tag{4.3.12}$$

Field Trials

Two data sets were taken from field scale trials, which consisted of a set of scenarios for different fertiliser techniques measuring plant P uptake (offtake), one

winter barley and one spring barley. The winter barley data has values for P offtake at two different time periods, growth stages 39 and 92; 232 and 313 days respectively. The spring barley data has values for P offtake at three different time periods, growth stages 31, 45 and 91; 61, 77 and 151 days respectively. The spring barley variety used was Shuffle, being grown from seed, with typical farm inputs used (e.g. fertiliser, herbicide, fungicide, e.t.c.) except P which was imposed based on experimental requirements. The trial was based near Aberdeen in Scotland, approximately 57^{o}N. The trial was ploughed in January and ground power harrowed on the day of sowing (23-March-2011). The crop was rolled after sowing to consolidate the seedbed and reduce the risk of stone damage to harvesting equipment.

The field scale data only uses one Olsen P value for a given plot and there is no distinction concerning how P is distributed with depth. Therefore, to assess how P might be distributed within the soil profile, P concentrations were calculated at intervals of 10 cm down to a depth of 1 m, for three sets of soils; Olsen P index 5, 3 and 2, Figure 4.1. To match the data a constant P profile with depth and an exponentially decaying P profile with depth will be compared when running model simulations.

To provide a description of how plant-available P varies with soil depth, soil was collected from different depths within a spring wheat field trial located at Abergwyngregyn, North Wales. The soil is classified as a free draining, sand textured Eutric Cambisol. Samples were taken from four replicate plots (3 m $\times$ 12 m in size) at growth stage 39 at 10 cm intervals down the soil profile. Plant-available P was determined by extracting the soil with 0.5 M acetic acid (1:5 w/v) for 30 min, centrifuging the extracts (4000 g, 15 min) and colorimetric determination of P [126].

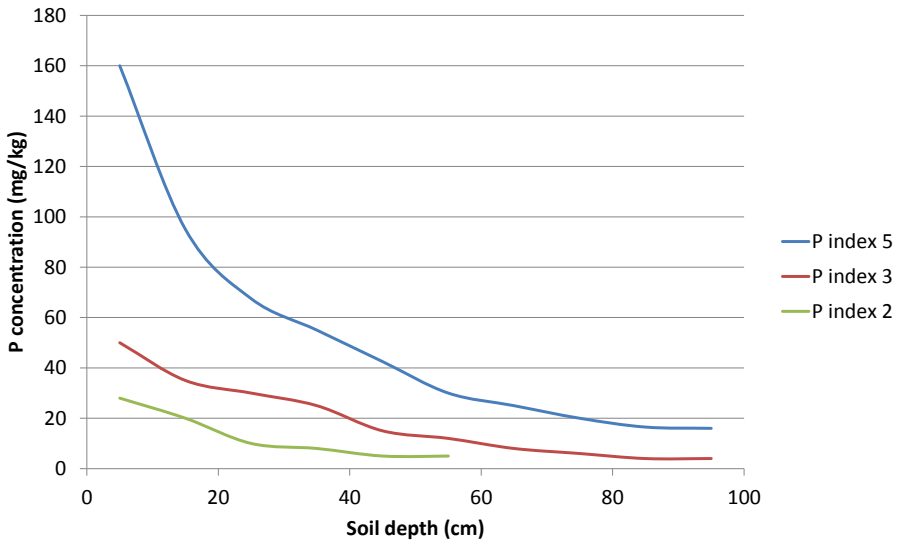

Figure 4.1: The concentration of P down the soil profile, taken at intervals of 10 cm down to 1 m, for three different sites; Olsen P index 2, 3 and 5.

4.3.5 Fertiliser Strategies

The model adapted in this paper is used to mimic field trials and predict plant P uptake (kg P/ha). In addition to the scenarios used in the field trial experimental data, we analyse the effects of different environmental conditions for a range of fertiliser and soil cultivation strategies.

We estimate that on average the ploughing depth is 25 cm. We use detailed climate data acquired from a site in Newbury, UK, consisting of hourly values for temperature, humidity, wind speed and rainfall (as in [70]). We used the climate data to calibrate the plant water uptake model from Chapter 3, and therefore the calibrated parameters and data are used within the adapted model.

The amount of fertiliser applied in an average cropping season ranges from 0 to 120 kg P/ha. Fertiliser can be applied in two different ways, branded and broadcasted. The branded application involves injecting fertiliser pellets 5-10 cm

below the soil and 5-10 cm away from the seed. This is represented in the model as fertiliser placed 9 cm below the seed. The aim is to put fertiliser next to where most of the roots are likely to grow to try to maximise root P uptake. The broadcasted approach spreads fertiliser on top of the soil. Note that the model can also be used to compare different fertiliser products that release P into the soil at different rates [184].

The adapted model estimates how different fertiliser strategies influence plant P uptake. The set of fertiliser strategies compared in the model are shown in Figure 4.2. The soil is first cultivated and then fertiliser is applied. During the cultivation phase, different methods are used to mix P in the soil. Ploughing evenly mixes P to a specific depth between 10-25 cm, whereas a reduced till gradient distributes P into bands; 0-5 cm, 5-10 cm and 10-15 cm with a P concentration ratio of 1.5:1:0.5 respectively, inverted plough inverts the P concentration between 0-15 cm, and lastly there is an option of no cultivation. We model either top soil fertilisation, fertilisation applied at 9 cm below the seed or no fertilisation, and use climate data with or without an increased amount of rainfall. For each strategy the model estimates plant P uptake which is then compared to a control with no fertilisation or cultivation for a given soil type and climate data.

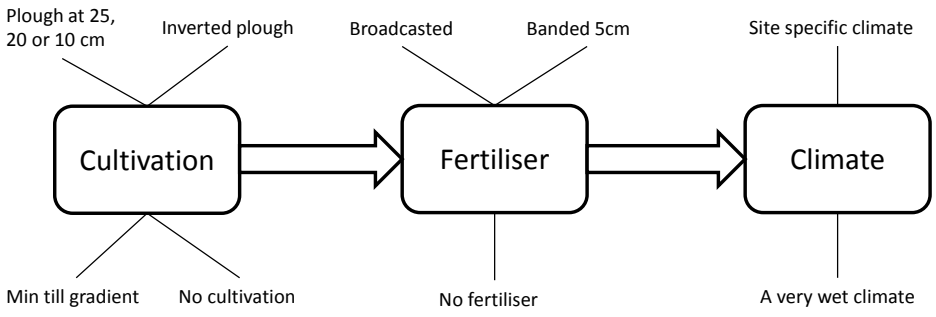

Figure 4.2: A set of scenarios to test the mathematical model; ploughing at 25, 20 or 10 cm, an inverted plough or using the reduced till gradient, top soil fertilisation, no fertilisation or fertiliser applied at 5 cm below and to the side of the seed, and finally using climate data with or without an additional constant heavy rainfall.

4.4 Results

Our adapted model based on the one by [159] estimates plant P uptake per soil surface area (kg P/ha). This adapted model is fitted against experimental field trial data to produce a site specific model. A selection of fertiliser strategies are then simulated using the model (Figure 4.2), and values for plant P uptake are compared to predict which strategy might, under certain climate conditions, estimate the highest plant P uptake.

By looking at the experimental data we find that the initial P distribution in the soil has a high concentration at the top of the soil and then the concentration decays with depth; at 1 m there is very little P left, Figure 4.1. This decay is much stronger for higher initial P concentrations, whereas at P index 1 there are almost indistinguishable changes in the P distribution (no decay). To assess the difference at P index 1 between a constant and an exponentially decaying P profile, we will model both profiles. In each case (constant and exponentially decaying P profiles) the total P down to 0.55 m is kept identical to represent similar amounts of P being available to the root system. The P profiles for a constant and exponentially decaying distribution are represented in Figures 4.5a and 4.5c, respectively, for time = 0 days.

A decimal code system is used to measure the growth stages of barley based on description stages [22], and we will also be using their notation. The model fits the winter barley data better at growth stage 39 (GS 39) compared with growth stage 92 (GS 92). At GS 39 the model predictions are within the error bars except for the scenario; 30 kg P/ha placed, Figure 4.3a. At GS 92 the model under predicts on all scenarios, but follows the trend of increasing plant P uptake values for increasing amounts of TSP applied, Figure 4.3b. The main reason for the under prediction stems from the unknown parameters, which include soil buffer power and the initial P profile in the soil. The initial P profile, at index

1, is depleted before the end of harvest and the final total plant P uptake is therefore capped. This depletion effect is also seen when modelling the spring barley data (Figures 4.4b and 4.4c), and in addition at GS 31 the model fails to capture the effects between small and large amounts of TSP applied, fitting well at 0-20 kg/ha but not at 30-90 kg/ha, Figure 4.4a. In regards to the spring barley crop, GS 31 is only a short time of 61 days and this is perhaps why little effects are seen between modelling different amounts of applied TSP. The amount of available P is unaffected by an additional supply as there is only a small root system generated by GS 31. The plant P uptake estimate from the model, on average decreases from a constant P distribution to an exponentially decaying P distribution. There is a decrease of 4.7% (GS 39) and 18.3% (GS 92) for winter barley, and -10.5% (GS 31), -12.3% (GS 45) and 5.0% (GS 91) for spring barley. The reason for a negative value (an increase in plant P uptake) for spring barley at GS 31 and 45 is due to a small root system, and as a consequence the P deeper in the soil profile has yet to be utilised.

The depletion of P for different initial P profiles can be seen in Figure 4.5. In a low P content soil (P1) with an exponentially decaying initial P distribution there is a reduction in plant P uptake rate after 147 days. This is because the majority of the available P is taken up at an early growth stage. This effect is not seen with a constant initial P distribution as P is spread out more evenly with depth; however the available P is still all taken up by the end of the simulation (GS 92, 313 days). For a high P content soil (P3) there is no decrease in the plant P uptake rate and most of the available P is taken up by the root system.

We tested the sensitivity of the model's output, plant P uptake, for two different parameters (soil buffer power and initial volumetric soil water content) to see if unknown or badly measured parameters would have an effect. We compared four different soil buffer power values 20, 23.28, 30 and 40 and found that plant

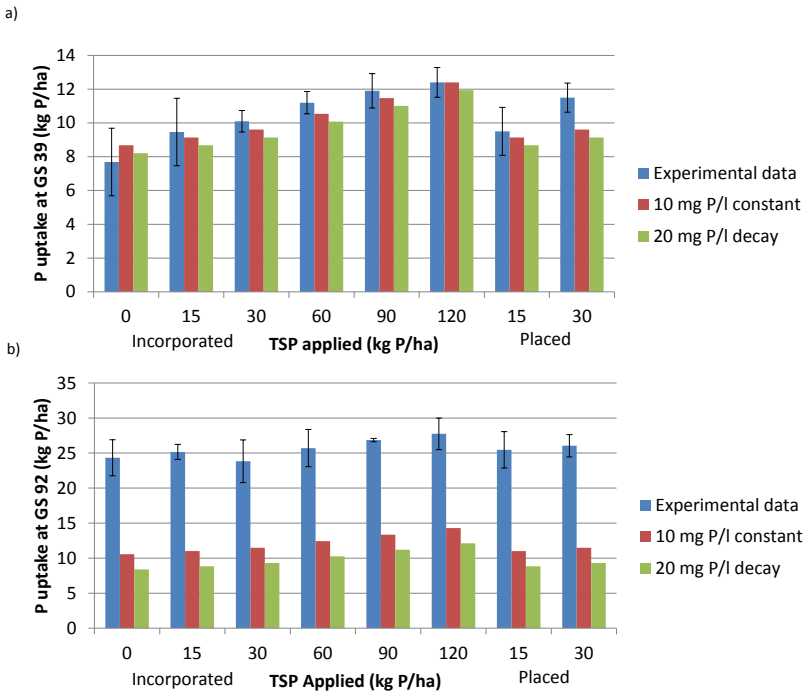

Figure 4.3: Experimental data and model predictions for winter barley at growth stages 39 (a) and 92 (b), for two modelled distributions for the initial P concentration, 10 mg P/l 'flat' and 20 mg P/l 'decay'.

P uptake is sensitive to the soil buffer power value, Figure 4.6a. Plant P uptake values at GS39 ranged between 8-12 kg P/ha, a large difference for only a small change in realistically measured soil buffer power values.

The initial volumetric soil water content is also changed to check its sensitivity, however little differences of 1% are seen between starting values of 0.1 to 0.5, Figure 4.6b. Thus, the initial volumetric soil water content has little effect on plant P uptake. Instead, the climate conditions throughout the cropping season affect plant P uptake as discussed below.

The model is simulated for a range of fertiliser and soil cultivation strategies under wet and normal climate conditions at GS 92, for an initial low P Olsen index soil (P1 20 mg/l P 'decay'; Figure 4.7a-normal, Figure 4.7b-wet) and a high P Olsen index soil (P3 60 mg/l P 'decay'; Figure 4.7c-normal, Figure 4.7d-

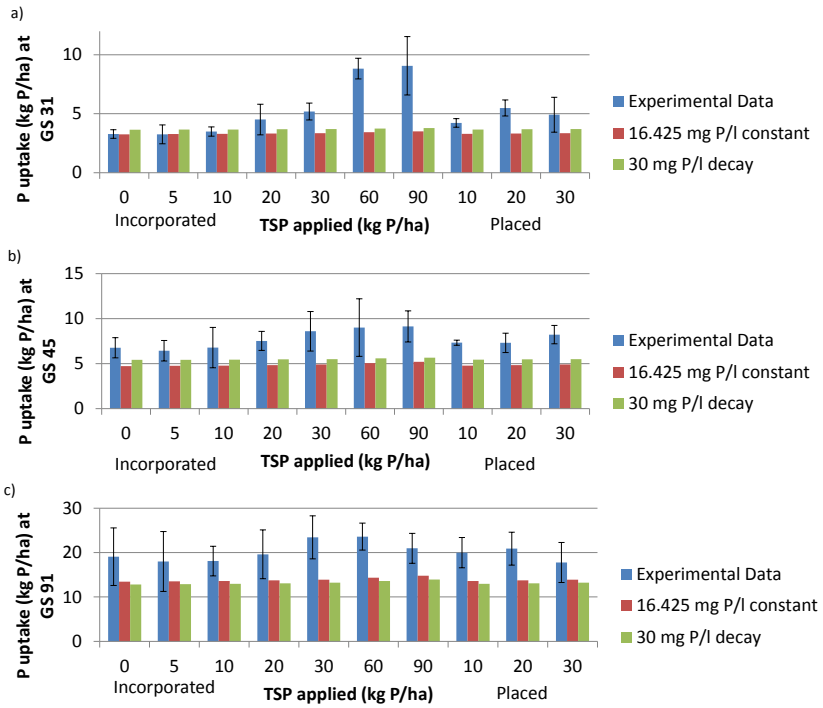

Figure 4.4: Experimental data and model predictions for spring barley at growth stages 31 (a), 45 (b) and 91 (c), for two modelled distributions for the initial P concentration, 16.425 mg P/l 'constant' and 30 mg P/l 'decay'.

wet). Instead of considering different amounts of applied fertiliser, six cultivation techniques are simulated (mix 25, 20 and 10 cm, inverted plough, min till and no cultivation) alongside 3 fertiliser treatments (placed 90 kg P/ha, incorporated 90 kg P/ha and no fertiliser). At GS 92 the highest plant P uptake is achieved from an inverted plough down to 15 cm and placing 90 kg P/ha, followed by mixing the soil to 25 cm and placing 90 kg P/ha. Under a wet climate, plant P uptake values are increased on average by 2% across all fertiliser and soil cultivation strategies; the highest increase of 5% was seen when broadcasting fertiliser. When broadcasting fertiliser the increased water helped diffuse the top soil P and allowed more to be taken up by the plant. In a high P index soil (P3) there is almost no response to plant P uptake values when adding P fertiliser, which is to be expected. For a low P index soil, plant P uptake is limited due to a lack of available P (depletion

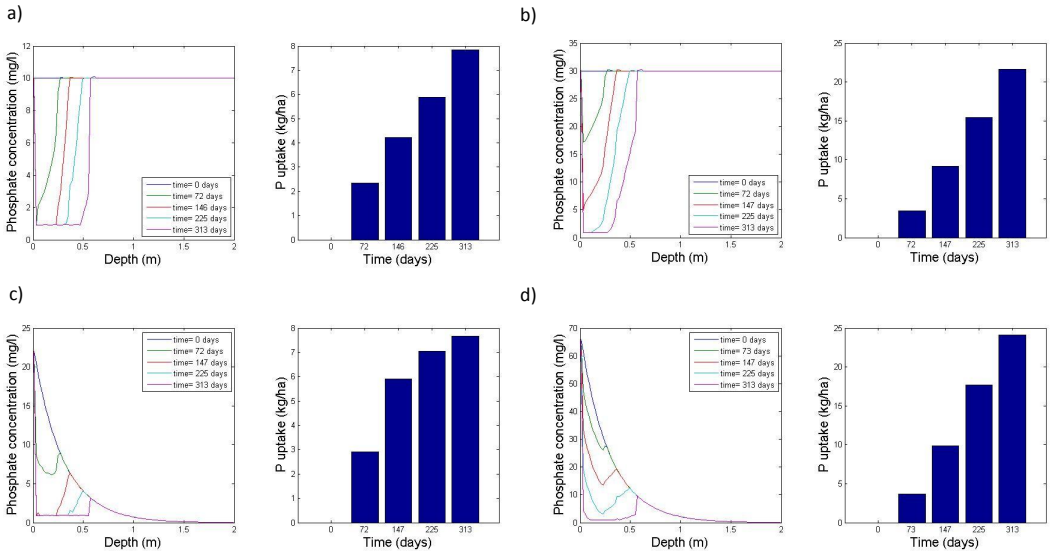

Figure 4.5: Model predictions for plant P uptake and P concentration against depth at five different times, 0, 72, 146, 225 and 313 (GS92) days, for a) an initial P concentration of 10 mg P/l 'flat' (P1-low), b) an initial P concentration of 30 mg P/l 'flat' (P1-high), c) an initial P concentration of 20 mg P/l 'decay' (P3-low) and d) an initial P concentration of 60 mg P/l 'decay' (P3-high).

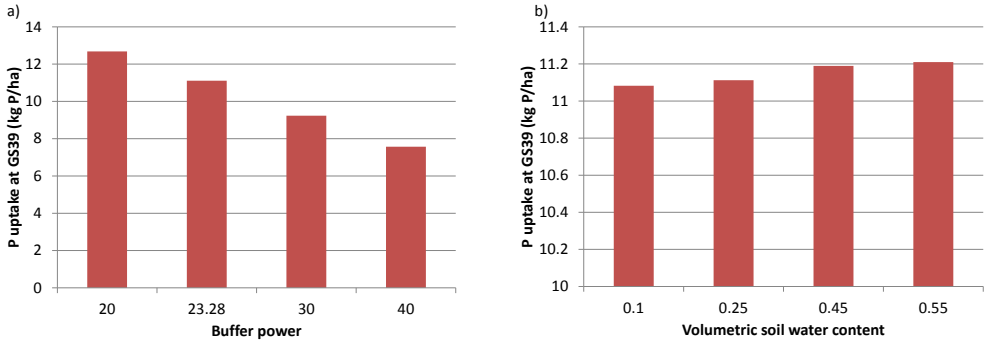

Figure 4.6: Model estimates for plant P uptake by the root system at growth stage 39 for a) four different soil buffer power values, 20, 23.28, 30 and 40; b) four different initial volumetric soil water content values, 0.1, 0.25, 0.45 and 0.55.

of P as seen in Figure 4.5) and this results in little distinction between ploughing techniques. Perhaps the simplistic implementation of the ploughing techniques does not capture certain subtleties, such as changing of the soil structure.

In summary, applying P near the rooting zone (inverted plough and mixing

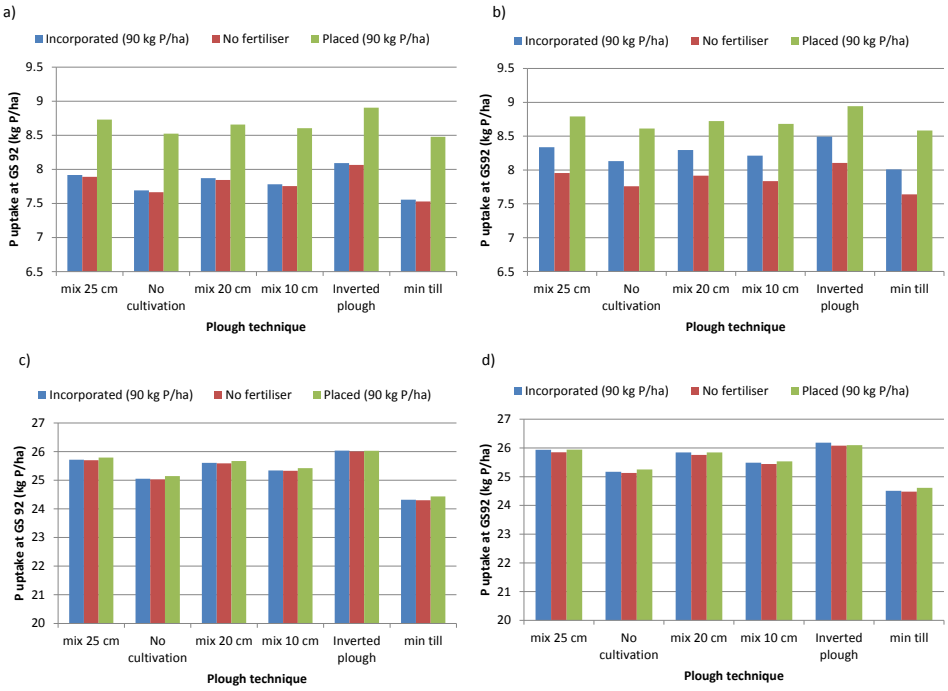

Figure 4.7: Model predictions for the set of scenarios described in Figure 4.2, for 6 cultivation strategies (mix at 25, 20 and 10 cm, no cultivation, inverted plough and min till) and 3 fertiliser placement options (90 kg P/ha incorporated (broadcast) or placed (banded) and no fertiliser), for a) and b) an initial P concentration of 20 mg P/l 'decay' (P1-low) for a normal and wet climate respectively, and c) and d) an initial P concentration of 60 mg P/l 'decay' (P3-high) for a normal and wet climate respectively.

at 25 cm while placing fertiliser) provides the best chance for maximising plant P uptake, and could result in a 4% increase to plant P uptake over doing nothing.

4.5 Discussion

To determine the optimal strategy for maximising plant P uptake, a set of fertiliser and soil cultivation strategies are simulated in the model. The difference between broadcasting and banding fertiliser depends upon price, accessibility and soil cultivation, etc. [111]. For example, applying fertiliser 20 cm away from the plant and at a depth of 10 cm in the soil gave optimal conditions for a certain

Maize plant study [141], and placing (banding) P was found to be better than broadcasting because of the enhanced P concentration within the rooting zone [152]. However, similar yields were seen between applying large amounts of P fertiliser via broadcasting or banding, and it was effects from starter P with rates as low as 20 lb P_2O_5/A that dramatically increased corn yields [180]. The model predicted that in a single harvest the ability to mix P in the rooting zone (inverted plough and mix at 25 cm) is highly desired over a min till gradient. In addition, placing fertiliser (banding) below the seed, rather than broadcasting, gave a sizeable increase of 11% to plant P uptake (6% for a wet climate). The effect of a heavy rainfall throughout the cropping season slightly increased average plant P uptake by 2% across all scenarios. The additional water could help increase the availability of P in the soil, and hence enhance plant P uptake.

The field trial data only had one Olsen P index to characterise the amount of available P in the soil. To represent this in the model, we let the P concentration in the soil have either an exponentially decaying or constant distribution with depth. By only knowing sparse information about the initial P concentration in the soil, a number of problems can arise. Firstly, if the concentration of P found in the soil is near a boundary (between Olsen P index 2 and 3, for example) then it is treated as an average in that category. Set amounts of fertiliser are prescribed to such soils and in certain cases this can cause a waste of resources [77]. In countries such as Ireland, there are stricter rules to the amount of applied P added to soils. Obtaining only one soil test for a field site can be misrepresentative and allow for more fertiliser to be added where perhaps it is not necessary. Secondly, there is a range between each Olsen P index and modelling a particular indexed soil can be ambiguous. For example, the model estimates that in a P index 1 soil, using an initial constant P distribution of 10 mg P/l will give a lower plant P uptake than 15 mg P/l by 33%. Perhaps further classification is needed when characterising

soils, to more accurately prescribe an optimal amount of fertiliser to add. This is the case in Scotland, where soils are given extra classification (namely descriptive features including, colour, texture, structure, consistence, organic matter, roots, stones, moisture, mottles and thickness of the horizon) to help use fertiliser more efficiently [181].

Current methods for calculating available P in soil are not consistent across Europe, with a wide range of techniques, each with their own methods, causing similar soils to have uncorrelated results [90, 129]. This provides confirmation that due to these current methods, site specific treatments are needed and one method cannot be used on all soils. However, new methods are being developed that calculate the amount of available P within the soil, that use more advanced methods compared to the very sensitive approach of Olsen P for example [195]. One method, Diffusive Gradients in Thin films (DGT) measures the diffusion of P taken from a soil sample to calculate the available P [185]. These new methods are trying to develop a robust method for all soils and if successful could result in a breakthrough and a better understanding of P within the soil.

Within some field sites there is little notion of how available P is distributed within the soil profile, with respect to depth. The idea that the majority of P added through fertilisers is given to the crop is partly true, as a set amount is locked up by the soil. However, from the modelling work presented in this paper we can conclude that the distribution of initial P within the soil profile affects total plant P uptake. There was a increase in plant P uptake, from a constant P distribution to an exponentially decaying P distribution, of 18.3% (GS 92) for winter barley, and 5.0% (GS 91) for spring barley. The field data for the distribution of P with depth showed an exponential decay of available P, with the majority of P situated within the top 30 cm. The steepness of the decay differs from P index to P index, decreasing with lower P content. In addition, it has been

shown that the steepness of decay for similar P content soils also differs from site to site [83] and this could alter the optimal fertiliser strategy. Data concerning the state and distribution of P within the soil is now becoming more available, as it can be used to save on fertiliser costs [209].

The soil buffer power value, a term used to describe the relationship between available and non-available P (in equilibrium), is very sensitive within the model. The higher the soil buffer power value the greater amount of P is bound to the soil and made unavailable. Small changes to the soil buffer power value causes plant P uptake values to vary by 50% (for soil buffer power values of 40 and 23.28, Figure 4.5). Field trial data generally has at best one value for the soil buffer power for a plot of land (sometimes its not even measured), despite the fact that there is evidence to show that this value changes within plots, and even with depth [13]. Therefore, to accurately model the available P within the soil, the soil buffer power value should be validated for site specific data and this could affect the optimal fertiliser and soil cultivation strategy. For example, for a high soil buffer power value a lot of applied P will be bound straight into the soil and form non-available P pools which the plant cannot access. For a high soil buffer power value there is a lower chance of adding P and getting a response in plant P uptake. In addition, when P is saturated so highly in a soil, possibly due to over-fertilisation [17], there is an increased loss of P due to eutrophication [68].

The idea to run down sites from a high P index 3, to 1 and 2 is achievable, but happening at a much slower rate due to over fertilisation where it is not necessarily needed [96]. It is therefore important to study which processes can help improve crop yields in low P content soils and perhaps more information is needed in this area. For example, field tests and the collection of more data in conjunction with models are necessary for the future.

Within this paper we have studied the effect of plant P uptake in barley for

different fertiliser and soil cultivation strategies given certain initial conditions. However in reality, these initial conditions change from year to year and what is best in one year is not necessarily best in the following year. A sustainable strategy is needed as well as a way of estimating how this will affect the soil 5 or 10 years from now. As long term field trials are expensive, models provide the ability to simulate the effects of different strategies.

Our advanced plant and soil model from Chapter 4 has been validated with experimental field study data, as well as climate data, resulting in a tool for estimating plant P uptake over the course of a crop life cycle. This work has given us a better understanding of the important factors concerning cultivation methods and fertiliser treatments for crops on a field scale. The aim of the modelling work is to guide future experimental studies on potential optimal strategies which can improve P efficiency in crops.

As a case study, the model from Chapter 4 was used to estimate how plant P uptake would be affected by adding combinations of struvite (slow release P fertiliser) and/or di-ammonium phosphate (DAP, fast release P fertiliser) to wheat. We found that a combination of both P fertilisers was optimal for plant P uptake, providing P early to boost initial root mass and later to maintain P uptake once the root system was at its biggest. For more details please see Appendix C.

Chapter 5

Conclusions and Future Work

In this Chapter we first summarise the findings from Chapters 1-4 and then discuss future ideas that would be extensions of the work carried out within this thesis.

5.1 Summary of Thesis Work

At the start of the thesis we began by introducing plant and soil management ideas focusing on the role of water and phosphorus (P). The use of models was discussed, which estimate water and P movement within the soil, from which predicting optimal soil cultivation and fertiliser management strategies can be achieved, via estimating plant P uptake. We use operational research techniques to find optimal parameter values, which maximise plant P uptake, and hence find potentially optimal strategies.

In Chapter 2 the root branching structure of a wheat crop was altered to see the effects it had on plant P uptake in a low P soil. Experimental work was carried out to validate the model and we found that changing from a linear to an exponential distribution of first order branches (a high number of branches at the top of the soil) improved plant P uptake by 142% for low P soils. This was however not enough to compensate plant P uptake for a drop from, a high P soil

to a low P soil (35.5 to 12.5 mg P l^{-1} respectively, using Olsen P index).

In Chapter 3 we described the movement of water in the soil around a plant root system during a year. The adapted model provided an estimate of the water content levels within the soil at different depths, and the uptake of water by the root system [160]. This model was validated using field data, which included hourly water content values at five different soil depths under a grass/herb cover over one year, and obtained a fully calibrated system for plant water uptake with respect to climate conditions. When compared quantitatively to a simple water balance model, our model achieved a better fit to the experimental data due to its ability to vary water content with depth. We found that to accurately model the water content levels in the soil profile, the sensitive Van Genuchten soil suction parameter and hydraulic conductivity values need to vary with depth. The Kriging algorithm was used to find optimal parameter values which fitted the model to the data set.

In Chapter 4 we considered different fertiliser strategies to find which one maximises total P taken up by the plant, estimated from advances to the model by [159]. The adapted model represented the development of the water and P profiles within the soil as spatial systems. Current cultivation techniques such as ploughing and a reduced till gradient were simulated along with fertiliser options to feed the top soil or below the seed. We found that a well-mixed soil (inverted and 25 cm ploughing) is critical for optimal plant P uptake and provided the best environment for the root system.

5.2 Future Work

A great deal of work has been presented within this thesis, looking at different models for predicting plant P and water uptake, and as a result a number of

extensions could be made to advance scientific understanding. Extensions 1 and 2 are part of the brief of an accepted-pending Post Doctoral Research Assistant position for the author, and are the subject for future publications.

5.2.1 Extension 1 - Coupling Root and Leaf Growth Models

Introduction

The model in Chapter 4 estimates plant P and water uptake by the root system and captures processes in the soil such as the root system and water and P diffusion. To more accurately model the whole plant, an above ground model could be added (leaf model), which tracks leaf growth and photosynthetic rates to estimate carbon mass stored by the plant. With the addition of a leaf model, carbon and leaf mass can be estimated during the crop life cycle. The role of carbon is used in conjunction with temperature to set the root growth rate [112]. As the two models are coupled they generate a feedback loop (in this case positive); an increase in plant P uptake from the roots increases carbon production via photosynthesis in the leaves, and vice versa.

This new model (root and leaf) can be compared against field trial data, and the set of scenarios from Chapter 4 Figure 4.2 can be evaluated to track the new models behaviour and predicted outcomes. Leaf mass estimates provide extra validation against experimental data (as leaf mass results at harvest are often recorded). In addition, carbon and leaf mass values provide a simple step to being able to estimate grain yield, another important validation against experimental data.

Two changes to the root model in Chapter 4 include, addition of a leaf model and root growth rate dependence upon temperature and carbon, which will be

discussed below in respective order.

The Leaf Model

We use a leaf model taken from Thornley [187], which estimates the mass of the leaf M_L (KgL), carbon M_c (KgC) and phosphorus M_p (KgP) as well as the concentration of free Carbon $[C] = M_c/M$ (KgC/KgL) and free P $[P] = M_p/M$ (KgP/KgL) within the plant. The leaf model takes into account photosynthesis, leaf litter and we have altered the leaf growth term, G_{sh}, to also be dependent upon the air temperature (A_T), as well as carbon and P. The governing equations are given below,

$$\frac{dM_L}{dt} = G_{sh} - \frac{K_{litt}}{1 + \frac{K_{mlitt}}{M_L}} M_L, \tag{5.2.1}$$

$$\frac{dM_c}{dt} = \epsilon k_1 [P] - f_c G_{sh} - \beta_c [C], \tag{5.2.2}$$

$$\frac{dM_p}{dt} = -f_p G_{sh} + (\alpha + \delta) - \beta_p [P] - k_p \epsilon [P] k_1, \tag{5.2.3}$$

where,

$$G_{sh} = k_g M_L [C][P] \frac{A_T^{s1}}{s_2^{s1} + A_T^{s1}}, \tag{5.2.4}$$

$$\epsilon = \frac{K_C M_L}{\left(1 + \frac{M_L}{k_m}\right)\left(1 + \frac{[C]}{J_C}\right)}, \tag{5.2.5}$$

where k_g is the leaf growth rate constant, K_{litt} is the litter rate constant, K_{mlitt} is the litter Michealis-Menten constant, K_C is the photosynthesis constant, k_m is the self shading constant, J_C is the product inhibition constant, f_c is the fraction of carbon (C) used for leaf growth, f_p is the fraction of phosphorus used for leaf growth, k_1 is the amount of P used for photosynthesis, k_p is the P:C ratio for photosynthesis production, β_c is the rate of C output to the phloem, β_p is the rate of phosphorus output to the phloem, α is the rate of P entry from the xylem, δ is

the rate of P entry from foliar application and s_1 and s_2 are fitting parameters. The parameter values and units for the leaf model are given in Table 5.1.

Parameter	Definition	Value	Units	Acquired
k_g	leaf growth rate constant	1000	$\left(\frac{\text{KgC}}{\text{KgL}}\frac{\text{KgP}}{\text{KgL}}\text{day}\right)^{-1}$	Thornley [187]
k_{litt}	litter rate constant	0.05	day^{-1}	Thornley [187]
k_{mlitt}	litter Michealis-Menten constant	0.5	KgL	Thornley [187]
k_C	photosynthesis constant	0.1	$\frac{\text{KgC}}{\text{KgL}}\text{day}^{-1}$	Thornley [187]
k_m	self shading constant	1	KgL	Thornley [187]
J_C	product inhibition constant	0.1	$\frac{\text{KgC}}{\text{KgL}}$	Thornley [187]
f_c	fraction of C used for leaf growth	0.5	$\frac{\text{KgC}}{\text{KgL}}$	Thornley [187]
f_p	fraction of P used for leaf growth	0.005	$\frac{\text{KgP}}{\text{KgL}}$	Thornley [187]
k_1	P used for photosynthesis	400	$\frac{\text{KgL}}{\text{KgP}}$	[183]
k_p	P:C ratio for photosynthesis production	0.005-0.05	$\frac{\text{KgP}}{\text{KgC}}$	estimated
β_p	rate of P output to phloem	0	$\frac{\text{KgL}}{\text{day}}$	n/a
α	rate of P entry from xylem	Root Model	$\frac{\text{KgP}}{\text{day}}$	Root Model
δ	rate of P entry from foliar application	0	$\frac{\text{KgP}}{\text{day}}$	n/a
A_T	Air temperature	Taken from data	^{o}C	Climate station
Fitting Parameter	**Definition**	**Bounds**	**Units**	**Acquired**
β_c	rate of C output to phloem	Fitting variable	$\frac{\text{KgL}}{\text{day}}$	Fitting
s_1	Air temperature slope constant	0-20	-	Fitting
s_2	Air temperature Transition constant	0-30	^{o}C	Fitting

Table 5.1: Parameter values and units used in the adapted Thornley leaf model.

The leaf model (Equation (5.2.1)-(5.2.3)) is coupled with the root model from Chapter 4 to obtain a full crop model. The equations are solved at the same time, where plant P uptake is an output from the root model (F in Equation (4.3.2)) and an input to the leaf model (α in Equation (5.2.3)), and carbon mass is an output of the leaf model (M_c in Equation (5.2.2)) and an input to the root model (C in Equation (5.2.6)). The main outputs of the coupled model are, plant P uptake by the root system (F in Equation (4.3.2)) and leaf mass (M_L in Equation (5.2.1)) which can be validated against experimental data. Other outputs of the model include, carbon mass (M_c in Equation (5.2.2)), different ordered root lengths (l in Equation (4.3.8)) and by extension, root mass.

Unknown parameters in the leaf model, β_c, s_1 and s_2, are fitted when validating against experimental field data for plant P uptake (Figures 4.3 and 4.4) and leaf mass values (Tables 5.2 and 5.3).

P fertilisation (kg P/ha)	Treatment	GS 31	s.e	GS 45	s.e	GS 91	s.e
0	n/a	1377.22	45.64	3016.13	162.93	14255.56	1462.39
5	inc	1342.94	98.39	2876.68	124.28	13783.33	2209.60
10	inc	1527.33	21.30	3310.92	395.58	13734.72	954.98
20	inc	1901.52	275.14	3502.36	221.67	13734.72	964.95
30	inc	2021.98	168.94	3706.82	367.20	13825.00	376.04
60	inc	2882.25	296.63	4232.44	560.19	14966.67	669.05
90	inc	3069.20	416.45	4111.29	222.79	15647.22	1148.89
10	plac	1679.89	92.90	3284.96	116.38	13894.44	833.62
20	plac	2129.09	192.46	3522.21	324.82	14715.28	967.73
30	plac	1893.09	296.84	4214.00	210.20	13122.22	1332.26

Table 5.2: Leafmass values (kg/ha) for spring barley at GS 31, 45 and 91 for different treatments of fertiliser, incorporated (inc) and placed (plac).

P fertilisation (kg P/ha)	Treatment	GS 39	s.e	GS 92	s.e
0	n/a	490.34	24.50	11147.22	553.14
15	inc	579.37	51.82	11616.96	567.39
30	inc	622.04	22.18	11123.91	168.39
60	inc	657.34	21.19	11429.05	717.31
90	inc	684.23	10.66	11979.22	221.34
120	inc	693.18	14.00	12167.73	525.69
15	plac	591.78	7.70	11763.60	719.50
30	plac	660.28	16.55	11788.30	198.42

Table 5.3: Leafmass values (kg/ha) for winter barley at GS 39 and 92 for different treatments of fertiliser, incorporated (inc) and placed (plac).

Root Growth Rate

The root growth rate used in Chapter 4, Equation (4.3.11), depends only upon temperature. Carbon mass is now estimated by the leaf model and can therefore also be used to affect the root growth rate. However, the root growth rate values

from Chapter 4 Table 4.1 measured at different temperatures, do not have values for carbon mass. We therefore let the root growth rate $r(T, C)$ be a function of carbon multiplied by a function of temperature, i.e. $r(T, C) = f(C)g(T)$. The function of carbon is a saturating one,

$$f(C) = \frac{C}{\gamma + C}, \tag{5.2.6}$$

where γ is the plant carbon mass when the root growth rate is half of its possible maximum. The value of γ is estimated by multiplying the fraction of structural carbon in structural dry matter by half the maximum root mass [187].

The function of temperature is similar to the one in Chapter 4 where the growth is represented by a linear distribution, Equation (4.3.12),

$$R_T = \begin{cases} 0 & \text{for} \quad T \leq 5^0 C \\ A(T-5) & \text{for} \quad T > 5^0 C \end{cases}, \tag{5.2.7}$$

where the constant A is set to fit the experimental data. As in Chapter 4 we set the root growth rate equal to zero when the temperature is less than or equal to 5^oC. The function of temperature is only valid for temperatures below 30^oC as the experimental data does not go beyond this. The root growth rate will eventually start to decrease as the temperature rises above a survivable threshold. For the UK climate this is not an issue with rarely maintained high temperatures above 30^oC, however higher temperature experiments would need to be carried out to provide values for possible root growth rates, for hotter climates.

Therefore, to match the root growth rate experimental data (Table 4.1), we set $A = 0.1961$ to minimise the SOS error and this fits the temperature profile as most curves are within the error bars, Figure 5.1.

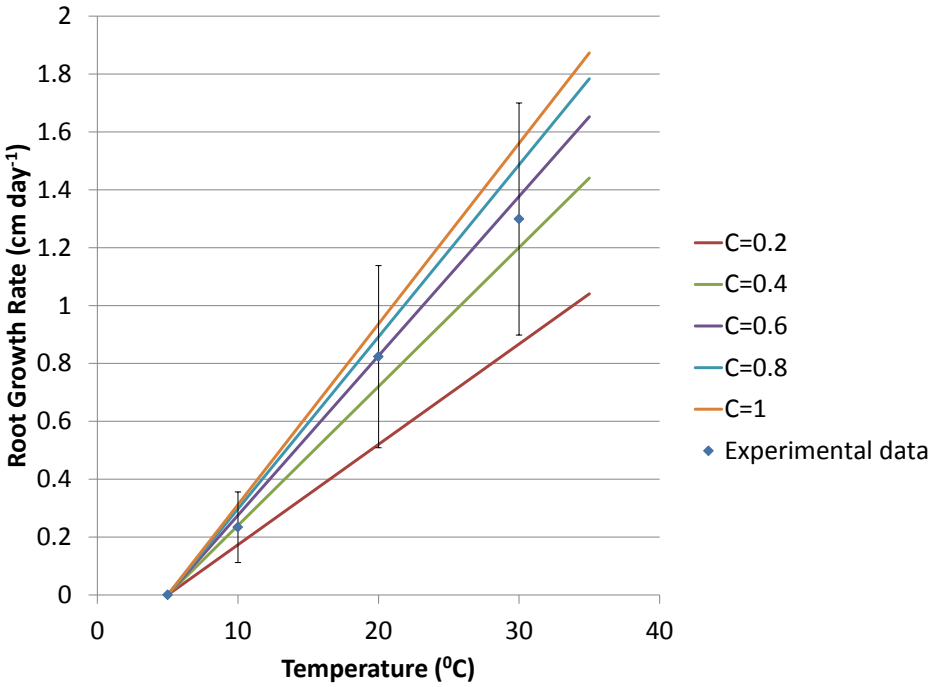

Figure 5.1: Comparison of experimental root growth rates against a function of carbon and temperature.

Results

The unknown parameters for the root and leaf model (β_c, s_1 and s_2) can be fitted by validating the model with the experimental data for plant P uptake from Chapter 4 and leaf mass values for the two barley sites, Tables 5.2 and 5.3.

It is possible to simulate the set of scenarios seen in Chapter 4, Figure 4.2. This will allow for a direct comparison with the root model alone. In addition, leaf mass estimates can be compared against experimental data available for the two barley trials.

Conclusion

The model in Chapter 4 underestimated plant P uptake compared with the experimental data at growth stage 91 and 92, for spring and winter barley respectively, perhaps because some processes were missing. With the addition of the leaf model

we hope to more accurately describe the whole crop system and capture the effects seen at harvest (plant P uptake and leaf mass values).

5.2.2 Extension 2 - P Dependent Root Growth

At present we use the model prescribed in Chapter 4 and Subsection 5.2.1 to estimate plant P and water uptake and the distribution of water and P within the soil profile. The model has only been partially validated from experimental data found in the literature, and two site specific data sets. However, in order to be fully predictive and to enable the model to be linked to graphical information systems (GIS) and maps to aid government decision-making, it needs to be validated to site specific data collected from farms across the whole country. Therefore, the model requires further enhancements that include, updating the model for new site specific data sets and to combine extra processes, such as groundwater movement and P dependant root growth (which occur in the soil). Currently the model uses one value for the buffer power which denotes the amount of available P within the soil. However, new evidence has shown that the amount of available and non-available P differs substantially between soil types and location [13]. When modelling the different sites it will be useful to compare buffer power values against plant P uptake.

To build upon the model from Chapter 4 and Subsection 5.2.1, we would initially validate the model against site specific data collected from farmers and industrial companies such as Agrii, ADAS and Teagasc. Secondly, additional features could be added into the model if they were found to be significant. The primary target would be to include a method to model the available P in the soil by using the buffer power, as it is very sensitive within each site and potentially with depth. Data provided by Agrii, for depth dependant P concentrations within the soil, will enable us to validate and test the model. P dependent root growth

rates can be collected experimentally from pot trials, similar to data obtained by Pete Talboys from Bangor University. In addition, water movement within the soil can be measured from TDR probes, and climate data for specific sites is available from the Met office.

The main aim of this research is to get a better understanding of the exact state of P within the soil, and therefore, relaying this valuable information to farmers via the external companies, agronomists (David Langton, Agrii), and the RB209 document from the Department of Environment, Food and Rural Affairs (DEFRA). This extension will give us a model which can be carried forward and applied to other sites and address other important questions of timings and amounts of fertiliser, for where there is only experimental evidence available. The combination of experimental data and modelling is key to efficiently use resources and predict possible outcomes.

5.2.3 Small Extensions

Grain Yield Approximation

We use plant P uptake (estimated from the models within this thesis) as a measure for P use efficiency, and hence try to find scenarios that maximise it. Another measure for P use efficiency is crop yield. Additionally, there are more crop yield data available to validate the model, and when conversing with industries, agronomists and farmers, having model outputs that are easy to understand and meaningfully (such as crop yield) are essential.

There are two main ways of estimating grain yield for the current models used within this thesis. The first and easiest, would be to convert the plant P uptake and leaf mass estimates into an estimate for grain yield. Data collected consisting of values for grain yield, plant mass and plant P uptake can be used to calculate a correlation between plant mass and plant P uptake against grain yield,

i.e. $A_1 * \text{plant mass} + B_1 * \text{plant P uptake} = \text{grain yield}$, where the parameters A_1 and B_1 can be estimated from the best fit of the data.

A more advanced technique, using the model from Subsection 5.2.1 (where carbon and leaf mass are estimated), is to actually model grain production. During the crop life cycle, part of the carbon produced from photosynthesis is stored within the plant, and along with the uptake of P, they are used to convert the leaf mass into grain. This process could be modelled by switching the crop's ability to store carbon and P, and instead grow grain depending upon the total amounts of carbon and P stored.

Implementing the Depth Dependent Van Genuchten Soil Suction Parameter

In Chapter 3 we found evidence that the Van Genuchten soil suction parameter along with the saturated hydraulic conductivity should change with the depth of the soil rather than remain constant. This could be further validated by taking the Cropwat model used as a comparison within the paper in Chapter 3 and adapting it, such that it does not use a constant value for the saturated hydraulic conductivity. The differences in the Cropwat model, between a constant and depth dependent saturated hydraulic conductivity, could then be assessed. The Cropwat model has the advantages of being quick to compute and it would be interesting to see how much the prediction of the water profile changes.

Comparing P Soil Test Methods

A number of soil tests for measuring P concentration within the soil were touched upon in Section 1.1.1, and different soil tests are more appropriate for different types of soil. Experimental data used within this thesis only used Olsen P values to estimate P concentration, but other sites have a range of soil test results. It

would be possible to estimate the error in the model's prediction for plant P uptake, from using other soil test methods. In addition, we may need to add additional processes to the model to account for different soil tests, such as the pH of the soil.

Virtual Plant Platform

A very long term plan for the work presented in this thesis is for the models to become part of a Virtual Plant Platform, which can take any model and estimate fertiliser requirements and soil cultivation strategies given certain site specific conditions. Our models along with others in the literature would go towards providing information based on agricultural problems facing farmers [44, 46, 60, 89, 101, 108, 115, 119, 142].

The Virtual Plant Platform would need to manage high amounts of computational data and require co-ordination between the many groups involved. This is because its aim is to use data from all sites and methods and link all treatments, such that each site can be given the best choice when it comes to managing crops.

All parties involved will be able to share techniques and resources to benefit the community. It is however still important to keep diversity among different methods in case of failures, but perhaps techniques for a number of different sites can be improved via the community getting involved together.

To some extent this is already being started, for example the International Soil Modelling Consortium (ISMC) has a range of models for agricultural and climate purposes.

Appendix A

Dissolution curves for P release

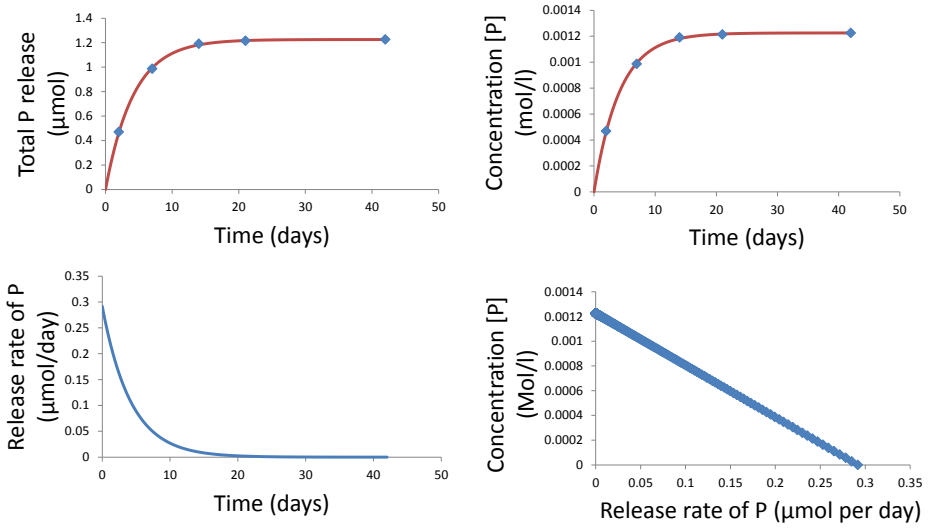

Figure A.1: Experimental release rates for a slow release fertiliser, Struvite.

Using the experimental data for struvite and DAP, we can plot curves for total P release against time and concentration against time, Figures A.1 and A.2. Integrating under the area of the total P release curve generates a plot for release rate of P against time. It is then possible to plot concentration of P against

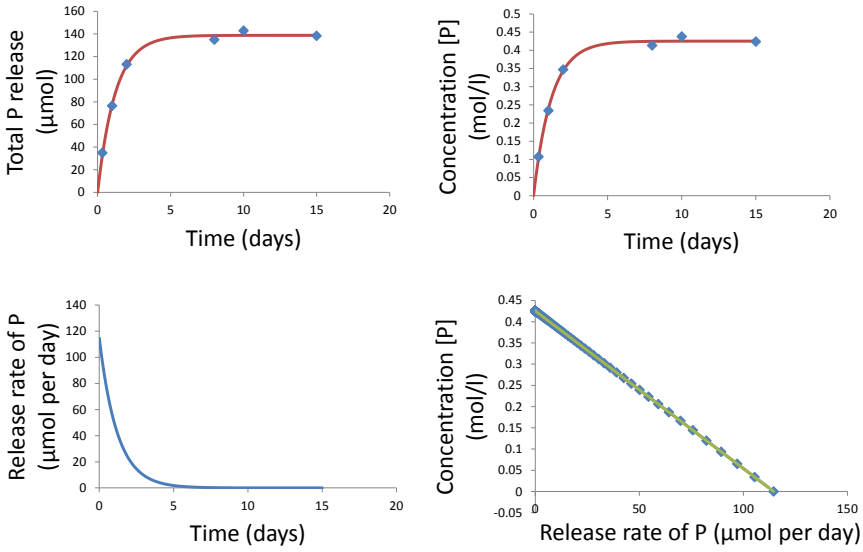

Figure A.2: Experimental release rates for a fast release fertiliser, DAP.

release rate of P (Figures A.1 and A.2) which is used as an input into the model in Chapter C. For a given concentration of P within the soil, an amount of P will be released. There is a maximum and minimum release rate for Struvite and DAP; at zero P concentration the release rates are 0.29 μ mol day^{-1} and 115 μ mol day^{-1} respectively, and the release rates for each drop to zero when the concentration is above 0.001225 Mol/l and 0.4244 Mol/l, respectively.

Appendix B

Root Structure for Struvite and DAP Experiments

Combinations of fertiliser are experimentally tested to see how plant P uptake and dissolved P recovery differs. Ratios tested (Struvite:DAP) are equivalent to 0:0, 80:0, 24:40, 24:56, 15:64, 8:72 and 0:80 kg/ha P_2O_5.

To adjust for the fast release fertiliser (DAP) stimulating earlier root growth, we adjust the branching frequency of first- and second-order roots. As in Chapter 2, we let the root branching distribution become exponential instead of linear, where at one extreme we have linear branching and the other, the majority of roots branch nearer the top of the soil. In addition, we also set the first 5 or 20 cm of the main ordered root to have a constant branching rate which then exponentially decreases, as this behaviour is seen from experimental data. We set the maximum branching density factor at 2.3, producing a maximum branching rate of 2.3*(0.7 cm^{-1}). Therefore, by adding only fast release fertiliser (DAP) we have the maximum branching rate and when adding no fertiliser (control) we have the minimum or standard branching rate (density factor is 1). To find the density factor for the mixed scenarios of slow and fast release fertiliser we fit a logarithm

curve bounded by the minimum and maximum values.

To fit a logarithm curve we first take the amount of P that is dissolved within the 90 day experiments for each ratio of fertiliser added. We add an amount to each (105 μmol P) and then calculate the percentage increase from the control, x_i. We then fit these data points to a logarithmic equation $\log(a(x_i + b))$, for fitting parameters a and b and match the ends points where the density factor is 1 and 2.3, for 0:0 and 0:80, respectively. A best fit is achieved by setting $a = 0.007946$ and $b = 342.0861$, minimising the SOS. To conserve the total number of root branches, the value for how exponential the branching density is (b from Equation (2.3.11)), is different for the two cases, 5 and 20 cm of constant branching. In Table B.1 the value of b for each strategy is shown.

Application	5 cm b value	20 cm b value
0:0	0	0
80:0	0.28	0.4
24:40	1.62	2.62
24:56	1.93	3.24
16:64	2.05	3.51
8:72	2.18	3.79
0:80	2.29	4.05

Table B.1: The value for the exponential branching constant b, for each fertiliser scenario for 5 or 20 cm of constant branching at the top of the root.

We can run the model for different ratios of fertiliser, to estimate plant P uptake and dissolved P recovery rates.

Appendix C

Struvite: A Slow-Release P Fertiliser for Sustainable Intensification?

Peter J Talboys[1], James Heppell[2], Jessica Daniel[1], Tiina Roose[3] John R Healey[1], Davey L Jones[1], Paul J A Withers[1]

[1]School of Environment, Natural Resources and Geography; Deiniol Road; Bangor; Gwynedd; LL57 2UW [2]Institute for Complex Systems Simulation; University of Southampton; UK; SO17 1BJ [3]Faculty of Engineering and the Environment; University of Southampton; UK; SO17 1BJ

C.1 Abstract

The increasing costs and inefficiency of using high rates of water-soluble phosphorus (P) fertilisers in global agriculture and the rapid depletion of finite rock phosphate reserves have led to a growing interest in the use of recycled sources of P, such as struvite extracted from wastewater. Struvite is markedly less soluble than conventional P fertilisers such as triple super phosphate (TSP) and di-ammonium phosphate (DAP), but is potentially more efficient because it continues to release P late in the growing season to meet total crop P demand. Using laboratory experiments, pot trials and mathematical modelling of the root system we found that struvite can be a component of an effective P fertiliser management strategy for crops. We show that struvite has greatly enhanced solubility in the

presence of organic acid anions; buckwheat which exudes a high level of organic acid was more effective at mobilising struvite P than the low level exuder spring wheat. Furthermore fertiliser mixes containing struvite and DAP applied to spring wheat demonstrated higher rates of P-fertiliser recovery, whilst also allowing optimal early P-uptake. These results indicate the potential resource savings and efficiency benefits of utilising a recycled slow release fertiliser like struvite and offers a more sustainable alternative to only using conventional, high solubility, rock phosphate based fertilisers.

C.2 Introduction

Phosphorus (P) is a plant macro-nutrient essential for cellular function and plant growth. In agriculture, P is often applied in the form of processed phosphate salt granules which dissolve into soil pore water allowing plant P uptake. Alongside other nutrient inputs, the application of these P fertiliser salts has enabled the rapid expansion in agricultural productivity in the developed countries during the 20^{th} century. Conventional mineral P fertilisers are derived from rock phosphate, global reserves of which, whilst not as limited as previously thought [47], remain finite and concentrated in only a handful of countries [81]. Our high dependency on P and the likely increase in their cost as rock phosphate reserves become harder to mine cost-effectively has prompted a renewed and urgent interest in the concept of re-cycled P [208]. For example, the P extracted from sources such as animal manures [61] or wastewater [98] can be processed into user-friendly fertiliser products for agriculture.

The development of fertilisers for agricultural use at a commercial scale using the P recycled from wastewater has gained much recent attention [33]. The greater usage of recycled P enabled by such products has the potential to be more efficient

from a global resource management perspective, prolonging the lifespan of existing rock P reserves, whilst also competing with rock P to ensure that P fertiliser prices remain affordable [47, 207]. The use of un-processed waste material that contains P is often difficult to spread and logistically complex; low P content can limit its value [125] and metal contamination can restrict its maximum limit of safe application [131]. Fertiliser-grade struvite ($NH_4MgPO_4 \cdot 6H_2O$) is one recycled P product that has good potential to overcome these difficulties, as it is easy to spread, has a high P content and can be produced with minimal heavy metal contamination [6].

Struvite is produced as a by-product of wastewater treatment; at locations within treatment plants where there are rapid pressure changes, it forms a scale on lines and clogs pipes [80]. However, controlled struvite precipitation can be triggered in specialised reactors by manipulation of the sludge digestion process to overcome these problems [9]. This can produce struvite granules that are useable as a fertiliser product for agriculture, whilst also removing > 85 % of solution P complying with UK environmental emission standards [6, 9, 168, 205]. Previous experimental evidence has shown that struvite can be at least as effective as mineral P sources when used as the sole P fertiliser [6, 113]. However, these have been end-point studies with results collected only at grain harvest, which have not assessed the potential pitfalls of using struvite as the sole P fertiliser on P uptake in the crucial early stages of plant growth and establishment [16, 20, 59, 62].

In addition to savings in resource use, the use of struvite provides potential efficiency savings and environmental benefits over conventional fertilisers due to its low solubility [14, 85, 113]. Conventional mineral P fertilisers are readily soluble and are either applied before crop sowing or top-dressed onto the soil surface. When applied in the seedbed, highly water-soluble P fertilisers causes high soil solution P concentrations in the early stages of crop development, but much of this

P becomes adsorbed onto soil particle surfaces [26]. This results in a much more limited P supply to crops in the later stages of growth, contrary to the timing of crop P demand which is far higher during the later stages of plant development [199]. When applied onto the soil surface, highly water-soluble fertilisers also cause high P concentrations in land runoff when rain falls soon after application [67, 206], with increased risk of eutrophication of receiving waterbodies. Struvite, as a less soluble slow release fertiliser, could provide longer term source of P for crop growth than readily soluble forms of P, thus more closely matching the plants demand for P later in the growing season and increasing its efficiency of use [208]. The slower dissolution of struvite could also reduce the amount of fertiliser P that becomes adsorbed on to soil particles, or released to land runoff. Un-processed rock P has previously been used as a slow release fertiliser with qualified success [28]. However, struvite is more soluble than rock P, whilst remaining significantly less so than conventional processed P fertilisers, which makes it more promising as a predictable slow release fertiliser [113]. These benefits could therefore potentially be used to either increase crop yields, or allow reduced application rates of P whilst maintaining or increasing yields with minimum environmental impact: all of which would be economically advantageous to the agricultural industry as it moves towards sustainable intensification in the future.

In this study, we investigated in laboratory and pot experiments whether struvite represents a more efficient and sustainable alternative fertiliser to conventional rock phosphate based fertilisers by answering the following questions. (1) Given that struvite is readily soluble in low pH conditions [136], does pH in the range found in UK agricultural soils (5.5-8.0) significantly affect its potential as a P fertiliser? (2) Do compounds exuded from plant roots, such as organic acids, affect the dissolution of struvite P, and does this influence its plant uptake? (3) Is replacing the application of readily soluble P fertiliser with struvite beneficial

for plant P uptake? (4) Does the slow release of P from struvite negatively impact early plant growth, and can this be compensated for by fertilisation with mixtures of soluble P and struvite? We uniquely included mathematical modelling to help answer these questions because of its ability to predict root uptake of nutrients [54, 60, 107]. Early root system models aimed to re-create detailed three-dimensional root systems [108], which were not conducive to simulating field scale growing conditions [163]. In the present study, in combination with pot-based experiments, we use the field scale root system model of [71, 159] which allows the significant up-scaling required to translate pot experiments into field scale predictions. This enabled us to assess with greater confidence which fertilisation strategies from the work in short term pot trials are viable candidates for future field experimentation.

C.3 Materials and Methods

C.3.1 Struvite Source

Struvite granules commercially distributed under the trade name Crystal Green® were provided by Ostara Nutrient Recovery Technologies Inc. These white granules have been classified as fertiliser grade material in the UK and measured approximately 2.4 mm in diameter. Crystal Green is precipitated from wastewater using the WASSTRIP™ [9] and PEARL® processes and the granules contain > 99 % struvite ($NH_4MgPO_4{\cdot}6H_2O$) equivalent to 12% P (28 % P_2O_5).

C.3.2 Struvite Solubility Assays

Reactions to test struvite solubility under varying pH conditions, using different counter-ions and in the presence of different organic acids including nil addition controls were performed in 1.5 ml tubes filled with deionised water. The deionised

water was buffered with 0.01 M Di-sodium EDTA and 0.01 M NaCl to stabilise both the pH, and salinity during the early period of dissolution. Solution pH was adjusted to between 5.5 and 8.0 using HCl and NaOH. Struvite granules weighing between 30 mg and 40 mg were then submerged in 1 ml of these solutions per replicate, and the resulting reaction mixtures were kept at room temperature. Solution aliquots of 5 μl were taken at successive time intervals, and their P content was determined using the ascorbate/molybdate blue method of Murphy and Riley [126]. Changes in solution P concentrations with time were plotted using a modified Mitscherlich Equation, which has been previously used to model rock P dissolution [109]:

$$c = a(1 - b^t), \tag{C.3.1}$$

where b is the curvature coefficient, a is the asymptote (equilibrium P concentration), c is the solution P concentration in mM and t is time elapsed in days.

Initial dissolution rates were calculated from the differential of Equation (C.3.1):

$$\frac{dc}{dt} = -a\ln(b)e^{t\ln b}. \tag{C.3.2}$$

For the assays including organic acids or counter-ions, all replicates were adjusted to pH 6.0 after the addition of either acetic acid, malic acid, oxalic acid, citric acid, $MgCl_2$, NH_4Cl or K_2HPO_4. The organic acids selected are known to be exuded by plant root systems [86], and are mono- (acetic acid), di- (malic acid, oxalic acid) or tri-valent (citric acid). The counter-ions are those present in struvite and therefore might be expected to affect dissolution rates.

C.3.3 Pot Experiments

The pot experiments used P fertilisers in the form of di-ammonium phosphate (DAP), triple super phosphate (TSP) or struvite, applied as granules placed at a

depth of 5 cm beneath the soil surface. Varying mixtures of DAP and struvite were also examined in the same manner. Placement of P fertilisers in this manner has previously been shown to offer significant advantages in P uptake over broadcast application, by enhancing the P content in the rooting zone [152]. Three seeds of *Triticum aestivum* (spring wheat) or *Fagopyrum esculentum* (buckwheat) were planted in 8 cm diameter 6.5 cm deep pots filled with 300 g sandy loam soil (30 and 36 day experiments), or for the long-term experiment (90 days) to mature grain yield in 11 cm diameter 30 cm deep drainpipes filled to the top with 3 kg of the same sandy loam soil. This soil (from Abergwyngregyn, UK) had a low Olsen P concentration of 12 mg l^{-1} which provided a P-limiting environment for plant growth according to current recommendation systems used in England and Wales [40]. The mass of each fertiliser (or mixtures of fertilisers) applied per pot was adjusted according to the pot surface area to produce a recommended constant rate of P fertilisation equivalent to 35 kg P ha^{-1} (80 kg ha^{-1} $P_2O_5^{3-}$). An additional mixture of struvite and DAP supplying 28 kg P ha^{-1} (64 kg $P_2O_5^{3-}$) was also included in one pot trial.

At crop emergence, the excess seedlings were removed to leave only the largest seedling in each pot. The pots were kept in a heated greenhouse with artificial lighting set to produce an air temperature of 20 ^oC and a minimum 16 hours of day length. Soil water holding capacity was measured gravimetrically, and the pots were watered thrice weekly by filling saucers at the bottom of the drainpipes for the long-term experiments or by maintaining the soil at 80 % of water holding capacity for the short-term experiments. To ensure that P was the only limiting macronutrient, the equivalent of 60 kg ha^{-1} N (as 1 M NH_4NO_3 solution) and 60 kg ha^{-1} K_2O (as 1 M KCl solution) were applied to each pot at seedling emergence. For the long-term experiment, an additional 60 kg ha^{-1} N was also applied at the stem extension growth stage as per current recommendations [40]. Micronutrients

were supplied in a weekly application of 10 ml of a solution containing: 5 mM $CaCl_2$; 2 mM $MgSO_4$; 765 nM $ZnSO_4$; 320 nM $CuSO_4$; 46.3 μM H_3BO_3; Na_2MoO_4 497 μM; 9.14 μM $MnCl_2$ and 38.7 μM Fe. EDTA (all Sigma Aldrich, Poole, UK). At harvest, the whole plant was extracted from the pot, the seed removed and weighed (if applicable), and then the root system washed in deionised water to remove any soil particles. All plant tissue was then dried at 85 ^{o}C overnight, weighed, and dry-ashed (550 ^{o}C, 16 h). The residue was dissolved in 0.5 M HCl and the P content was determined [126]. Any remaining stuvite granules were extracted from the soil, air dried, any adhering soil particles brushed off, and re-weighed at the end of each experiment. There were no discernable TSP or DAP granules remaining at the end of the short or long-term experimental periods.

C.3.4 Modelling P Uptake From a Growing Root System

A model that has previously been used to simulate P uptake from wheat root systems by accounting for P-fertiliser inputs and the resulting alterations in root branching was used [71, 159]. To account for the variations in solubility of different P fertilisers, a source term was added at a given soil depth to the P conservation equation used in the model. By varying the rate of fertiliser source over time, the model mimicked the effect of different combinations of soluble P (in this case DAP) and slow release P (in this case struvite) fertiliser on P uptake. The model was set up so that fertiliser P was released at depths between 0 cm and 10 cm below the seed, with peak release rates at 5 cm and a linear decline to zero at 0 cm and 10 cm. In order to match the release of fertiliser P in the model to the dissolution of DAP and struvite, a set of dissolution curves were produced (see Appendix A). This was done by placing a granule of DAP or struvite into 1 ml deionised water, and measuring the solution P concentration over time [126]. This was performed in triplicate for both fertilisers, with granule weights ranging from

30 to 40 mg as used in the pot trials.

The DAP and struvite P dissolution rates were first fitted by a modified Mitscherlich Equation (Equation C.3.1). The total release of P (μmol) was fitted against time, and integrated to acquire the release rate of P over time (μmol day^{-1}). Plots of concentration of P (mol l^{-1}, x) against release rate of P (μmol day^{-1}, y) were best fitted by a straight line. For DAP the equation was $y = (x - x_0)/y_0$, where x_0 is 0.4253 mol l^{-1} and y_0 is -0.003712 10^6day l^{-1}, whereas for struvite the equation was $y = (x - x_1)/y_1$, where x_1 is 0.0.001225 mol l^{-1} and y_1 is -0.004200 10^6day l^{-1}. Therefore, at a given soil solution P concentration, P was released from each fertiliser at an experimentally measured rate. When the soil solution P concentration rose above the point where P dissolution reached equilibrium for a fertiliser granule, its P release was halted. For DAP and struvite these values were estimated at 0.4253 mol l^{-1} and 0.001225 mol l^{-1} respectively. The two orders of magnitude difference in these values reflect the large difference in solubility between the two fertiliser types. In order to determine the change in soil P content as a result of P application for the model simulations, air dried samples were extracted according to the Olsen P method [137], or the acetic acid method [150] and P determined by colour [126].

To account for the differences between treatments in root branching structure following fertiliser application, the maximum root branching rates for plants under DAP, struvite and control (no fertiliser) treatments were calculated from images of intact 36-day-old *T. aestivum* root systems grown as described in Section C.3.3. The resulting maximum branching densities expressed relative to the controls as density factors were used to create root branching structures. The untreated control simulations used a constant root branching rate as has been done previously [71, 159] and the fertiliser treatments used a branching rate that decreased exponentially with increasing depth from a maximum that was calculated

by multiplying the relevant density factor by the normal branching rate measured previously [71]. In all simulations, the volume of the root system at 90 days was kept constant so that the final simulation results were comparable in terms of efficacy of treatments (see Appendix B).

The short-term pot experiments provided plant P uptake values 36 days after sowing. In the model we set an initial root length between 5 cm and 10 cm, which took approximately four days to reach in the experiments. The model was therefore run for 32 days to mirror the pot experimental data for this time-point. The model simulations used identical DAP and struvite treatments to the pot experiments described in Section C.3.3, and was run to a 90 day time-point to assess the effects of these treatments on total P uptake at harvest.

C.3.5 Statistical Details

Statistical testing was performed using Students t-test in Microsoft Excel, and two way ANOVAs in SPSS. P recovery is calculated as plant P content minus control treatment average plant P content, divided by applied fertiliser P.

C.4 Results

The solubility curves for struvite P over the pH range 5.5-8.0 provided good fits ($r^2 > 0.9$ for each replicate) to the modified Mitscherlich Equation, Figure C.1A. The initial struvite P dissolution rate showed a strong negative correlation with increasing pH ($r^2 = 0.78$, Figure C.1B), but there was no discernible impact of pH on the equilibrium P concentration in solution at the end point of the experiment. When the initial concentration of the counter-ions Mg^{2+}, NH_4^+ and PO_4^{3-} was varied at constant pH, there was a significant inhibitory effect of increasing initial PO_4^{3-} concentration on both initial dissolution rate and equilibrium P con-

centration ($p < 0.05$). Increased NH_4^+ concentration also significantly reduced the end-point equilibrium P concentration ($p < 0.05$). Initial P dissolution rate was not significantly affected by altering the starting NH_4^+ or Mg_2^+ concentration, with Mg_2^+ also having no significant effect upon equilibrium P concentration ($p > 0.05$).

The addition of four organic acids commonly exuded by plant roots [86], with equal pH to no organic acid controls, resulted in marked increases in struvite P solubility, Figure C.2. Both the initial rate of dissolution and the equilibrium P concentration (Figure C.2B) showed significant increases (by up to 69 % and 39 %, respectively) in the presence of 1 mM acetate, oxalate, malate and citrate. Furthermore, a pot experiment (Figure C.2C) found that the plant recovery of the P applied in struvite was very similar to that of the P applied in DAP (a positive control) when growing *F. esculentum*, which exudes organic acids in large quantities [211]. However, for *T. aestivum*, which does not exude large quantities of organic acids [128], the recovery of P applied in struvite remained at just 30 % of the level of that applied in DAP over the 36 day experimental period.

When *T. aestivum* was grown to harvest, use of struvite produced very similar rates of total P uptake (Figure C.3A) and grain yield (Figure C.3B) per plant to those obtained with use of TSP. However the number of mature grain heads produced was significantly increased ($p < 0.05$) by TSP application (control = 4.6 heads plant^{-1}, struvite 4.8 heads plant^{-1}, TSP 5.6 heads plant^{-1}). The rate of plant recovery of P from struvite was 175 % greater than from TSP (which had been added at the same P application rate per pot) (Figure C.3C). Any residue from the applied TSP granules could not be identified from the bulk soil and so has been assumed for these purposes to be completely dissolved. However, there were sizeable quantities of un-dissolved struvite after harvest in the long-term pot experiments (ranging from 65.6 % to 82.3 % of the initial mass).

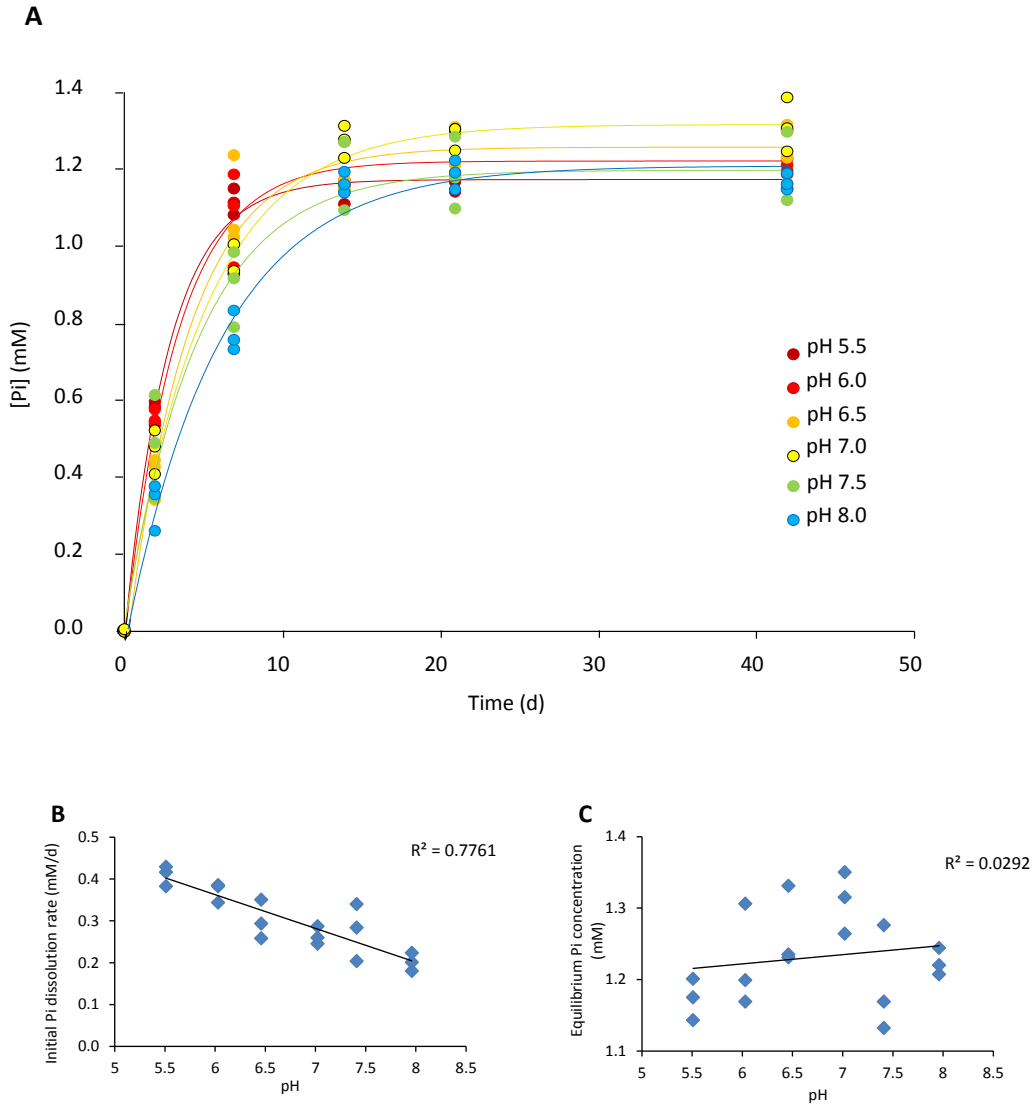

Figure C.1: The effects of solution pH on struvite dissolution. 2.4 mm diameter Struvite granules were submerged in 1 ml deionised water, adjusted to a pH range of 5.5 8.0. There were three replicates per initial pH. The concentration of solution P was measured over time, and the curve $f(x) = a(1 - bx)$ fitted to the data for each initial pH (A). All three replicates were used to fit each curve in A. The curve $f(x) = a(1-bx)$ was then fitted to each replicate individually, to calculate their initial P dissolution rate (B), and final equilibrium P concentration (C). The Pearson product-moment correlation coefficient for both datasets was calculated: showing a strong negative correlation between increasing pH and dissolution rate (B, r = -0.88), but no strong correlation between pH and equilibrium P concentration (C, r = 0.17).

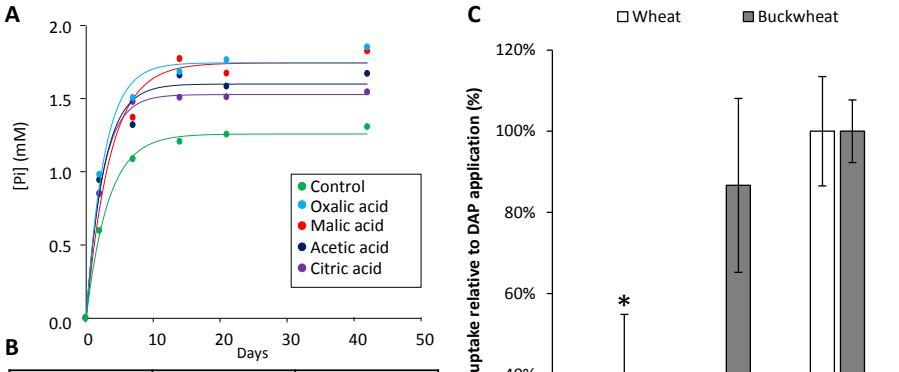

B

Organic anion (1 mM)	Equilibrium [Pi] (mM)	Initial dissolution rate (mM/day)
Control	1.258	0.381
Oxalic acid	1.745*	0.645*
Acetic acid	1.600*	0.616*
Malic acid	1.744*	0.489*
Citric acid	1.528*	0.635*

Figure C.2: Organic acids promote Struvite P dissolution and uptake. 2.4 mm diameter Struvite granules were submerged in 1 ml solutions containing 1 μM oxalic acid, malic acid, acetic acid, or citric acid; alongside an untreated control. There were three replicates per treatment. The concentration of solution P was measured over time, and the curve $f(x) = a(1-bx)$ was then fitted for each treatment to its average value for each time (A). The curve $f(x) = a(1-bx)$ was then fitted to each replicate individually: and used to calculate their initial P dissolution rate and final equilibrium P concentration and the mean of the three values for each treatment are shown (B). Asterisks represent values that are significantly different from the controls using students t-test ($p < 0.05$). (C) A 30-day pot experiment was conducted, growing seedlings of Triticum aestivum and Fagopyrum esculentum in 8 cm diameter pots containing a low-P loamy sand soil. P was applied at the equivalent of 80 kg ha^{-1} P_2O_5 in the form of DAP or struvite alongside untreated controls. At the end of the experiment remaining struvite granules were recovered from the soil dried and re-weighed. Any remaining undissolved DAP granules were not discernable from the bulk soil, and so were assumed to be 100 % dissolved The total plant P content, minus the average P content of untreated control plants, was divided by the total quantity of P dissolved from the fertiliser to determine the recovery rate of dissolved fertiliser P, which is expressed as a percentage of the DAP treatments P uptake for each species. Asterisks represent values that are significantly different from the DAP positive controls for each species using students t-test ($p < 0.05$, $n \geq 4$). Error bars are standard errors of the mean.

The 36 day pot experiments showed clearly that there was a significant reduction (by 39 %) in plant uptake of P within the first 36 days of growth using struvite

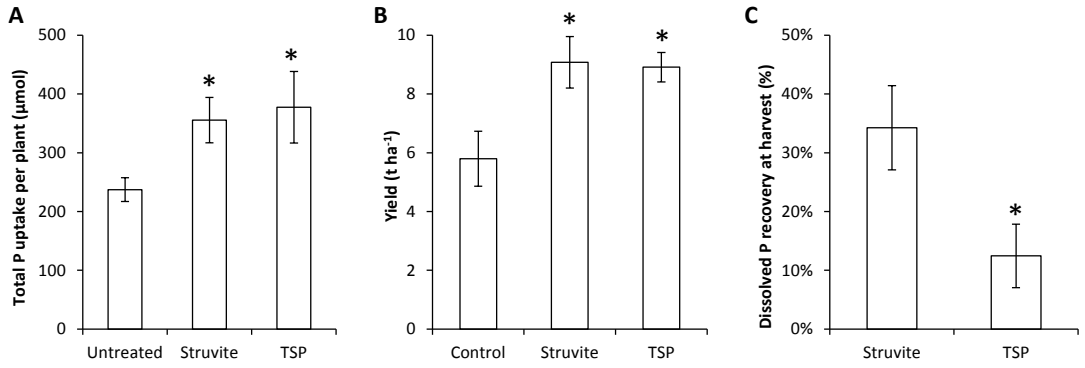

Figure C.3: Struvite fertilisation produces comparable outcomes of Triticum aestivum P uptake and yield to readily soluble P sources, with gains in P recovery rate. A pot experiment was conducted, growing *T. aestivum* to mature grain yield in 11 cm diameter, 30 cm deep pots containing a low-P loamy sand soil. P was applied at the equivalent of 80 kg ha^{-1} P_2O_5 in the form of Struvite or TSP alongside untreated controls. (A) The total P uptake resulting from each treatment, expressed in μmol plant^{-1}. (B) The grain yield, scaled up to t ha^{-1}, of each treatment. (C) The recovery rate in the harvested plants of the amount of P that had dissolved from the fertiliser granules at the end point of the experiment. At the end of the experiment remaining struvite granules were recovered from the soil dried and re-weighed. Any remaining undissolved TSP granules were not discernable from the bulk soil, and so were assumed to be 100 % dissolved The total plant P content, minus the average P content of untreated control plants, was divided by the total quantity of P dissolved from the fertiliser to determine the recovery rate of dissolved fertiliser P. In A and B, asterisks mark values that are significantly different from the untreated negative controls, and in C they mark values significantly different from the TSP positive control using students t-test ($p < 0.05$, n = 5-8). Error bars are standard errors of the mean.

in comparison with the readily soluble P fertiliser DAP, Figure C.4A. The use of mixtures of struvite with readily soluble P (where the struvite accounted for no more than 20 % of the total applied P) provided comparable levels of initial plant P uptake to the use of the readily soluble P fertiliser alone, Figure C.4A. Hence DAP at 80 % of the P applied was required to maximise early growth. Mixtures

of struvite with DAP in any ratio did not improve the rate of recovery in the plant of the P dissolved from the fertiliser compared with the treatment in which DAP alone was applied, Figure C.4B. This can be attributed to the presence of DAP in the mixture, which reduced the rate of recovery of dissolved P to less than 35 % of that achieved when struvite alone was used.

The outputs of the root P-uptake model are broadly corroborated by the results of the 36 day pot trial regarding both P uptake and recovery rate. In models using either Olsen P or acetic acid P to account for changes in soil P, plant P uptake over 36 days was very similar to that with DAP fertiliser alone for the 20:60 and 10:70 struvite:DAP treatments, whereas the P uptake for application of struvite alone and other mixtures was lower and similar to untreated controls, Figure C.4A. Similarly both models showed that recovery rates of dissolved P were very similar to the DAP only application for all struvite:DAP mixtures, and much lower than for struvite alone.

When the models were run to grain harvest at 90 days, exactly the same trends were observed as after 36 days. However, the total plant P uptake rates, and dissolved fertiliser P recovery rates were drastically different between the Olsen P and the acetic acid models, with the Olsen P model predicting control P uptake rates only 70 % of those predicted by the acetic acid model, Figure C.5A. The effectiveness of P fertilisation over the controls was also greater for DAP fertilisation alone (0:80) in the acetic acid model (87.8 %) than the Olsen P model (66 %), whereas this was not the case for struvite fertilisation alone (80:0) where the values were similar (10 % acetic acid model, 10 % Olsen P model).

C.5 Discussion

C.5.1 Struvite P is recovered by roots in greater quantities than for more soluble P fertilisers

The greater recovery rate in plants of P applied in struvite compared with the readily soluble P fertilisers (Figures C.2C, C.3B and C.4B) supports the theory that the slow rate of P release from struvite is closer to the development of the crop root systems capacity to take up P [113]. Increasing the proportion of applied fertiliser P taken up by the crop, as opposed to it replenishing stocks of residual soil P taken up by current or previous years crops offers a number of potential benefits to agricultural systems. Firstly, it decreases the crops allocation of photosynthate to root growth, exudates or mycorrhizas required to access and take up soil P, which is a significant cost for plants [97]. This may allow either a decrease in application of non-P fertilisers or an increase in yield for the same rate of P application. Secondly, the use of readily soluble P fertilisers has been shown to significantly increase the transfers of dissolved P in land run-off [67, 206], which has long been known to have the potential for serious environmental costs including eutrophication of water bodies [41, 169]. By increasing the proportion of applied fertiliser P taken up by the crop root system, potential pollution of water-courses is reduced. Thirdly, any dissolved fertiliser P that does becomes adsorbed to soil particle surfaces, or precipitated out by complexion with cations, may be bound with a sufficiently high binding energy to make it less available for plant uptake in the short term [10, 74]. This is of particular importance in soils with a high P-binding capacity that occur in many tropical areas where lack of food security is a serious issue for human well-being [166]. Strongly-bound residual P is also a source of P in land runoff due to erosion. Thus, minimising the amount of fertiliser P immobilised by the soil is economically and environmentally

important and the use of slow release P fertilisers such as struvite can contribute greatly to more sustainable crop production systems by maximising the proportion of applied P that is up-taken by the crop root system.

C.5.2 Struvite application alone does not allow sufficient early P uptake, but similar P uptake levels at harvest indicate benefits at later growth stages

The results show that use of struvite alone produces lower rates of P uptake early in plant development than does use of more readily soluble P fertilisers, Figure C.4A. This is a potential problem in agricultural systems, where initial establishment and early growth are dependent upon early P uptake, and correlate well with final crop yield [16, 20, 60, 62]. Good early growth is also viewed by the agricultural industry as an insurance against problems such as adverse weather conditions, pests, or diseases which may occur later in the growing period. Vigorous early growth also provides quicker soil surface cover, and therefore is useful in the reduction of soil erosion which can be a significant driver of environmental problems [145] and weed competition.

While in the pot experiments in controlled glasshouse conditions the yield of grain obtained from plants fertilised with struvite alone was the same as that for plants fertilised only with soluble P fertiliser, Figure C.3B, the plants grown with struvite had a visibly reduced number of reproductive shoots and grain heads in later growth stages. The number of grain heads has long been known to be both a very significant driver of final yield and is also determined at early growth stages [20], so this could be a disadvantage of use of struvite fertiliser alone in field conditions. It is possible that, in the pot experiment, early disadvantages for plant development of the slower release of P from struvite compared with more soluble P

fertiliser, Figure C.4A, were subsequently compensated by a more sustained rate of P release from struvite which was better able to meet plant P demand later in the growing season. Although the re-distribution of P already taken up by the plants meets a significant proportion of P demand for grain-filling, P-uptake from the soil at later growth stages may still be required to augment this [15, 60, 121], and also to facilitate carbohydrate translocation into the ripening grain [182].

C.5.3 Mixing struvite with a more soluble P source potentially enhances crop recovery of applied P

This study also attempted to couple the early P uptake levels of readily soluble DAP fertiliser (Section C.5.2) with the slow release and high plant P recovery rates of struvite (Section C.5.1), by combining the benefits of both approaches through the use of mixtures of the two fertiliser types. At 36 days, only a minimal quantity of the applied struvite had dissolved (9 %, when applied alone at 35 kg P ha^{-1}), but a much greater proportion had dissolved in a struvite only set of replicates in the pot trial taken to mature grain yield (26 %). These data further confirm that struvite provides a source of late season P which may significantly enhance yield [182]. In addition, the large quantities of undissolved struvite remaining after harvest could also provide a valuable resource of P for future growing seasons which is potentially a more readily plant available source of P than immobilised residual soil P.

The prediction stated in this section, that mixtures of struvite and readily soluble P fertilisers could maintain early plant P uptake, whilst elevating plant recovery rates of P dissolved from fertiliser, is corroborated by the model simulations, Figures C.4 and C.5. When using Olsen P to calibrate the model, the total P uptakes after 36 days fit the experimentally derived results reasonably well for the majority of treatments, Figure C.4A. However, using acetic acid extractable

P produced notable over-estimations of P-uptake at 36 days. As acetic acid extracted much more P that Olsen in this sandy soil, this suggests that the release of P from DAP increased soil available P beyond the level required for plant P uptake at this stage.

Interestingly, the model simulations predicted P uptake better when grown to harvest (90 days) when using acetic acid extractable P than Olsen extractable P to calibrate the model, Figures C.3A and C.5A. This is probably due to the model not including plant uptake from non-labile P-pools in the soil. The model simulations show clear indications that substituting struvite for readily soluble P in a fertiliser mixture has the potential to maintain soil P supplies for both early and late crop growth stages. Whilst fertiliser P recovery rates at 36 days were significantly lower for the fertiliser mixture treatments than for the application of struvite alone, the model results indicate a potential gain in dissolved P recovery rate after 90 days in the mixed treatments compared with use of the DAP alone, Figure C.5. It is interesting to note that the model simulations, despite being calibrated using struvite dissolution rates in controlled conditions, consistently under-estimated the degree of fertiliser P uptake resulting from struvite treatment alone (Figures C.4A and C.5A compared with Figures C.2C and C.3A respectively). This under-estimation may be due to an increase in struvite dissolution rate when in close proximity to roots exuding organic acid anions, with the amount of struvite dissolved in the model simulations only reaching 53 % (Olsen P model) or 1 % (Acetic acid model) of the experimentally derived values at 36 days, and 55.4 % (Olsen P model) or 6 % (acetic acid model) at harvest.

The results obtained from this model, validated against and then extrapolating from pot experiments, show its potential to provide a quick, cheap tool for assessing potential fertilisation strategies. Future utilisation of this method to predict field trials would however require fitting the model to field data as an

additional calibration step.

C.5.4 Struvites effectiveness as a P fertiliser may be enhanced for crop species that exude organic acids in large quantities

The results of the struvite solubility experiments showed a clear increase in both struvites P dissolution rate and the final solution equilibrium P concentration when treated with 1 mM of each of the organic acid anions tested, Figure C.2A. *Fagopyrum esculentum* also proved to be significantly more effective at taking up P after struvite fertilisation than *T. aestivum*, a result that could be attributed to its higher rate of organic acid exudation [210, 211]. The *F. esculentum* root system is known to exude large quantities of oxalic acid even when unstressed [211] and here we show that oxalic acid had the biggest impact on struvite solubility of the organic acids tested, Figure C.2B. This shows the potential benefit of increasing struvite use to fertilise other commercially valuable species whose root systems also exude organic acids in large quantities: this includes *Brassica napus* which exudes large quantities of malate and citrate [103] which were also shown to significantly enhance struvite dissolution in the present study, Figure C.2B. This interaction creates a specific advantage of struvite over conventional fertilisers for sustainable nutrition of crops when it is applied at depth in the soil: given the slow release of P from struvite in the absence of organic acids, relatively little of the P applied in struvite would have dissolved before the root system reaches the depth of the fertiliser. Then the proximity of the growing root system to the struvite granules could result in elevated organic acid concentrations and an increased rate of P release from the struvite in close proximity to the roots that can take up that P. This therefore has the potential to be a far more spatially precise, efficient

method of fertilising plants with P than application of conventional, readily soluble P fertilisers. Provided that it can be applied at the right depth relative to the growing root system of a young plant the increased initial struvite P dissolution rate in the presence of organic acid anions (Figure C.2) could also eliminate the need for mixing struvite with readily soluble P fertiliser to fulfil the crops early P uptake demands.

C.5.5 Soil pH, Mg^{2+} and NH_4^+ concentrations, are unlikely to be detrimental to struvite P-fertilisation

The present study showed the expected result [14] that the initial solubility of struvite was increased by a reduction in pH, but the final equilibrium P concentration was unaffected by pH, Figure C.1. When applied to soil in combination with readily soluble P fertilisers, the initial P dissolution rate of struvite is rendered unimportant: the soil solution P concentration will rapidly far exceed the point at which struvite dissolution is arrested (Figure C.1A) until either soil P-fixation, leaching or plant uptake removes sufficient of the dissolved P from solution. An important factor in this mixed fertilisation method is the equilibrium P concentration that struvite can maintain later in the growing season, once the effects of the readily soluble fertiliser P have diminished. This is unlikely to be significantly impacted by soil solution pH for this kind of fertiliser mix. The pot experiments used only soils with a pH of 6.0, but [113] have previously shown struvite fertilisation to be effective in moderately alkaline soils (pH 7.6), which adds further evidence that there is not a significant impact of pH within the range found in agricultural soils upon struvite effectiveness.

Experimentation on the effects of the presence of counter-ions on struvite P dissolution found that solution NH_4^+ concentration had a negative effect on the equilibrium P concentration. However, this effect was only small even over

the wide range of concentrations tested, so it is unlikely to be an important consideration when planning crop fertilisation strategies.

C.5.6 Conclusions

This study shows that replacement of readily soluble P fertilisers with struvite significantly alters a plant P uptake profile over time, with positive impacts on the proportion of fertiliser P recovered by the crop. Using mixtures of struvite and readily soluble P have shown promise as a more sustainable fertiliser strategy that maximises early crop nutrition, whilst also supplying P at later stages of plant development when P demand is at its peak. Our experimental evidence indicates that organic acids have a major impact on the rate of dissolution of P from struvite and a plant species whose root system exudes large quantities of organic acids is extremely effective at taking up P from struvite granules. Therefore struvite has an especially high potential for spatial and temporal targeting of P for root uptake for such crops. Further field experimentation is now required to assess the effectiveness of these proposed P fertilisation strategies under field conditions, for a wider range of soil types and cropping systems.

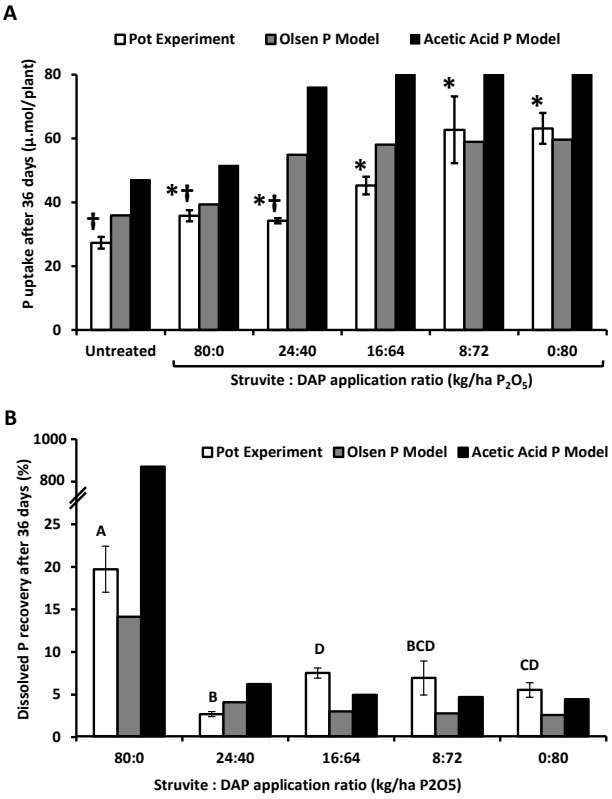

Figure C.4: Applying Struvite together with DAP allows the maintenance of early P uptake, whilst increasing P recovery in Triticum aestivum. In a 36-day pot experiment with *T. aestivum* P was applied at the equivalent of 80 kg ha^{-1} P_2O_5 in the form of Struvite and/or DAP alongside untreated controls. These were compared with model simulations carried out using measured concentrations of either acetic acid extractable P (black bars) or Olsen extractable P (white bars) to calibrate the total plant available P in the soil. (A) The total P uptake resulting from each treatment, expressed in μmol plant^{-1}. Asterisks mark pot trial values that are significantly different from the untreated negative controls, and daggers mark those that are significantly different from the 100 % DAP (0 : 80) positive control using students t-test ($p < 0.05$, $n \geq 3$). (B) The recovery rate of P that had dissolved from the fertiliser granules at the end point of the experiment. At the end of the experiment remaining struvite granules were recovered from the soil dried and re-weighed. Any remaining undissolved DAP granules were not discernable from the bulk soil, and so were assumed to be 100 % dissolved. The total plant P content, minus the average P content of untreated control plants, was divided by the total quantity of P dissolved from the fertiliser to determine the recovery rate of dissolved fertiliser P. Letters denote pot trial values significantly different from each other using students t-test ($p < 0.05$, $n \geq 3$). Error bars are standard errors of the mean.

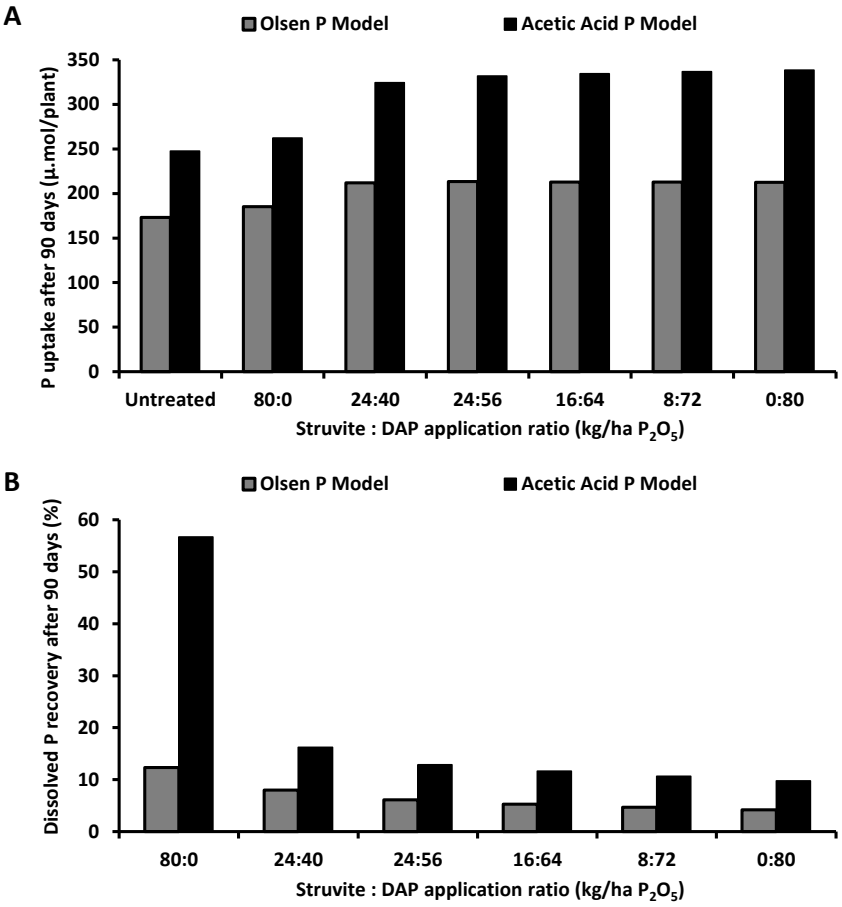

Figure C.5: Model results showing the benefit of applying struvite together with DAP for recovery of dissolved P compared with DAP alone without compromising P uptake in 90 day old *Triticum aestivum* plants. A-B Model simulations to 90 days after planting where P was applied at the equivalent of 80 kg ha^{-1} P_2O_5 in the form of Struvite and/or DAP and/or alongside untreated controls. These were compared with model simulations carried out using measured concentrations of either acetic acid extractable P (black bars) or Olsen extractable P (gray bars) to calibrate the total plant available P in the soil. (A) The total P uptake resulting from each treatment, expressed in μmol plant^{-1}. (B) The recovery rate of P that had dissolved from the fertiliser granules at the end point of the experiment.

Bibliography

[1] Aarts, E., and Korst, J. *Simulated Annealing and Boltzmann Machines*. J. Wiley and Sons, 1988.

[2] Al-Sultan, K., and Al-Fawzan, M. A tabu search hooke and jeeves algorithm for unconstrained optimization. *European Journal of Operational Research 103*, 1 (1997), 198–208.

[3] Allen, R., Smith, M., Perrier, A., and Pereira, L. An update for the calculation of reference evapotranspiration. *ICID Bulletin of the International Commission on Irrigation and Drainage 43*, 2 (1994), 35–92.

[4] Anderson, M., Hubbard, M., and Kneale, O. The influence of shrinkage cracks on pore water pressures within a clay embankment. *Quarterly Journal of Engineering Geology and Hydrogeology 15*, 1 (1982), 9–14.

[5] Andrei, A. Embankment stabilisation works between rayners lane and south harrow underground stations. *Ground Engineering 33*, 1 (2000), 24–26.

[6] Antonini, S., Arias, M., Eichert, T., and Clemens, J. Greenhouse evaluation and environmental impact assessment of different urine-derived struvite fertilizers as phosphorus sources for plants. *Chemosphere 89*, 10 (2012), 1202–1210.

[7] Barber, S. *Soil nutrient bioavailability: a mechanistic approach.* Wiley-Interscience, 1984.

[8] Battiti, R. First- and second-order methods for learning: between steepest descent and newton's method. *Neural Computation 4*, 2 (1992), 141–166.

[9] Baur, R. Waste activated sludge stripping to remove internal phosphorus. *US Patent 7* (2009), 604–740. US 7604740 B2.

[10] Beauchemin, S., Hesterberg, D., Chou, J., Beauchmin, M., Simard, R., and Sayers, D. Speciation of phosphorus in phosphorus-enriched agricultural soils using x-ray absorption near-edge structure spectroscopy and chemical fractionation. *Journal of Environmental Quality 32*, 5 (2003), 1809.

[11] Benton, T., Gallani, B., Jones, C., Lewis, K., Tiffin, R., and Donohoe, T. Severe weather and uk food chain resilience - detailed appendix to synthesis report. *Global food security* (2012). http://www.bis.gov.uk/go-science.

[12] Beven, K. A sensitivity analysis of the penman-monteith actual evapotranspiration estimates. *Journal of Hydrology 44*, 3-4 (1979), 169–190.

[13] Bhadoria, P., Kaselowsky, J., Classen, N., and Jungk, A. Soil phosphate diffusion coefficients: Their dependence on phosphorus concentration and buffer power. *Soil Science of America Journal 55*, 1 (1991), 56–60.

[14] Bhuiyan, M., Mavinic, D., and Beckie, R. A solubility and thermodynamic study of struvite. *Environmental Science & Technology 28*, 9 (2003), 1015–1026.

[15] Boatwright, G., and Haas, H. Development and composition of spring wheat as influenced by nitrogen and phosphorus fertilization. *Agronomy Journal 53*, 1 (1961), 33–36.

[16] Boatwright, G., and Viets, F. Phosphorus absorption during various growth stages of spring wheat and intermediate wheatgrass. *Agronomy Journal 58*, 2 (1966), 185–188.

[17] Borda, T., Celi, L., Zavattaro, L., Sacco, D., and Barberis, E. Effect of agronomic management on risk of suspended solids and phosphorus losses from soil to waters. *Journal of Soils and Sediments 11*, 3 (2011), 440–451.

[18] Bormann, H. Sensitivity analysis of 18 different potential evapotranspiration models to observed climate change at german stations. *Climate change 104*, 3-4 (2011), 729–753. DOI 10.1007/s10584-010-9869-7.

[19] Bray, R., and Kurtz, L. Determination of total, organic, and available forms of phosphorus in soils. *Soil Science 59*, 1 (1945), 39–46.

[20] Brenchley, W. The phosphate requirement of barley at different periods of growth. *Annals of Botany 43*, 169 (1929), 89–112.

[21] Briggs, K., Smethurst, J., Powrie, W., and O'Brien, A. Wet winter pore pressures in railway embankments. *Proceedings of the Institution of Civil Engineers - Geotechnical engineering 166*, 5 (2013), 451–465.

[22] Broad, H. The decimal code for the growth stages of cereals, with illustrations. *Annals of Applied Biology 110* (1987), 441–454.

[23] Bryd, R., Schnabel, R., and Shultz, G. A trust region algorithm for nonlinearly constrained optimization. *Society for Industrial and Applied*

Mathematics (SIAM) Journal on Numerical Analysis 24, 5 (1987), 1152–1170.

[24] Bucher, M. Functional biology of plant phosphate uptake at root mycorrhiza interfaces. *New Phytologist 173*, 1 (2007), 11–26.

[25] Cetin, B., Barben, J., and Burdick, J. Terminal repeller unconstrained subenergy tunneling (trust) for fast global optimization. *Journal of Optimization Theory and Applications 77*, 1 (1993), 97–126.

[26] Chang, S., and Chu, W. The fate of soluble phosphate applied to soils. *Journal of Soil Science 12*, 2 (1961), 286–293.

[27] Chen, Y., Dunbabin, V., Postma, J., Diggle, A., Siddique, K., and Rengel, Z. Modelling root plasticity and responce of narrow-leafed lupin to heterogeneous phosphorus supply. *Plant and Soil 372*, 1-2 (2013), 319–337.

[28] Chien, S., and Menon, R. Factors affecting the agronomic effectiveness of phosphate rock for direct application. *Fertilizer Research 41*, 3 (1955), 227–234.

[29] Clarke, D., and Smethurst, J. Effect of climate change on cycels of wetting and drying in engineered clay slopes in england. *Quartely Journal of Engineering Geology and Hydrogeology 43*, 4 (2010), 473–486.

[30] Clarke, D., Smith, M., and El-Askari, K. Cropwat for windows: User guide, version 4.2. See http://www.fao.org/nr/water/infores_databases_cropwat.html (accessed 09/06/2014).

[31] Clarke, D., Smith, M., and El-Askari, K. New software for crop water requirements and irrgation scheduling. *ICID Bulletin of the International Commission on Irrigation and Drainage 47*, 2 (1998), 45–58.

[32] Cordell, D., Drangert, J., and White, S. The story of phosphorus: Global food security and food for thought. *Global Environmental Change 19*, 2 (2009), 292–305.

[33] Cordell, D., and White, S. Sustainable phosphorus measures: strategies and technologies for achieving phosphorus security. *Agronomy 3*, 2 (2013), 86–116.

[34] Croney, D. *Design and Performance of Road Pavements*. Her Majesty's Stationery Office, London, UK, 1977.

[35] Déry, P., and Anderson, B. Peak phosphorus. *Energy Bulletin* (2007). Post Carbon Institute. energybulletin.net/node/33164.

[36] De Wit, C. Photosynthesis of leaf canopies. *Agricultural Research Reports 663 663* (1965). Wageningen: Pudoc.

[37] De Wit, C., Brouwer, R., and Penning De Vries, F. The simulation of photosynthesis systems. in: I. setlik (ed.); prediction and measurement of photosynthetic productivity. *Proceeding International Biological Program/Plant Production Technical Meeting Trebon* (1970). Wageningen: Pudoc.

[38] De Wit, C., and Goudriaan, J. Simulation of assimilation, respiration and transpiration of crops. *Simulation Monographs* (1978), 140. Wageningen: Pudoc, D.F1.22.50.

[39] Dennis, J., and Moré, J. Quasi-newton methods, motivation and theory. *Society for Industrial and Applied Mathematics (SIAM) Review 19*, 1 (1977), 46–89.

[40] Department for Environment, F., and (DEFRA), R. A. *Fertiliser Manual (RB209)*. The Stationery Office, Uk, PO Box 29, Norwich, NR3 1GN, 2010.

[41] Dodds, W., Bouska, W., Eitzmann, J., Pilger, T., Pitts, K., Riley, A., Schloesser, J., and Thornbrugh, D. Eutrophication of u.s. freshwaters: Analysis of potential economic damages. *Environmental Science & Technology 43*, 1 (2009), 12–19.

[42] Drew, M. Comparison of the effects of a localised supply of phsophate, nitrate, ammonium and potassium on the growth of the seminal root system and shoot in barley. *New Phytologist 75*, 3 (1975), 479–490.

[43] Driscoll, R. The influence of vegetation on the swelling and shrinking of clay soils in britain. *Géotechnique 33*, 2 (1983), 93–105.

[44] Dunbabin, V., Postma, J., Schnepf, A., Pagès, L., Javaux, M., Wu, L., Leitner, D., Chen, Y., Rengel, Z., and Diggle, A. Modelling root-soil interactions using three-dimensional models of root growth, architecture and function. *Plant and soil 372*, 1-2 (2013), 93–124. DOI 10.1007/s11104-013-1769-y.

[45] Dungait, J., Cardenas, L., Blackwell, M., Wu, L., Withers, P., Whitmore, A., Murray, P., Chadwick, D., Bol, R., Macdonald, A., and Goulding, K. Advances in the understanding of nutrient dynamics and management in uk agriculture. *Science of the Total Environment 434* (2012), 39–50. doi:10.1016/j.scitotenv.2012.04.029.

[46] Dupuy, L., Gregory, P., and Bengough, A. Root growth models: towards a new generation of continuous approaches. *Journal of Experimental Botany 61*, 8 (2010), 2131–2143.

[47] Elser, J., and bennett, E. Phosphorus cycle: A broken biogeochemical cycle. *Nature 478*, October (2011), 29–31.

[48] Finkel, D. Direct optimization algorithm user guide. *North Carolina State University* (2003).

[49] Fisher, J., DeBiase, T., Qi, Y., Xu, M., and Goldstein, A. Evapotranspiration models compared on a sierra nevada forest ecosystem. *Environmental Modelling & Software 20*, 6 (2005), 783–796.

[50] Forrester, A., Sóbester, A., and Keane, A. *Engineering Design via Surrogate Modelling: A practical Guide.* John Wiley & Sons, 2008.

[51] Frank, K., Beegle, D., and Denning, J. Recommended chemical soil test procedurec for the north central region. *Phosphorus (J.R. Brown, edition)* (1998), 21–30. Missouri Agricultural Experiment Station SB1001.

[52] Gahoonia, T., and Nielsen, N. Barley genotypes with long root hairs sustain high grain yields in low-p field. *Plant and Soil 262*, 1-2 (2003), 55–62.

[53] Gahoonia, T., and Nielsen, N. Root traits as tools for creating phosphorus efficient crop varieties. *Plant and Soil 260*, 1-2 (2004), 47–57.

[54] Ge, Z., Rubio, G., and Lynch, J. The importance of root gravitropism for inter-root competition and phosphorus acquisition efficiency: results from a geometric simulation model. *Plant and Soil 218*, 1-2 (2000), 159–171.

[55] Gentle, J. *Random Number Generation and Monte Carlo Methods.* 264 Kurasa, Kuchapishwa na Springer, 2004.

[56] Ghanbarian-Alavijeh, B., Liaghat, A., Guan-Hua, H., and Van Genuchten, M. Estimation of the van genuchten soil water retention properties from soil textural data. *Pedosphere 20*, 4 (2010), 456–465.

[57] Gilbert, J., and Nocedal, J. Global convergence properties of conjugate gradient methods for optimization. *Society for Industrial and Applied Mathematics (SIAM) Journal on Optimization 2*, 1 (1992), 21–42.

[58] Gormus, O., and Yucel, C. Different planting date and potassium fertility effects on cotton yield and fiber properties in the cukurova region, turkey. *Field Crops Research 78*, 2-3 (2002), 141–149.

[59] Grant, C., Flaten, D., Tomasiewicz, D., and Sheppard, S. The importance of early season phosphorus nutrition. *Canadian Journal of Plant Science 81*, 2 (2001), 211–224.

[60] Grant, R., and Robertson, J. Phosphorus uptake by root systems: mathematical modelling in ecosys. *Plant and Soil 118*, 2 (1997), 279–297.

[61] Greaves, J., Hobbs, P., Chadwick, D., and Haygarth, P. Prospects for the recovery of phosphorus from animal manures: a review. *Environmental Science & Technology 20*, 7 (1999), 697–708.

[62] Green, D., Ferguson, W., and Warder, F. Accumulation of toxic levels of phosphorus in the leaves of phosphorus-deficient barley. *Canadian Journal of Plant Science 53*, 2 (1973), 241–264.

[63] Grefenstette, J., and Baker, J. How genetic algorithms work: A critical look at implicit parallelism. *Proceedings of the Third International Conference on Genetic Algorithms* (1989), 20–27.

[64] Guely, F., and Siarry, P. Gradient descent method for optimizing various fuzzy rule bases. *Fuzzy Systems, Second IEEE International Conference 2* (1993), 1241–1246.

[65] Hansen, E. *Global optimization using interval analysis*. M Dekker, New York, 1990.

[66] Hargreaves, C., Gregory, P., and Bengough, A. Measuring root traits in barley (hordeum vulgare ssp. vulgare and ssp. spontaneum) seedlings using gel chambers, soil sacs and x-ray microtomography. *Plant and Soil 316*, 1-2 (2009), 285–297.

[67] Hart, M., Quin, B., and Nguyen, M. Phosphorus runoff from agricultural land and direct fertilizer effects. *Journal of Environmental Quality 33*, 6 (2004), 1954.

[68] Hartikainen, H., Rasa, K., and Withers, P. Phosphorus exchange properties of european soils and sediments derived from them. *European Journal of Soil Science 61*, 6 (2010), 1033–1042.

[69] Hasancebi, O., and Erbatur, F. Evaluation of crossover techniques in genetic algorithm based optimum structural design. *Computers and Structures 78*, 1-3 (2000), 435–448.

[70] Heppell, J., Payvandi, S., Zygalakis, K., Smethurst, J., Fliege, J., and Roose, T. Validation of a spatial-temporal soil water movement and plant water uptake model. *Geotechnique 64*, 7 (2014), 526–539.

[71] Heppell, J., Talboys, P., Payvandi, S., Zygalakis, K., Fliege, J., Withers, P., Jones, D., and Roose, T. How changing root system architecture can help tackle a reduction in soil phosphate (p) levels for better

plant p acquisition. *Plant, Cell & Environment 'In press'* (2014), 1–33. doi: 10.1111/pce.12376.

[72] Hermans, C., Hammond, J., White, P., and Verbruggen, N. How do plants respond to nutrient shotage by biomass allocation? *TRENDS in Plant Science 11*, 12 (2006), 1360–1385. doi:10.1016/j.tplants.2006.10.007.

[73] Ho, M., Rosas, J., Brown, K., and Lynch, J. Root architectural tradeoffs for water and phosphorus acquisition. *Functional Plant Biology 32*, 8 (2005), 737–748.

[74] Holford, I., and Mattingly, G. The high- and low-energy phosphate adsorbing surfaces in calcareous soils. *Journal of Soil Science 26*, 4 (1975), 407–417.

[75] Holland, J. *Adaptation in Natural and Artificial Systems.* 2nd Ed, MIT Press, 1992.

[76] Holloway, G., and Paris, Q. Production efficiency in the von liebig model. *Agricultural and Applied Economics Association 84*, 5 (2002), 1271–1278.

[77] Hooda, P., Truesdale, V., Edwards, A., Withers, P., Aitken, M., Miller, A., and Rendell, A. Manuring and fertilization effects on phosphorus accumulation in soils and potential environment implications. *Advances in Environmental Research 5*, 1 (2001), 13–21.

[78] Huyer, W., and Neumaier, A. Global optimization by multilevel coordinate search. *Journal of Global Optimization 14*, 4 (1999), 331–355.

[79] Iman, R., Davenport, J., and Zeigler, D. *Latin hypercube sampling (a program users guide), Technical Report SAND791473.* Albuquerque, NM, USA: Sandia National Laboratories, 1980.

[80] Jaffer, Y., Clark, T., Pearce, P., and Parsons, S. Potential phosphorus recovery by struvite formation. *Water Research 36*, 7 (2002), 1834–1842.

[81] Jasinski, S. Usgs minerals information: Phosphate rock. *U.S. Geological Survey* (2013).

[82] Jeuffroy, M., Vocanson, A., Roger-Estrade, J., and Meynard, J. The use of models at field and farm levels for the ex ante assessment of new pea genotypes. *European Journal of Agronomy 42*, October (2012), 68–78.

[83] Jobbágy, E., and Jackson, R. The distribution of soil nutrients with depth: Global patterns and the imprints of plants. *Biogeochemistry 53*, 1 (2001), 51–77.

[84] Johnson, M., Moore, L., and D., Y. Minimax and maximin distance designs. *Journal of Statistical Planning and Inference 26*, 2 (1990), 131–148.

[85] Johnston, A., and Richards, I. Effectiveness of different precipitated phosphates as phosphorus sources for plants. *Soil Use and Management 19*, 1 (2003), 45–49.

[86] Jones, D. Organic acids in the rhizosphere a critical review. *Plant and Soil 205*, 1 (1998), 25–44.

[87] Jones, D., Perttunen, C., and Stuckman, B. Lipschitzian optimization without the lipschitz constant. *Journal of Optimization Theory And Aplpications 79*, 1 (1993), 157–181.

[88] Jones, D., Shannon, D., Murphy, D., and Farrar, J. Role of dissolved organic nitrogen (don) in soil n cycling in grassland soils. *Soil Biology and Biochemistry 36*, 5 (2004), 749–756.

[89] Jones, J., Hoogenboom, G., Porter, C., Boote, K., Batchelor, W., Hunt, L., Wilkens, P., Singh, U., Gijsman, A., and Ritchie, J. The dassat cropping system model. *European Journal of Agronomy 18*, 3-4 (2003), 235–265.

[90] Jordan-Meille, L., Rub, G. Ehlert, P., Genot, V., Hofman, G., Goulding, K., Recknagel, J., Provolo, G., and Barraclough, P. An overview of fertilizer - p recommendations in europe: soil testing, calibration and fertilizer recommendations. *Soil Use and Management 28*, 4 (2012), 419–435.

[91] Jungk, A., and Claassen, N. Ion diffucion in the soil-root system. *Advances in Agronomy 61* (1997), 53–110.

[92] Jury, A., and Claassen, N. The role of science in solving the world's emerging water problems. *Proceedings of the National Academy of Sciences of the United States of America (PNAS) 102*, 44 (2005), 15715–15720.

[93] Kamprath, E., Beegle, D., Fixen, P., Hodges, S., Joern, B., Mallarino, A., Miller, R., Sims, J., Ward, R., and Wolf, A. Relevance of soil testing to agriculture and the environment. *Council for Agricultural Science and Technology Issue paper*, 15 (2000).

[94] Krige, D. A statistical approach to some of the borehole values in the orange free state goldfields. *Journal Chemical Metallurgical and Mining Scoiety South Africa 53* (1952), 47.

[95] Kurganov, A., and Tadmor, E. New high-resolution cantral schemes for non-linear conservation laws and convection-diffusion equations. *Journal of Computational Physics 160*, 1 (2000), 241–282.

[96] Lalor, S., Wall, D., and Plunkett, M. Maintaining optimum soil fertility - focus on offtake. *Proceedings of Spring Scientific Meeting 2013, The fertilizer association of Ireland 48* (2013).

[97] Lambers, H., Raven, J., Shaver, G., and Smith, S. Plant nutrient-acquisition strategies change with soil age. *Trends in Ecology & Evolution 23*, 2 (2008), 95–103.

[98] Le Corre, K., Valsami-Jones, E., Hobbs, P., and Parsons, S. Phosphorus recovery from wastewater by struvite crystallization: a review. *Critical Reviews in Environmental Science and Technology 39*, 6 (2009), 433–477.

[99] L'Ecuyer, P. Uniform random number generation. *Annals of Operational Research 53*, 1 (1994), 77–120.

[100] Leitner, D., Klepsch, S. Bodner, G., and Schnepf, A. A dynamic root system growth model based on l-systems. tropisms and coupling to nutrient uptake from soil. *Plant and Soil 332*, 1-2 (2010a), 117–192.

[101] Leitner, D., Klepsch, S., Ptashnyk, M., Marchant, A., Kirk, G., Schnepf, A., and Roose, T. A dynamic model of nutrient uptake by root hairs. *New Phytologist 185*, 3 (2010b), 792–802.

[102] Li, L., Zhang, L., and Kwong, B. Field permeability at shollow depth in a compacted fill. *Proceedings of the Institution of Civil Engineers: Geotechnical Engineering 164*, 3 (2011), 211–221.

[103] Ligaba, A., Shen, H., Shibata, K., Yamamoto, Y., Tanakamaru, S., and Matsumoto, H. The role of phosphorus in aluminium-induced citrate and malate exudation from rape (brassica napus). *Physiol Plant 120*, 4 (2004), 575–584.

[104] Loveridge, F., Spink, T., O'Brien, A., Briggs, K., and Butcher, D. The impact of climate and climate change on uk infrastructure slopes. *Quartely Journal of Engineering Geology and Hydrogeology 43*, 4 (2010), 461–472.

[105] Luersen, M., and Riche, R. Globalized nelder-mead method for engineering optimization. *Computers and Sturctures 82*, 23-26 (2004), 2251–2260.

[106] Lynch, J. Roots of the second green revolution. *Australian Journal of Botany 55*, 5 (2007), 493–512.

[107] Lynch, J., and Brown, K. Topsoil foraging - an architectural adaptation of plants to low phosphorus availability. *Plant and Soil 237*, 2 (2001), 225–237.

[108] Lynch, J., Nielsen, K., Davis, R., and Jablokow, A. Simroot: Modelling and visualization of root systems. *Plant and Soil 188*, 1 (1997), 139–151.

[109] Mackay, A., Syers, J., Tillman, R., and Gregg, P. A simple model to describe the dissolution of phosphate rock in soils. *Soil Science Society of America Journal 50*, 2 (1986), 291–296.

[110] Maguire, R., Sims, J., and Coale, F. Phosphorus solubility in biosolids-amended farm soils in the mid-atlantic region of the usa. *American Society of Agronomy 29*, 4 (2000), 1225–1233.

[111] Mahler, R. *Fertilizer Placement. CIS 757.* Soil Scientist, Department of plant, Soil, and Entomological Sciences, University of Idoha, 2001.

[112] Marschner, P. *Mineral Nutrition of Higher Plants*, third ed. Elsevier, 32 Jamestown Road, london, NW1 7BY, UK, 2012.

[113] Massey, A., Syers, J., Tillman, R., and Gregg, P. Effectivness of recovered magnesium phosphates as fertilizers in neutral and slightly alkaline soils. *Agronomy Journal 101* (1986), 323–329.

[114] McConnell, S., Sander, D., and Peterson, G. Effect of fertilizer phosphorus placement depth on winter wheat yield. *Soil Science Society of America 50*, 1 (1985), 148–153.

[115] McCown, R., Hammer, G., Hargreaves, J., Holzworth, D., and Freebairn, D. Apsim: a novel software system for model development, model testing and simulation in agricultural systems research. *Agricultural Systems 50*, 3 (1996), 255–271.

[116] McKay, M., Backman, R., and Conover, W. A comparison of three methods for selecting values of imput variables in the analysis of output from a computer code. *Technometrics 21*, 2 (1979), 239–245.

[117] Mehlich, A. Determination of p, k, ca, mg, and nh_4. *Soil Test Div. Mimeo, N.C. Department of Agriculture, Raleigh. 1-53* (1953). www.ncagr.com/agronomi/pdffiles/mehlich53.pdf, accessed June 30, 2014.

[118] Mehlich, A. Mehlich 3 soil test extractant: A modification of mehlich-2 extractant. *Communications in Soil Science and Plant Analysis 15*, 12 (1984), 1409–1416.

[119] Miglietta, F., and Bindi, M. Crop growth simulation models for research, farm management and agrometeorology. *EARSeL ADVANCES IN REMOTE SENSING 2*, 2 (1993), 148–157.

[120] Mockus, J. *Bayesian Approach to Global Optimization*. Kluwer Academic Publishers, 1989.

[121] Mohammed, G., and Marshall, C. The pattern of distribution of phosphorus and dry matter with time in spring wheat. *Annals of Botany 44*, 6 (1979), 721–730.

[122] Mor*é*, J. The levenberg-marquardt algorithm: Implementation and theory. *Numerical Analysis 630* (1978), 105–116.

[123] Morgan, M. Microchemical soil tests. *Connecticut Agricultural Experiment Station Bulliten 333* (1932). 1935. The universal soil testing system. Conn. Agri. Expt. Sta. Bul. 372.

[124] Morris, M., and Mitchell, T. Exploratory designs for computational experiments. *Journal of Statistical Planning and Inference 43*, 3 (1995), 1749–1842.

[125] Morse, G., Brett, S., Guy, J., and Lester, J. Review: Phosphorus removal and recovery technologies. *Science of the Total Environment 212*, 1 (1998), 69–81.

[126] Murphy, J., and Riley, J. A modified single solution method for the determination of phosphate in natural waters. *Analytica Chimica Acta 27* (1962), 31–36.

[127] Nelder, J., and Mead, R. A simplex method for function minimization. *Computer Journal 7*, 4 (1965), 308–313.

[128] Neumann, G., and Römheld, V. Root excretion of carboxylic acids and protons in phosphorus-deficient plants. *Plant and Soil 211*, 1 (1999), 121–130.

[129] Neyroud, J., and Lischer, P. Do different methods used to estimate soil phosphorus availability across europe give comparable results? *Journal of Plant Nutrition Soil Science 166*, 4 (2002), 422–431.

[130] Ng, C., and Pang, Y. Experimental investigations of the soil-water characteristics of a volcanic soil. *Canadian Geotechnical Journal 37*, 6 (2000), 1252–1264.

[131] Nicholson, F., Smith, S., Alloway, B., Carlton-Smith, C., and Chambers, B. An inventory of heavy metals inputs to agricultural soils in england and wales. *Science of the Total Environment 311*, 1-3 (2003), 205–219.

[132] Nyambyo, V., and Potts, D. Numerical simulation of evapotranspiration using a root water uptake model. *Computers and Geotechnics 37*, 1-2 (2010), 175–186.

[133] Nye, P., and Tinker, P. *Solute movement in the soil-root system*. Blackwell science publishers, 1977.

[134] O'Brien, A. Rehabilitation of urban railway embankments: investigation, analysis and stabilisation. *In Proceedings of the 14th European conference on soil mechanics and geotechnical engineering, Madrid (eds V.cuellar, E. Dapena, E. Alonso et al.* (2007), 125–143. Amsterdam, the Netherlands: Millpress.

[135] of Agriculture, U. S. D. Economic research service: Wheat data [www document] url http://www.ers.usda.gov/data-products/wheat-data.aspx.u5sjgfldx-t [accessed 31/05/2013]. *USDA* (2013).

[136] Ohlinger, K., Young, T., and Schroeder, E. Predicting struvite formation in digestion. *Water Research 32*, 12 (1998), 3607–3614.

[137] Olsen, S., Cole, R., Watanabe, R., and Dean, L. Estimation of available phosphorus in soils by extraction with sodium bicarbonate. *US Department of Agriculture, Washington DC, Circular 939* (1954), 1–19.

[138] Olsen, S., and Kemper, W. Movement of nutirents to plant roots. *Advances in Agronomg 20* (1968), 91–151. (doi:10.1016/S0065-2113(08)60855-x).

[139] Orbović, V., Jifin, J., and Syvertsen, J. Foliar-applied surfactants and urea temporarily reduce carbon assimilation of grapefruit leaves. *Journal of the American Society for Horticultural Science 126*, 4 (2001), 486–490.

[140] O'Sullivan, J., Asher, C., and Blamey, F. Nutrient disorders of sweet potato. *Australian Centre for International Agricultual Research (ACIAR) Monograph 48* (1997), 136p. ISBN: 1 86320 210 2.

[141] Owusu-Gyimah, V., Nyatuame, M., Ampiaw, F., and Ampadu, P. Effect of depth and placement distance of fertilizer npk 15-15-15 on the performance and yield of maize plant. *International Journal of Agronomy and Plant Production 4*, 12 (2013), 3197–3204.

[142] Pagès, L., Jourdan, M., and Picard, D. A simulation model of the three-dimensional architecture of the maize root system. *Plant and Soil 199*, 1 (1989), 147–154.

[143] Pardalos, P., and Romeijn, H. *Handbook of Global Optimization Volume 2*. Kluwer Academic Publishers, 2002.

[144] Pierzynski, G., J., S., and Vance, G. *Soils and Environmental Quality, Second Edition*. CRC Press, Boca Raton, FL, 2000.

[145] Pimentel, D., Berger, B., Filiberto, D., Newton, M., Wolfe, B., Karabinakis, E., Clark, S., Poon, E., Abbett, E., and Nandagopal, S. Water resources: Agricultural and environmental issues. *BioScience 54*, 10 (2004), 909–918.

[146] Pimentel, D., Harvey, C., Resosudarmo, P., Sinclair, K., Kurz, D., McNair, M., Crist, S., Shpritz, L., Fitton, L., Saffouri, R., and Blair, R. Environmental and economic costs of soil erosion and conservation benefits. *Science 267*, 5201 (1995), 1117–1123.

[147] Pintér, J. *Global Optimization in Action: Continuous and Lipschitz Optimization. Algorithms, Implementations and Applications. Nonconvex Optimization and its Applications*. Kluwer, Dordrecht, 1995.

[148] Powell, M. An efficient method for finding the minimum of a function of several variables without calculating derivatives. *Computer Journal 7*, 2 (1964), 155–162.

[149] Qiu, J. Phosphate fertilizer warning for china. *Nature 'http://www.nature.com/news/2010/100929/full/news.2010.498.html' last accessed 13/06/2014* (2010). Doi: 10.1038/news.2012.498.

[150] Quilliam, R., Marsden, K., Gertler, C., Rousk, J., DeLuca, T., and Jones, D. Nutrient dynamics, microbial growth and weed emergence in biochar amended soil are influenced by time since application and reapplication rate. *Agriculture, Ecosystems & Environmental Journal 158*, 1 (2012), 192–199.

[151] Rahardjo, H., Li, X., Toll, D., and Leong, E. The effect of antecedent rainfall on slope stability. *Geotechical and Geological Engineering 19*, 3-4 (2001), 371–399.

[152] Randall, G., and Hoeft, R. Placement methods for improved efficiency of p and k fertilisers: A review. *Journal of Production Agriculture 1*, 1 (1988), 70–79. Doi:10.2134/jpa1988.0070.

[153] Reijneveld, J., Ehlert, P., Termorshuizen, A., and Oenema, O. Changes in the soil phosphorus status of agricultural land in the netherlands during the 20th century. *Soil Use and Management 26*, 4 (2010), 399–411.

[154] Rennenberg, H. The fate of excess sulfur in higher plants. *Annual Review of Plant Physiology 35* (1984), 121–53.

[155] Reynolds, M., and Ortiz, R. *Adapting Crops to Climate Change*. Edited by M Reynolds, Principal Scientist, CIMMYT, Mexico, 2010.

[156] Richardson, A., Lynch, J., Ryan, P., Delhaize, E., Smith, A., Smith, S., Harvey, P., Ryan, M., Veneklass, E., Lambers, H., Obersonm, A., Culvenor, R., and Simpson, R. Plant and microbial strategies to improve the phosphorus efficiency of agriculture. *Plant and Soil 349*, 1-2 (2011), 121–156.

[157] Rios, L., and Sahinidis, N. Derivative-free optimization: a review of algorithms and comparison of software implementations. *Journal of Global Optimization 56*, 3 (2013), 1247–1293.

[158] Roger-Estrade, J., Richard, G., Boizard, H., Boiffin, J., Caneill, J., and Manichon, H. Modelling structural changes in tilled topsoil over time as a function of cropping systems. *European Journal of Soil Science 51*, 3 (2000), 455–474.

[159] Roose, T., and Fowler, A. A mathematical model for water and nutrient uptake by plant root systems. *Journal of theoretical biology 288*, 2 (2004), 173–184.

[160] Roose, T., and Fowler, A. A model for water uptake by plant roots. *Journal of theoretical biology 288*, 2 (2004), 155–171.

[161] Roose, T., Fowler, A., and Darrah, P. A mathematical model of plant nutrient uptake. *Mathematical biology 42*, 4 (2001), 347–360.

[162] Roose, T., and Kirk, G. The solution of convection-diffusion equations for solute transport to plant roots. *Plant and Soil 316*, 1-2 (2009), 257–264.

[163] Roose, T., and Schnepf, A. Mathematical models of plant-soil interaction. *Philosophical transactions Series A, Mathematical, physical, and engineering sciences 336*, 1885 (2008), 4597–4661.

[164] Rouainia, M., Davies, O., O'Brien, A., and Glendinning, S. Numerical modelling of climate effects on slope stability. *Proceedings of the Institution of Civil Engineers - Engineering Sustainability 162*, 2 (2009), 81–89.

[165] Sacks, J., Welch, W., Mitchell, T., and Wynn, H. Design and analysis of computer experiments. *Statistical Science 4*, 4 (1989), 409–423.

[166] Sánchez, P. Tripling crop yields in tropical africa. *Nature Geoscience 3* (2010), 299–300.

[167] Schaap, M., Leij, F., and Van Genuchten, M. Rosetta: a computer program for estimating soil hydraulic parameters with hierarchical pedotransfer functions. *Journal of Hydrology 251*, 3-4 (2001), 163–176.

[168] Schauer, P., Baur, R., Barnard, J., and Britton, A. Increasing revenue while reducing nuisance struvite precipitation: pilot scale testing of the wasstrip process. *Proceedings of the Water Environment Federation 18* (2011), 848–865.

[169] Schindler, D. Evolution of phosphorus limitation in lakes. *Science (80-.) 195*, 4275 (1977), 260–262.

[170] Schreiner, R. Foliar sprays containing phosphorus (p) have minimal impact on 'pinot noir' growth and p status, mycorrhizal colonization, and fruit quality. *HortScience 45*, 5 (2010), 815–821.

[171] Selmants, P., and Hart, S. Phosphorus and soil development: Dose the walker and syers model apply to semiarid ecosystems? *Ecology 91*, 2 (2010), 474–484.

[172] Shubert, B. A sequential method seeking the global maximum of a function. *Society for Industrial and Applied Mathematics (SIAM) Journal on Numerical Analysis 9*, 3 (1972), 379–388.

[173] Siddique, K., Belford, R., Perry, M., and Tennant, D. Growth, development and light interception of old modern wheat cultivars in a mediterranean-type environment. *Australian Journal of Agricultural Research 40*, 3 (1989), 473–487.

[174] Sivaraj, R. A review of selection methods in genetic algorithms. *Internation Journal of Engineering Science and Technology 3*, 5 (2011), 3792–3797.

[175] Smethurst, J., Clarke, D., and Powrie, W. Seasonal changes in pore water pressure in a grass-covered cut slope in london clay. *Geotechnique 56*, 8 (2006), 523–537.

[176] Smethurst, J., Clarke, D., and Powrie, W. Factors controlling the seasonal variation in soil water content and pore water pressures within a lightly vegetated clay slope. *Geotechnique 62*, 5 (2012), 429–446.

[177] Smith, S. *The scientist and Engineer's Guide to Digital Signal Processing*. California Technical Publishing San Diedo, Ca, USE, 1997.

[178] Stŕeda, T., Dostal, V., Horakova, V., and Chloupek, O. Effective use of water by wheat varieties with different root system sizes in rainfed experiments in central europe. *Agricultural Water Management 104*, February (2012), 203–209.

[179] Stutter, M., Shand, C., George, T., Blackwell, M., Bol, R., MacKay, R., Richardson, A., Condron, L., Turner, B., and Haygarth, P. Recovering phosphorus from soil: A root solution. *Environmental Science & Technology 46*, 4 (2012), 1977–1978.

[180] Sultenfuss, J., and Doyle, W. Better crops with plant food. *Phosphorus Fertiliser Placement. A Publication of the International Plant Nutrition Institute (IPNI) 83*, 1 (1999), 34–39.

[181] survey of Scotland Staff, S. *Soil maps of Scotland at a scale of 1:250 000*. Macaulay Institute for Soil Research, Aberdeen, 1981.

[182] Sutton, P., Peterseon, G., and Sander, D. Dry matter production in tops and roots of winter wheat as affected by phosphorus availability during various growth stages. *Agronomy Journal 75*, 4 (1983), 657.

[183] Sylvester-Bradley, R., Scott, R., and Clare, R. The wheat growth guide. *London: Home Grown Cereals Authority* (1997). http://www.hgca.com/media/185687/g39-the-wheat-growth-guide.pdf, last accessed 12/09/2014.

[184] Talboys, P., Heppell, J., Daniel, J., Roose, T., Healey, J., Jones, D., and Withers, J. Struvite: a slow-release p fertiliser for sustainable intensification. *In Submission* (2014).

[185] Tandy, S., Mundus, S., Yngvesson, J., de Bang, T., Lombi, E., Schjoerring, J., and Husted, S. The use of dgt for prediction of plant

available cooper, zinc and phosphorus in agricultural soils. *Plant and Soil 346*, 1-2 (2011), 167–180.

[186] Törn, A. Cluster analysis using seed points and density determined hyperspheres as an aid to global optimization. *Institute of Electrical and Electronics Engineers (IEEE) Transactions on Systems Man and Cybernetics 7*, 8 (1977), 385–398.

[187] Thornley, J. Modelling allocation with transport/conversion processes. *Silva Fenica 31*, 3 (1997), 341–355.

[188] Thornley, J., and Johnson, I. *Plant and Crop Modelling: A mathematical approach to Plant and Crop Physiology*. Oxford University Press, Walton street, OxfordOX2 6DP, 1990.

[189] Tinsley, J., and Pizer, N. The morgan method of soil testing. part iv. use of the spekker absorptiometer for estimating phosphate. *Journal of the Soceity of Chemical Industry, London (Transactions) 65*, 7 (1946), 208–211.

[190] Tuzet, A., Perrier, A., and Leuning, R. A coupled model of stomatal conductance, photosynthesis and transpiration. *Plant, Cell & Environment 26*, 7 (2003), 1097–1116.

[191] Vaccari, D. Phosphorus: a looming crisis. *Scientific American 300*, 6 (2009), 54–59.

[192] Van den Putte, A., Govers, G., Diels, J., Gillijns, K., and Demuzere, M. Assessing the effect of soil tillage on crop growth: A meta-regression analysis on european crop yields under conservation agriculture. *European Journal of Agronomy 33*, 3 (2010), 231–241.

[193] Van Ganuchten, M. A closed-form equation for predicting the hydraulic conductivity of unsaturated soil. *Soil Science Society of America Journal 44*, 5 (1980), 892–898.

[194] Van Keulen, H., Penning De Vries, F., and Drees, E. A summary model for crop growth. in f.w.t. penning de vries and h.h. van laar (eds.): Simulation of plant growth and crop production. *Simulation Monographs* (1982). Wageningen: Pudoc.

[195] Van Rotterdam, A., Temminghoff, E., Schenkeveld, W., Hiemstra, T., and Riemdijk, W. Phosorus removal from soil using fe oxide-impregnated paper: Processes and applications. *Geoderma 151*, 3-4 (2009), 282–289.

[196] Vance, C. Uhde-Stone, C., and Allan, D. Phosphorus acquisition and use: critical adaptations by plants for securing a non-renewable resource. *New Phytologist 157*, 3 (2003), 423–447.

[197] Varney, G., Canny, M., Wang, X., and McCully, M. The branch roots of zea. i. first order branches, their number, sizes and division into classes. *Annals of Botany 67* (1991), 357–364.

[198] Vaughan, P., Kovacevic, N., and Potts, D. Then and now: some comments on the design and analysis of slopes and embankments. *In Advances in geotechnical engineering: Proceedings of the Skempton conference, Imperial College, London (eds R. J. Jardine, D. K. Potts and K. G. Higgins) 1* (2004), 241–290. London, UK: Thomas Telford.

[199] Veneklaas, E., Lambers, H., Bragg, J., Finnengan, P., Lovelock, C., Plaxton, W., Price, C., Scheible, W., Shance, M.,

White, P., and Raven, J. Opportunities for improving phosphorus-use efficiency in crop plants. *New Phytologist 195*, 2 (2012), 306–320.

[200] Vu, T., Tang, C., and Armstrong, R. Tillage system affects phosphorus form and depth distribution in three contrasting victorian soils. *Australian Journal of Soil Research 47*, 1 (2009), 33–45.

[201] Vu Tran, M. Nutrient mobility from biosolids land application sites. *All Graduate Theses and DIssertations Paper 74* (2008). http://digitalcommons.usu.edu/etd/74 last accessed 06/06/2014.

[202] Walker, T., and Syers, J. The fate of phosphorus during pedogenesis. *Geoderma 15*, 1 (1976), 1–19.

[203] Wallace, J. Increasing agricultural water use efficiency to meet future food production. *Agriculture, Ecosystems and Environment 82*, 1-3 (2000), 105–119.

[204] Williamson, L., Ribrioux, S., Fitter, A., and Leyser, H. Phosphate availability regulates root system architecture in arabidopsis. *Plant Physiology 126*, 2 (2001), 875–882.

[205] Wilsenach, J., Schuurbiers, C., Loosdrecht, M., and van Loosdrecht, M. Phosphare and potassium recovery from source separated urine through struvite precipitation. *Water Research 41*, 2 (2007), 458–466.

[206] Withers, P., Clay, S., and Breeze, V. Phosphorus transfer in runoff following application of fertilizer, manure, and sewage sludge. *Journal of Environmental Quality 30*, 1 (2001a), 180–188.

[207] Withers, P., Edwards, A., and Foy, R. Phosphorus cycling in uk agriculture and implications for phosphorus loss from soil. *Soil Use Management 17*, 3 (2001b), 139–149.

[208] Withers, P., Sylvester-Bradley, R., Jones, D., Healey, J., and Talboys, P. Feed the crop not the soil: rethinking phosphorus management in the food chain. *Environmental Sceince & Technology 48*, 12 (2014), 6523–6530. dx.doi.org/10.1021/es501670j.

[209] Yang, X., Post, W., Thornton, P., and Jain, A. The distribution of soil phosphorus for global biogeochemical modeling. *Biogeosciences Discussions 9*, 11 (2012), 16347–16380.

[210] Zhang, W., Ryan, P., and Tyerman, S. Malate-permeable channels and cation channels activated by aluminum in the apical cells of wheat roots. *Plant Physiology 125*, 3 (2001), 1459–1472.

[211] Zheng, J., Ma, F., and Matsumoto, H. High aluminum resistance in buckwheat. i. al-induced specific secretion of oxalic acid from root tips. *Plant Physiology 117*, 3 (1998), 745–751.

[212] Zhu, J., Kaeppler, M., and Lynch, J. Mapping of gtl controlling root hair length in maizw (zea mays l.) under phosphorus deficiency. *Plant and Soil 270*, 1 (2005), 299–310.

[213] Zhu, J., and Lynch, J. The contribution of lateral rooting to phosphorus acquisition efficiency in maize (zea mays) seedlings. *Functional Plant Biology 31*, 10 (2004), 949–958.